STABLE ISOTOPE GEOCHEMISTRY OF BIOAPATITE

by

Amanda E. Drewicz

A dissertation

submitted in partial fulfillment

of the requirements for the degree of

Doctor of Philosophy in Geosciences

Boise State University

December 2018

© 2018

Amanda E. Drewicz

ALL RIGHTS RESERVED

BOISE STATE UNIVERSITY GRADUATE COLLEGE

DEFENSE COMMITTEE AND FINAL READING APPROVALS

of the dissertation submitted by

Amanda E. Drewicz

Dissertation Title: Stable Isotope Geochemistry of Bioapatite

Date of Final Oral Examination: 22 August 2018

The following individuals read and discussed the dissertation submitted by student Amanda E. Drewicz, and they evaluated her presentation and response to questions during the final oral examination. They found that the student passed the final oral examination.

Matthew J. Kohn, Ph.D.	Chair, Supervisory Committee
Jennifer Pierce, Ph.D.	Member, Supervisory Committee
Marion L. Lytle, Ph.D.	Member, Supervisory Committee

The final reading approval of the dissertation was granted by Matthew J. Kohn, Ph.D., Chair of the Supervisory Committee. The dissertation was approved by the Graduate College.

DEDICATION

I dedicate this dissertation to my family and friend-family. Specifically, this work is dedicated to Andy Bray and Abel Jackson. You have been with me through this period in my life, and I cannot thank you enough. I also dedicate this work to Lisa, John, and Robert Drewicz, I love you all very much. Lastly, this research is dedicated to my friend-family in Boise (specifically Erin Murray, Andrea Leonard, and Darin Schwartz); you all mean the world to me, and I will remember these years for the rest of my life.

ACKNOWLEDGEMENTS

I thank my advisor Dr. Matthew Kohn for his scientific and writing insights, and encouragement. I thank also my committee, which consists of, Drs. Marion Lytle and Jennifer Pierce for their insights into my dissertation. This work was funded by a grant from Evolving Earth Foundation, Geological Society of America, Boise State University, and the Burnham Foundation. I am grateful to T. Fremd for fossil specimens, assistance with stratigraphic placement, and constructive reviews. W. Orr and N. Farmer for providing samples from collections at the University of Oregon and Hagerman Fossil Beds; S. Foss, L. Vella, M. Smith, L.R. Rogers, A. Pajak, and D. Findeisen of John Day Fossil Beds National Monument for field collections and curatorial assistance of fossils from Oregon; and M. Thompson and W. Akersten of the Idaho Museum of Natural History for providing samples from Idaho. I thank Jeff S. Pigati and Kathleen B. Springer at the United States Geological Survey (USGS) and Eric Scott at the Cogstone Resource Management for fossil specimens and tufa samples, as well as for temporal context for the Las Vegas Wash. Specifically I would like to thank Kathleen Springer and Jeff Pigati at the USGS for their insights into my work. I also thank Robin Trayler, Mariah Hollaway, and Samantha Evans for insights and for laboratory assistance.

ABSTRACT

The Cenozoic Era was a time period where dynamic shifts in climate created for both warm-wet greenhouse environments of the mid-Miocene Climatic Optimum (MMCO), and cool-dry, glacial periods of the late Pleistocene. The Cenozoic is close to our own time period, and although past climate reconstructions cannot be used as direct analogs for future climate change, understanding previous environmental responses can help inform policy surrounding future climate change. Presented here are climate reconstructions of the interior western United States, from two different geologic time periods. Each had a different climate, that differed greatly from modern day environments. The use of hydrogen isotopes in tooth enamel is also evaluated as a potential new approach for understanding climate. Expanding our isotopic toolbox for climate reconstructions allows for more certain interpretations, and the use of tooth enamel stable hydrogen (δD), oxygen ($\delta^{18}O$), and carbon ($\delta^{13}C$) compositions allow for more reliable climate reconstructions.

The MMCO, between ~17 and 14 Ma, represents the warmest period on Earth in the last 35 Ma, and is thought to reflect a high partial pressure of atmospheric CO_2 (pCO_2). Using tooth enamel $\delta^{13}C$ values from the interior Pacific Northwest, mean annual precipitation (MAP) was estimated before, during, and following the MMCO, to test whether MAP tracks pCO_2 levels. This work speculates high pCO_2 contributed to higher MAP at ~ 28 and 15.1 Ma, and lower pCO_2 contributed to lower MAP for other time periods. Terrestrial climates during the MMCO were likely more dynamic than originally

considered, with wet-warm and cool-dry cycles reflecting 20-, 40-, and 100-ka Milankovitch cycles. Modern climate models predict that the Pacific Northwest will become wetter and warmer with increased CO_2 levels, and this climate projection is consistent with MMCO climates associated with high pCO_2 levels.

Tooth enamel and tufa (low-temperature $CaCO_3$ precipitate) $\delta^{18}O$ and $\delta^{13}C$ values from well-dated late Pleistocene deposits in the Las Vegas Wash (LVW), Nevada, were used to reconstruct past precipitation seasonality, where enhanced net precipitation aided in the expansion of desert wetlands. Low late Pleistocene water $\delta^{18}O$ values, inferred from tufa and tooth enamel, indicate that paleowetland expansion likely resulted from increased winter precipitation derived from high latitudes in the Pacific Ocean. Low tooth enamel $\delta^{13}C$ and inferred $\%C_4$ grass values are again consistent with an increase in proportion of winter precipitation. Increased winter precipitation diverges from late Pleistocene climate reconstructions at lower latitudes in the American Southwest and modern-day climes that receive nearly equal proportions of winter and summer moisture.

Stable hydrogen and oxygen isotope compositions correlate between organic tissues and meteoric water. This correlation was tested for the first time in modern herbivore tooth enamel by measuring oxygen and hydrogen isotope compositions from localities where water compositions are well known. Against expectations, δD and $\delta^{18}O$ values of modern tooth enamel do not align with the Global Meteoric Water Line (GMWL) and hydrogen isotope compositions display little isotopic variation (~35‰) between vastly different geographic locations. However, a strong correlation ($R^2 = 0.84$) indicates a coupling between stable oxygen and hydrogen isotopes in tooth enamel. Tooth enamel δD values were compared to local water compositions, which generally correlate

(R^2 = 0.71), suggesting tooth enamel δD values at least partially reflect biogenic water compositions. However, when hydrogen amounts (H mg/sample mg) are compared to sample weights (mg), it is clear that additional, labile hydrogen is adsorbed onto bioapatite crystallites, and constitutes ~80% of measured hydrogen. The rate of exchange between adsorbed water and water vapor was determined by equilibrating powdered samples with enriched- and depleted-water for 48 hours, and then exposing samples to laboratory conditions for times ranging from a few minutes up to 8 hours. In both experiments, adsorbed water and laboratory water vapor equilibrate within 1 to 2 hours. Because adsorbed water (onto tooth enamel) and ambient water vapor equilibrate so quickly, it would be almost impossible to reconcile tooth enamel δD values for a single specimen across different laboratories, because of differences in local water compositions. Enamel heated at 70 °C in air for 48 hours shows lower δD values than samples equilibrated at room temperature, which likely reflects a different, temperature-dependent partition coefficient between adsorbed water (onto apatite) and water vapor.

TABLE OF CONTENTS

LIST OF TABLES

LIST OF FIGURES

LIST OF ABBREVIATIONS

MMCO	mid-Miocene Climatic Optimum
MAP	mean annual precipitation
MAT	mean annual temperature
CO_2	carbon dioxide
pCO_2	partial pressure of CO_2
ppm	parts per million
ppb	parts per billion
kyr	a thousand years
ka	a thousand years ago
Myr	a million years
m Myr^{-1}	meters per million years
mm/yr	millimeters per year
Ma	1,000,000 years ago
mg	milligram
VPDB	Vienna Pee Dee Belemnite
VSMOW	Vienna Standard Mean Ocean Water
$\delta^{13}C$	stable carbon isotope composition
$\delta^{18}O$	stable oxygen isotope composition
δD	stable hydrogen isotope composition
^{18}O	oxygen-18

^{16}O	oxygen-17
D	deuterium
^{1}H	hydrogen-1
^{14}C	carbon-14
σ	sigma
s.e.	standard error
LVW	Las Vegas Wash
GWD	groundwater discharge
SOW	shift of the westerlies
OOT	out of the tropics
$\%C_4$	percent of C_4 biomass
GMWL	Global Meteoric Water Line
[H]	hydrogen content

CHAPTER ONE: STABLE ISOTOPES IN LARGE HERBIVORE TOOTH ENAMEL CAPTURE A MID-MIOCENE PRECIPITATION SPIKE IN THE INTERIOR PACIFIC NORTHWEST

Introduction

The mid-Miocene Climatic Optimum (MMCO; 13.75-16.9 Ma; Holbourn et al., 2014, 2015) , represents the warmest period on Earth in the last 35 Ma, and is distinguished by low ice volume, high ocean water temperatures, and numerous distinct temperature maxima between 14.6 and 16.3 Ma (Fig 1; e.g., Flower and Kennett, 1993; Zachos et al., 2001; Shevenell et al., 2001; Pekar and DeConto, 2006; Holbourn et al., 2007; 2015; Lear et al., 2010; Cramer et al., 2011). In parallel with marine systems, warm and wet terrestrial ecosystems expanded to higher latitudes during the mid-Miocene (e.g., Wolfe, 1994; Bohme, 2003; Mosbrugger et al., 2005; Hinojasa and Villagran, 2005; Barreda and Palazzesi, 2007; Herold et al., 2008; Bruch et al., 2011; Pound et al., 2012). Carbon dioxide plays a major role in explaining the MMCO greenhouse. Paleosols and stomatal indices indicate a higher partial pressure of atmospheric CO_2 (pCO_2) during the MMCO than at any other time since 35 Ma, with typical atmospheric CO_2 estimates of 500-600 ppmv, and up to 850 ppmv (see summary of Beerling and Royer, 2011; ppmv = parts per million by volume, or µatm). Past marine pCO_2 estimates have been much lower - as low as ~300 ppmv based on boron isotopes or even as low as 180-290 ppmv

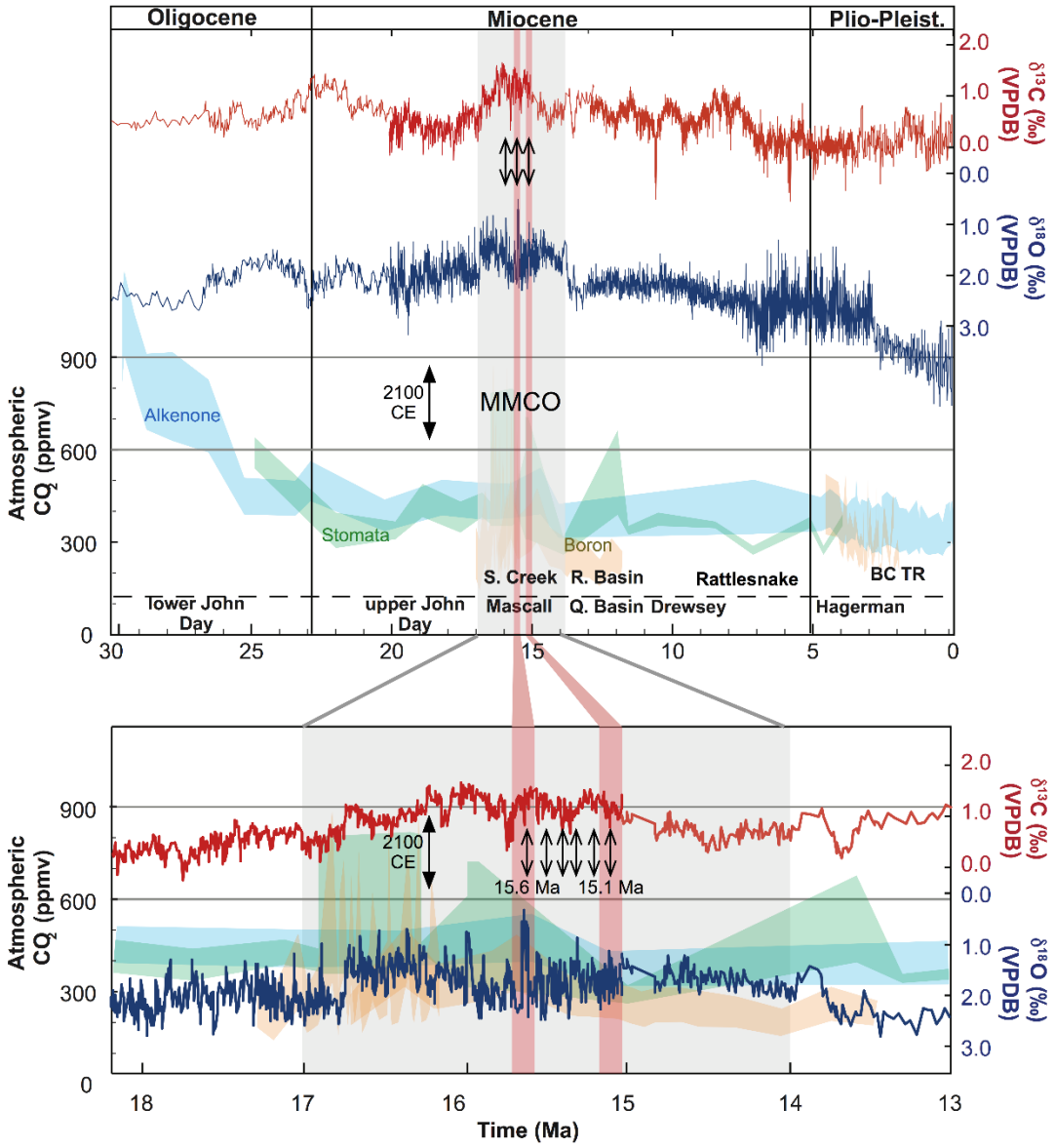

Figure 1. Comparison of climate records for the last 30 Ma: benthic marine $\delta^{13}C$ and $\delta^{18}O$ (Zachos et al., 2001, for 30 to c. 20 Ma and c. 3 to 0 Ma; Holbourn et al., 2013, for c. 13 to c. 8 Ma; Drury et al., 2016, for c. 8 to 3 Ma), and pCO_2 as determined from boron isotopes (Bartoli et al., 2011; Foster et al., 2012; Greenop et al., 2014), alkenone carbon isotopes (Zhang et al., 2013), and leaf stomata (Beerling and Royer, 2011). Arrows between $\delta^{13}C$ and $\delta^{18}O$ records show times of brief warming events, and events at 15.6 and 15.1 Ma are highlighted. The age of each fossil tooth locality is indicated. UJD = upper John Day, LM = lower Mascall, MM = middle Mascall, SC = Sucker Creek, QB = Quartz Basin, Rat. = Rattlesnake, BC = Birch Creek, and TR = Tyson Ranch. The dashed line at pCO_2 = 125 ppmv is the lower limit of C_3 plant

photosynthesis. The range between 550 and 900 ppmv labeled AD 2100 is the range of possible pCO_2 levels expected by year 2100.

based on carbon isotopes (Pagani et al., 1999; 2005; Pearson and Palmer, 2000). More recent work on marine sediments, however, suggests pCO_2 levels were higher and varied during the Miocene in tandem with perturbations in temperature (Bartoli et al., 2011; Foster et al., 2012; Zhang et al., 2013; Holbourn et al., 2013; 2014; 2015; Greenop et al., 2014). These studies suggest MMCO values of ~400±100 ppmv (Zhang et al., 2013), with spikes as high as 850 ppmv (Greenop et al., 2014). The pCO_2 spikes correspond with temperature spikes and perturbations in the C-cycle with a potential ~100 ka cyclicity (Holbourn et al., 2013; 2015).

Overall, climate proxies show that the MMCO represents an unusually warm and wet period in the Earth's history, likely driven in part by higher pCO_2 with some pulses of unusually high temperatures and pCO_2 (Holbourn et al., 2014). The high pCO_2 of the MMCO (400-850 ppmv) almost completely overlaps levels anticipated by A.D. 2100 (550-900 ppmv; (Meehl et al., 2005; 2007). Past climates cannot represent direct analogues for modern environments, but general circulation models (GCM's) for the MMCO provide insights into future climate forcing (You et al., 2009). Because boundary constraints are better known and more similar to modern conditions, the MMCO provides more reliable data-model intercomparisons than older high pCO_2 greenhouse worlds (e.g., the Eocene and Mesozoic). Such GCM's support pCO_2 > 500 to 800 ppmv during the MMCO to explain temperature, precipitation, and ice volume records (Langebroek et al., 2009; Herold et al., 2008; 2011; Henrot et al., 2010; Goldner et al., 2014). These conditions contrast with pCO_2 reconstructions for the cooler Late Miocene (7-11 Ma; Herbert et al., 2016), which

can be modelled with pre-industrial levels of pCO_2 (Knorr et al., 2011; LaRiviere et al., 2012).

The Pacific Northwest provides an excellent setting to study past climate, both temporally and spatially, due to the abundance of preserved herbivore fossils from Oligocene through Pliocene deposits (Fig 2). In this study, stable carbon and oxygen isotope compositions were measured from fossil tooth enamel to illuminate the relationships among changing climate, precipitation patterns, and ecology over the last 30 Myr in the interior Pacific Northwest, with an emphasis on the MMCO. These data help identify possible correspondence among thermal perturbations, pCO_2, and mean annual precipitation (MAP). Here, this work hypothesizes that MAP tracks pCO_2: MAP was high during the late Oligocene and the MMCO when pCO_2 was high, and low at other times when pCO_2 was low. That is, the warm and wet greenhouse conditions of the MMCO suggested by terrestrial records reflect high pCO_2. Stable carbon and oxygen isotope data were used from mammalian teeth from before, during, and after the MMCO to test whether regional climate and ecosystems correlate with previously known atmospheric CO_2 levels.

Stable Isotopes in Teeth

Mineralogically, teeth consist of hydroxylapatite with major substitution of CO_3 for PO_4 and OH groups. Stable carbon and oxygen isotope data from tooth enamel are commonly used for paleoecological and paleoenvironmental reconstructions (Koch, 1998; 2007; MacFadden, 2000; Kohn and Cerling, 2002; Kohn and Dettman, 2007; Clementz, 2012). Oxygen isotope compositions ($\delta^{18}O$ values) in herbivores correlate with local water compositions, which reflect moisture sources and regional climate, including temperature. Carbon isotopes ($\delta^{13}C$ values) in herbivores correlate with $\delta^{13}C$ values of

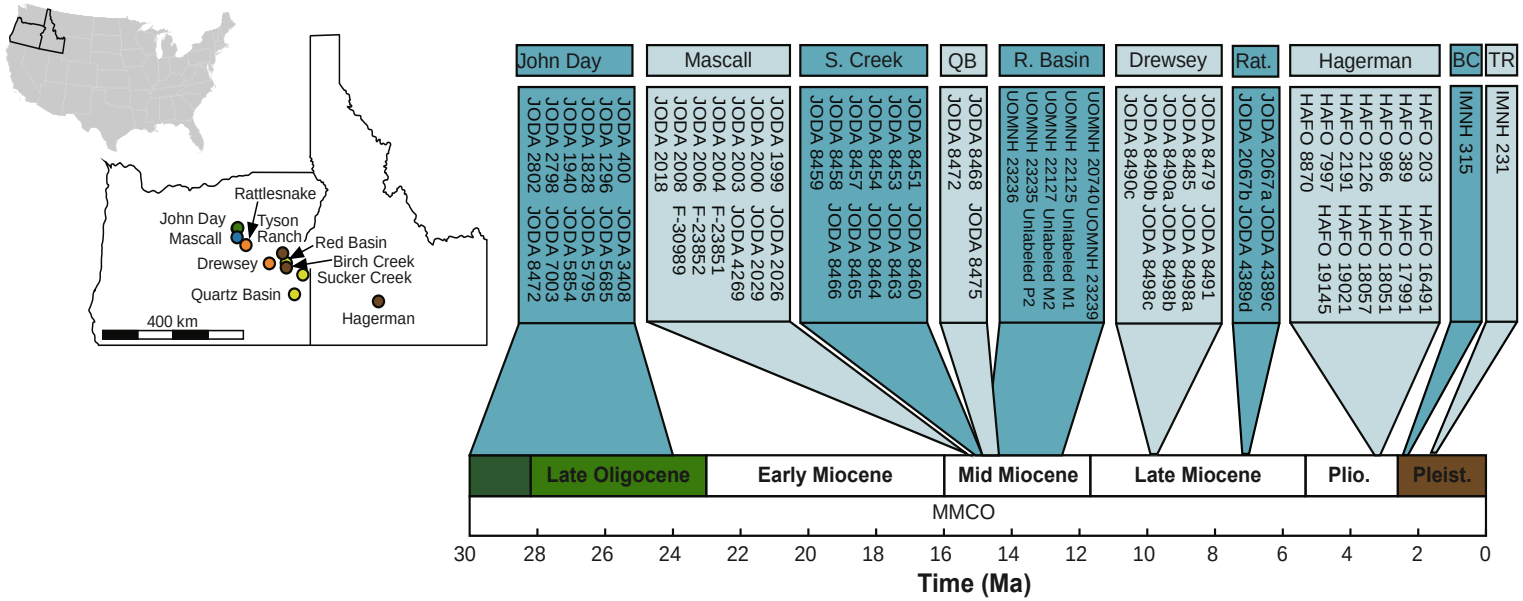

Figure 2. Specimen locations through geologic time. Map of interior Pacific Northwest shows locations of tooth specimens that were analyzed in this study. Different symbols represent different localities and different colors represent different time periods. IMNH=Idaho Museum of National History, HAFO=Hagerman Fossil Beds National Monument, JODA=John Day Fossil Beds National Monument, UOMHN=University of Oregon Museum of Natural History.

their diet. Although modern ecosystems contain both C_3 and C_4 plants, which exhibit a major difference in $\delta^{13}C$ values, C_4 plants were not abundant prior to c. 7 Ma, and constitute only a small portion of plant biomass in the Pacific Northwest today. Thus, once corrected for the fractionation between diet and tooth enamel (Cerling and Harris, 1999; Passey et al., 2005) and for changes in $\delta^{13}C$ values of atmospheric CO_2 (Tipple et al., 2010), isotopic compositions of the herbivores studied reflect C_3 plant $\delta^{13}C$ values.

In principle, tooth enamel $\delta^{13}C$ values allow us to constrain MAP (Kohn, 2010). Carbon isotope values in enamel depend on the $\delta^{13}C$ values of plants consumed, and the $\delta^{13}C$ values of plants that use the C_3 photosynthetic pathway depend quantitatively on MAP (Diefendorf et al., 2010; Kohn, 2010). The nonlinear negative correlation between modern plant $\delta^{13}C$ values and MAP implies that low plant $\delta^{13}C$ values correspond with high MAP and denser forests, while high plant $\delta^{13}C$ values correspond with environments with low MAP (500 mm/yr; Appendix Fig 2; Kohn, 2010). By measuring the $\delta^{13}C$ values of herbivore tooth enamel a correction for the known fractionation between diet and tooth enamel (Cerling and Harris, 1999; Passey et al., 2005) is used to recover $\delta^{13}C$ values of diet (vegetation). The offset between vegetation and atmospheric $\delta^{13}C$ values (Tipple et al., 2010) then allows us to calculate MAP.

Methods

Specimens and Research Area

Eighty-three fossil herbivore teeth were analyzed from ten stratigraphic units in central/eastern Oregon and southern Idaho, spanning the Oligocene, Miocene, and Pliocene (Fig 2; see also (Shotwell et al., 1963; 1968; Fremd et al., 1997; Sankey, 2002; Carrasco et al., 2009; Kohn and Fremd, 2007). These included: sixteen teeth (*Miohippus*

sp., and unidentified equids) from the Turtle Cove member of the middle Oligocene John Day Formation (c.27 Ma); thirteen teeth (*Merychippus* sp., and equid) from the middle Miocene Mascall Formation at or just above the Mascall tuff (15.112±0.017 Ma; Maguire et al., 2018); eleven teeth (*Merychippus* sp., equid, rhino, and artiodactyl) from the middle Miocene Sucker Creek Formation (14.92±0.10 Ma); three teeth (*Merychippus* sp., and equid) from the middle Miocene Quartz Basin locality, Deer Butte Formation (14.3-14.8 Ma); nine teeth (single species of *Dromomeryx* sp.) from the Red Basin locality, Butte Creek Volcanic Sandstone (12.5-14.8 Ma); ten teeth (*Pliohippus* sp., *Megatylopus* sp., gomphothere, equid, rhino) from the late Miocene Drewsey Formation (c.9.8 Ma; age corrected for revisions in standard ages in $^{40}Ar/^{39}Ar$ analysis subsequent to data collection; Kuiper et al., 2008); four equid teeth from the Rattlesnake Formation (7.1 Ma); fifteen teeth (*Mammut* sp., *Camelops* sp., *Castor* sp., Camelidae, Proboscidea, and *Equus* sp.) from the Hagerman locality, Glenns Ferry Formation (c.3.2 Ma); one *Equus* sp. tooth from Birch Creek (2.4 Ma); and one *Equus* sp. tooth from Tyson Ranch (1.9 Ma). We also consider $\delta^{13}C$ values for equids from the Mascall Formation published by Maguire (2015), who focused on paleoecology during the MMCO in central Oregon and did not directly estimate MAP.

Note that Maguire (2015) refers some "*Merychippus*" teeth from the Mascall Formation to "aff. *Acritohippus*". These taxa differ in size, such that the unworn tooth crown height for *Acritohippus* sp. is 30-38 mm (Kelly, 1998), whereas that of *Merychippus* sp. is less. The maximum "*Merychippus*" crown height that we analyzed was 20 mm. So, although some *Acritohippus* sp. teeth may well be present (because of tooth wear), we retain the assignment of *Merychippus* to these specimens.

Ages for John Day, Drewsey, Hagerman, Birch Creek, and Tyson Ranch specimens are constrained using precise $^{40}Ar/^{39}Ar$ dating of single-crystals extracted from interbedded tuffs, with associated errors of ±0.1 Ma, and from magnetostratigraphic correlations (Fields, 1996; Fremd et al., 1997; Sankey, 2002; Jefferson et al., 2002; Jordan et al., 2004; Kohn and Fremd, 2008), although sampling is so dispersed through the John Day Formation that we simply lump average all data at an average age of ~27 Ma. All our samples from Sucker Creek are from within 10 m above and below a tuff with a $^{40}Ar/^{39}Ar$ date of 14.92±0.10 Ma (Fields, 1996). An overall sedimentation rate derived from several ash bed ages ($^{40}Ar/^{39}Ar$ of plagioclase grains) from the Sucker Creek Formation (Downing, 1992) imply that ±10 m uncertainty in location of our fossils would contribute an age uncertainty of only ±0.03Ma. At Quartz Basin, an upper age limit of 14.30±0.12 Ma is derived from an overlying basalt (Fremd et al., 1997). The lower age limit for Quartz Basin is c.14.8 Ma, based on biostratigraphy (Miomap; Carrasco et al., 2009). Ages for Red Basin are based solely on biostratigraphy (12.5-14.8 Ma; Miomap; Carrasco et al., 2009). All specimens from the Rattlesnake Formation were collected proximal to the Rattlesnake ash flow tuff, which has a $^{40}Ar/^{39}Ar$ age of 7.14±0.03 (Jordan et al., 2004; corrected for recalibration of the Fish Canyon sanidine standard: Kuiper et al., 2008).

Because data from the Mascall Formation figure heavily in our interpretations, age control among specimens from our study vs. Maguire (2015) is especially important. Our samples were collected from the Mascall tuff bed and strata immediately overlying it, at the base of the middle member of the Mascall Formation (Bestland et al., 2008). An unpublished U-Pb zircon age for the Mascall tuff is 15.112±0.017 Ma (Maguire et al.,

2018), which is younger than has been previously assumed from $^{40}Ar/^{39}Ar$ data (c.15.8 Ma; Swisher, 1992). Although Maguire (2015) does not report detailed stratigraphy, some of the "middle Mascall" sample localities derive directly from the Mascall tuff (Downs, 1956), and appear to be denoted "middle" in her Table 1. Thus, we correlate isotopic data for the "middle Mascall" of Maguire (2015) with our new data. Precise stratigraphic positions for many of Maguire's other samples are not published or derivable from locality information of Downs (1956). In general, however, we assign an age of c.16 Ma to a series of samples that Maguire (2015) denotes "lower" and that appear to fall at or above the boundary between the John Day and Mascall Formations. This assumption is justified, because the underlying Dayville Basalt is dated between 16.5 - 16.3 Ma in this area (Long and Duncan, 1982; Hooper and Swanson, 1990). Specimens from Hawk Rim, lowermost Mascall Formation, were also assigned to the c.16 Ma group because their age is constrained between 16.26±0.01 and 16.43±0.04 Ma (McLaughlin et al., 2016). We assign an age of c.18 Ma to sample localities JDNM-49, JDNM-160, RV7608, RV7711 and RV7713) that fall within the upper John Day Formation (Hunt and Stepleton, 2004; Albright et al., 2008).

We emphasize equids in our interpretations both because of both their fossil abundance and their relatively conservative physiology, which confers greater accuracy and consistency when interpreting isotope compositions (Kohn and Fremd, 2008). Most equids from our composite dataset occupied open environments (Maguire, 2015), which can be drier with higher $\delta^{13}C$ values than more shaded, closed environments. If equids occupied drier ecosystems, or were disproportionately represented in drier periods, our data could be biased towards higher $\delta^{13}C$ values leading to lower calculated MAP values.

However, comparison of $\delta^{13}C$ values of equids vs. other fauna (grazers and browsers) shows no systematic offset (see supplementary materials), and equids from presumed forested environments (*Archaeohippus*) do not show lower $\delta^{13}C$ values than sympatric equids from more open environments (*Parahippus*, *Desmatippus*, and *affin. Acritohippus*; Maguire, 2015). Thus, we consider data in this study as representative, even though they are weighted towards equids.

Analytical Methods

Enamel was selected for analysis because of its resistance to diagenetic alteration, thus preserving biogenic isotope compositions (Kohn and Cerling, 2002). Enamel slices were cut along the length of each tooth, typically with a length of 1-2 cm, and subsampled every 1-2 mm using a slow-speed microsaw, as recommended for retrieving sub-annual isotope variations (Kohn, 2004) and preserving tooth mineralization geometry (Trayler and Kohn, 2017). Enamel was removed from dentine and was ground to a fine powder using a mortar and pestle. Samples were then pretreated as per Koch et al. (1997), first with H_2O_2 to remove remaining organic matter, then with an acetic acid-Ca acetate buffer to remove diagenetic or labile carbonates. 1.5-2 mg of powdered enamel were dissolved in supersaturated H_3PO_4 in a GasBench II, in-line with a Thermo Delta V Plus Mass Spectrometer, housed in the Stable Isotope Laboratory at Boise State University. Five to six NIST-120c ($\delta^{18}O$ = +28.5 ‰, VSMOW, $\delta^{13}C$ = –6.55 ‰, VPDB; Kohn et al., 2015) aliquots were prepared using the same cleaning and pretreatment methods and analyzed with each sample set. Eight to nine NBS-18 ($\delta^{13}C$ = –5.014 ‰ VPDB and $\delta^{18}O$ = –23.2 ‰ VPDB) and NBS-19 ($\delta^{13}C$ = +1.95 ‰ VPDB and $\delta^{18}O$ = –2.2 ‰ VPDB) calcite standards were also analyzed with each sample set to verify mass spectrometer

operation and calibrate reference gas. Analytical reproducibility for oxygen isotopes was: NIST-120c = ±0.86 ‰ (2σ); NBS-18 =±0.60 ‰; and NBS-19 = ±0.67 ‰. For carbon isotopes, reproducibility was: NIST-120c = ±0.53 ‰ (2σ); NBS-18 = ±0.48 ‰, and NBS-19 = ±0.49 ‰. Table 1 provides summary data, while the Supplemental file provides tooth enamel isotope measurements from this study and Maguire (2015). All tooth $\delta^{13}C$ and $\delta^{18}O$ values are reported relative to VPDB and VSMOW respectively.

Estimating MAP

MAP was estimated using the approach of Kohn (2010), which requires estimates of plant $\delta^{13}C$ values, atmospheric $\delta^{13}C$ values, altitude (in meters), and latitude (in absolute °). Because carbon isotope compositions were measured for herbivore tooth enamel, we corrected for fractionation between diet and tooth enamel and for changes in atmospheric $\delta^{13}C$ values (Tipple et al., 2010). Because different localities have different age resolution, we assumed different atmospheric $\delta^{13}C$ values corresponding with different smoothing functions (Tipple et al., 2010): high-resolution (typically ≤0.1 Ma) for Hagerman, Drewsey, Sucker Creek, Tyson Ranch, Birch Creek, and middle Mascall, 0.5 Ma for Quartz Basin, and 3 Ma for Red Basin, lower Mascall, upper John Day, and John Day. Reported atmospheric CO_2 $\delta^{13}C$ values are temporally sparse through the Rattlesnake Formation (~7.15 Ma), therefore CO_2 $\delta^{13}C$ values were calculated using benthic foraminifera data from Drury et al. (2016) following methods of Tipple et al. (2010). A higher correction value (*A*) was used for foraminifera $\delta^{13}C$ values to account for greater surface-bottom water disequilibrium, biologic pumps, and remineralization

Table 1. Identification number, taxa, mean, error, minimum, and maximum tooth enamel $\delta^{13}C$ and $\delta^{18}O$ values.

John Day Formation (~28 Ma)										
Identifier	Taxa	Mean $\delta^{13}C$ (enamel; ‰; VPDB)	Mean $\delta^{13}C$ (plant; ‰; VPDB)	2σ	Mean $\delta^{18}O$ (‰; VSMOW)	2σ	Min $\delta^{13}C$ (‰; VPDB)	Max $\delta^{13}C$ (‰; VPDB)	Min $\delta^{18}O$ (‰; VSMOW)	Max $\delta^{18}O$ (‰; VSMOW)
JODA 2802(B)	Merycoidodont	–10.7	–25.2	0.3	20.4	0.8	–10.8	–10.5	20.1	20.7
JODA 1940(A)	Merycoidodont	–12.1	–26.6	0.3	20.2	0.6	–12.2	–12	20	20.4
JODA 7003(B)	Merycoidodont	–14.6	–29.1		21.5					
JODA 400A+B	Merycoidodont	–11.9	–26.4	0.8	19.9	3.1	–12.3	–11.5	18.9	21.7
JODA 7003(D)	Merycoidodont	–13.1	–27.6	0.4	21.6	0.3	–13.4	–13	21.4	21.7
JODA 8472	Merycoidodont	–9.5	–24	1.2	21.1	1.4	–10.3	–8.9	20.5	22
JODA 1296-G	Merycoidodont	–9.3	–23.8		18.7					
JODA 5795/1	*Parahippus*	–10.4	–24.4	3.3	22.8	1.2	–12.9	–9.4	21.9	23.2
JODA 5795/1	*Parahippus*	–10.5	–24.5		25.1					
JODA 5685(B)	*Eporeodon*	–11.6	–26.1		26.1					
JODA 5685(A)	*Eporeodon*	–12.3	–26.8		23.4					

Identifier	Taxa	Mean $\delta^{13}C$ (enamel; ‰; VPDB)	Mean $\delta^{13}C$ (plant; ‰; VPDB)	2σ	Mean $\delta^{18}O$ (‰; VSMOW)	2σ	Min $\delta^{13}C$ (‰; VPDB)	Max $\delta^{13}C$ (‰; VPDB)	Min $\delta^{18}O$ (‰; VSMOW)	Max $\delta^{18}O$ (‰; VSMOW)
JODA 5854(A)	*Eporedon*	–12.7	–27.2	0.7	23.1	0.6	–12.9	–12.5	22.8	23.3
JODA 3408	*Diceratherium*	–11.4	–25.4	0.4	20.8	0.5		–11.1	20.5	21
JODA 1828	*Diceratherium*	–11	–25	0.4	21.2	1.4	–11.3	–10.6	20.2	22.4
JODA 1296	*Diceratherium*	–10.4	–24.4	0.6	19.3	1	–10.9	–10.2	18.7	19.9
JODA 2798	Rhino	–10.8	–24.8	0	23.2	0.4	–10.8	–10.7	23.1	23.4
Mascall Formation (~15.1 Ma)										
Identifier	Taxa	Mean $\delta^{13}C$ (enamel; ‰; VPDB)	Mean $\delta^{13}C$ (plant; ‰; VPDB)	2σ	Mean $\delta^{18}O$ (‰; VSMOW)	2σ	Min $\delta^{13}C$ (‰; VPDB)	Max $\delta^{13}C$ (‰; VPDB)	Min $\delta^{18}O$ (‰; VSMOW)	Max $\delta^{18}O$ (‰; VSMOW)
JODA 2004	*Merychippus*	–12.4	–26.4	1	21.4	2	–13.5	–11.8	19.7	23.1

Identifier	Taxa	Mean $\delta^{13}C$ (enamel; ‰; VPDB)	Mean $\delta^{13}C$ (plant; ‰; VPDB)	2σ	Mean $\delta^{18}O$ (‰; VSMOW)	2σ	Min $\delta^{13}C$ (‰; VPDB)	Max $\delta^{13}C$ (‰; VPDB)	Min $\delta^{18}O$ (‰; VSMOW)	Max $\delta^{18}O$ (‰; VSMOW)
JODA 1999	*Acritohippus*	–10.4	–24.4	1.7	22.8	1.8	–12.6	–9.4	21.3	24.3
JODA 2003	*Acritohippus*	–10.8	–24.8	0.9	22.5	1	–11.5	–10	22	23.8
JODA 2026	*Merychippus*	–10	–24	1	22.4	2.1	–10.7	–9.1	20.8	24
JODA 2029	*Merychippus*	–11.4	–25.4	1	21.3	2	–12.4	–10.8	19.6	23.3
F-23851	*Acritohippus*	–9.9	–23.9	0.6	19.1	1	–10.3	–9.5	18.3	19.8
F-23852	*Acritohippus*	–10.6	–24.6	0.9	19.9	1.6	–11.5	–10.1	18.7	20.9
JODA 2000	*Acritohippus*	–11.3	–25.3	0.5	21.1	1.6	–11.7	–10.8	19.7	22.1
JODA 2018	*Merychippus*	–12	–26	0.8	20.4	1	–12.5	–11.2	19.5	21.3

Identifier	Taxa	Mean $\delta^{13}C$ (enamel; ‰; VPDB)	Mean $\delta^{13}C$ (plant; ‰; VPDB)	2σ	Mean $\delta^{18}O$ (‰; VSMOW)	2σ	Min $\delta^{13}C$ (‰; VPDB)	Max $\delta^{13}C$ (‰; VPDB)	Min $\delta^{18}O$ (‰; VSMOW)	Max $\delta^{18}O$ (‰; VSMOW)
JODA 2008	*Merychippus*	–11.2	–25.2	0.5	20.6	1.7	–11.7	–10.8	19.4	21.9
Sucker Creek (~14.73 Ma)										
Identifier	Taxa	Mean $\delta^{13}C$ (enamel; ‰; VPDB)	Mean $\delta^{13}C$ (plant; ‰; VPDB)	2σ	Mean $\delta^{18}O$ (‰; VSMOW)	2σ	Min $\delta^{13}C$ (‰; VPDB)	Max $\delta^{13}C$ (‰; VPDB)	Min $\delta^{18}O$ (‰; VSMOW)	Max $\delta^{18}O$ (‰; VSMOW)
JODA 8460	*Merychippus*	–10.3	–24.3	0.6	20.1	0.3	–10.6	–9.9	19.9	20.3
JODA 8451	*Merychippus*	–8.9	–22.9	0.6	17.2	1.3	–9.3	–8.5	16.1	17.9
JODA 8464	*Merychippus*	–9.2	–23.2	0.9	19.2	0.7	–9.5	–8.5	18.8	19.6
JODA 8464	*Merychippus*	–9.2	–23.2	0.9	19.2	0.7	–9.5	–8.5	18.8	19.6
JODA 8463	Equid	–9.9	–23.9	0	18.3	6.4	–9.9	–9.9	16.1	20.6

Identifier	Taxa	Mean $\delta^{13}C$ (enamel; ‰; VPDB)	Mean $\delta^{13}C$ (plant; ‰; VPDB)	2σ	Mean $\delta^{18}O$ (‰; VSMOW)	2σ	Min $\delta^{13}C$ (‰; VPDB)	Max $\delta^{13}C$ (‰; VPDB)	Min $\delta^{18}O$ (‰; VSMOW)	Max $\delta^{18}O$ (‰; VSMOW)
JODA 8453	Equid	–9.1	–23.1	0.1	18	0.7	–9.2	–9.1	17.6	18.2
JODA 8454	Equid	–10.7	–24.7	1.1	18.8	0.7	–11.3	–10.1	18.4	19.1
JODA 8457	Equid	–10.3	–24.3	0.3	17.1	1.7	–10.5	–10.2	16.3	18
JODA 8458	Rhino	–9.9	–23.9	0.9	17.3	1.5	–10.3	–9.1	16.8	18.6
JODA 8465	Artiodactyl	–8.4	–22.9	0.6	15.7	6.7	–8.6	–8.2	13.3	18.1
JODA 8466	Artiodactyl	–9.2	–23.7	2.3	15.3	0.8	–10	–8.4	15	15.6
Quartz Basin (~14.8–14.12 Ma)										
JODA 8468	*Merychippus*	–9.6	–23.6	0.4	19.3	1.5	–9.9	–9.3	18.3	20.3
JODA 8472	*Merychippus*	–9.2	–23.2	0.2	20.7	0.5	–9.3	–9.1	20.5	21

Identifier	Taxa	Mean $\delta^{13}C$ (enamel; ‰; VPDB)	Mean $\delta^{13}C$ (plant; ‰; VPDB)	2σ	Mean $\delta^{18}O$ (‰; VSMOW)	2σ	Min $\delta^{13}C$ (‰; VPDB)	Max $\delta^{13}C$ (‰; VPDB)	Min $\delta^{18}O$ (‰; VSMOW)	Max $\delta^{18}O$ (‰; VSMOW)
JODA 8475	Equid	–9.4	–23.4	0.6	18.9	2	–9.6	–9.2	18.2	19.6
Red Basin (~14.8–12.5 Ma)										
Identifier	Taxa	Mean $\delta^{13}C$ (enamel; ‰; VPDB)	Mean $\delta^{13}C$ (plant; ‰; VPDB)	2σ	Mean $\delta^{18}O$ (‰; VSMOW)	2σ	Min $\delta^{13}C$ (‰; VPDB)	Max $\delta^{13}C$ (‰; VPDB)	Min $\delta^{18}O$ (‰; VSMOW)	Max $\delta^{18}O$ (‰; VSMOW)
23236–M1	*Dromomeryx*	–10.1	–24.6	2	27.5	2.2	–11.3	–9.5	26.2	28.2
unlabled–M1	*Dromomeryx*	–10.5	–25	1.5	27	1.6	–11.4	–10.1	26.1	27.5
20740–M2	*Dromomeryx*	–10.2	–24.7	1	27.4	1.1	–10.8	–9.8	26.7	27.9
unlabled–M2	*Dromomeryx*	–10.2	–24.7	0.6	27.4	0.7	–10.5	–9.9	27	27.7
23235–M3	*Dromomeryx*	–10.3	–24.8	1	27.3	1.1	–11	–9.9	26.6	27.7
21255–M3	*Dromomeryx*	–10.6	–25.1	0.8	26.9	0.9	–10.9	–10	26.7	27.6
22127–P2	*Dromomeryx*	–9.6	–24.1	1.4	28	1.5	–10.5	–9	27.1	28.7
unlabled–P2	*Dromomeryx*	–9.8	–24.3	0.2	27.8	0.2	–9.8	–9.7	27.8	27.9
23239–P4	*Dromomeryx*	–10.1	–24.6	0.4	27.5	0.4	–10.4	–9.9	27.2	27.7
Drewsey Formation (~9.7 Ma)										

Identifier	Taxa	Mean $\delta^{13}C$ (enamel; ‰; VPDB)	Mean $\delta^{13}C$ (plant; ‰; VPDB)	2σ	Mean $\delta^{18}O$ (‰; VSMOW)	2σ	Min $\delta^{13}C$ (‰; VPDB)	Max $\delta^{13}C$ (‰; VPDB)	Min $\delta^{18}O$ (‰; VSMOW)	Max $\delta^{18}O$ (‰; VSMOW)
JODA 8479	*Hipparion*	–8.5	–22.5	4.8	20.4	1.3	–10.7	–8.2	18.9	21.9
JODA 8485	*Pliohippus*	–8.8	–22.8	0.5	18.1	1.3	–9.3	–8.4	17.2	19.1
JODA 8491	*Pliohippus*	–8.9	–22.9	0.3	19.6	1.3	–9.1	–8.8	18.9	20.1
JODA 8494	*Pliohippus*	–7.3	–21.3	0.5	13.9	1	–7.5	–7	13.4	14.6
JODA 8498b	*Megatylopus*	–10	–24.5	0.4	23.3	0.7	–10.1	–9.7	22.9	23.5
JODA 8498c	*Megatylopus*	–9.3	–23.8	0.1	22.2	3.5	–9.3	–9.2	20.3	23.7
JODA 8498a	Gomphothere	–11.2	–25.45	0.3	20.9	0.2	–11.3	–11.1	20.8	21
JODA 8490a	Equid	–9.9	–23.9	1.9	18.2	2	–10.6	–9.3	17.4	18.9
JODA 8490b	Equid	–10	–24	0.3	19.6	1	–10.2	–9.8	19	20.4
JODA 8490c	Rhino	–9.9	–23.9	0.4	18.2	0.5	–10.1	–9.7	18	18.5
Rattlesnake Formation (~7.2 Ma)										

Identifier	Taxa	Mean $\delta^{13}C$ (enamel; ‰; VPDB)	Mean $\delta^{13}C$ (plant; ‰; VPDB)	2σ	Mean $\delta^{18}O$ (‰; VSMOW)	2σ	Min $\delta^{13}C$ (‰; VPDB)	Max $\delta^{13}C$ (‰; VPDB)	Min $\delta^{18}O$ (‰; VSMOW)	Max $\delta^{18}O$ (‰; VSMOW)
JODA 4389c	Equid	–10.31	–24.31	0.57	22.97	0.53	–11.83	–8.84	21.85	23.93
JODA 4389d	Equid	–11.20	–25.20	0.17	20.37	1.21	–11.34	–11.04	19.69	21.57
JODA 2067a	Equid	–11.98	–25.98	0.33	23.84	1.62	–12.04	–11.66	22.48	25.97
JODA 2067b	Equid	–12.12	–26.12	0.43	23.67	1.01	–12.56	–11.38	22.93	25.5
Glenns Ferry Formation (Hagerman; ~3.2 Ma)										
Identifier	Taxa	Mean $\delta^{13}C$ (enamel; ‰; VPDB)	Mean $\delta^{13}C$ (plant; ‰; VPDB)	2σ	Mean $\delta^{18}O$ (‰; VSMOW)	2σ	Min $\delta^{13}C$ (‰; VPDB)	Max $\delta^{13}C$ (‰; VPDB)	Min $\delta^{18}O$ (‰; VSMOW)	Max $\delta^{18}O$ (‰; VSMOW)
HAFO 2126	*Castor*	–9.3		1.1	18.3	1	–10	–8.4	17.2	19.4
HAFO 19021	Castoridae	–7.8		0.2	17.8	0.8	–8	–7.7	17.2	18.2
HAFO 389	*Mammut*	–9.8	–24.05	0.3	21.4	0.9	–9.9	–9.4	20.8	22
HAFO 986	*Mammut*	–10.2	–24.45	0.3	18.9	0.4	–10.4	–10	18.6	19.2
HAFO 8870	*Mammut*	–9.7	–23.95	0.4	18	0.3	–10.1	–9.4	17.8	18.2

Identifier	Taxa	Mean $\delta^{13}C$ (enamel; ‰; VPDB)	Mean $\delta^{13}C$ (plant; ‰; VPDB)	2σ	Mean $\delta^{18}O$ (‰; VSMOW)	2σ	Min $\delta^{13}C$ (‰; VPDB)	Max $\delta^{13}C$ (‰; VPDB)	Min $\delta^{18}O$ (‰; VSMOW)	Max $\delta^{18}O$ (‰; VSMOW)
HAFO 7997	*Mammut*	–10.0	–24.25	0.7	19	0.4	–10.3	–9	18.7	19.5
HAFO 19145	Proboscidea	–9.3	–23.55	1.2	19.7	2.8	–9.7	–8.2	17.2	20.6
HAFO 203	Camelidae	–10.6	–25.1	0.4	21.8	2	–10.8	–10.2	19.4	22.8
HAFO 16491	*Camelops*	–10	–24.5	1.1	19.6	3	–10.6	–9.5	18.3	21.1
Birch Creek (~2.4 Ma)										
Identifier	Taxa	Mean $\delta^{13}C$ (enamel; ‰; VPDB)	Mean $\delta^{13}C$ (plant; ‰; VPDB)	2σ	Mean $\delta^{18}O$ (‰; VSMOW)	2σ	Min $\delta^{13}C$ (‰; VPDB)	Max $\delta^{13}C$ (‰; VPDB)	Min $\delta^{18}O$ (‰; VSMOW)	Max $\delta^{18}O$ (‰; VSMOW)
IMNH 315	*Equus*	–10.77	–24.77	0.28	19.4	0.3	–13.4	–9.2	17.2	22.1
Tyson Ranch (~1.9 Ma)										
Identifier	Taxa	Mean $\delta^{13}C$ (enamel; ‰; VPDB)	Mean $\delta^{13}C$ (plant; ‰; VPDB)	2σ	Mean $\delta^{18}O$ (‰; VSMOW)	2σ	Min $\delta^{13}C$ (‰; VPDB)	Max $\delta^{13}C$ (‰; VPDB)	Min $\delta^{18}O$ (‰; VSMOW)	Max $\delta^{18}O$ (‰; VSMOW)
IMNH 231	*Equus*	–8.08	–22.08	0.23	22.9	0.5	–11.0	–6.9	16.6	26

(Tipple et al., 2010; Drury et al., 2016). Enamel-diet $\delta^{13}C$ value offsets of 14.5 ‰ for artiodactyls (Passey et al., 2005), and 14 ‰ for perissodactyls (Cerling and Harris, 1999) were applied. For elephantids, an intermediate offset of 14.25 ‰ was assumed. We did not attempt to calculate leaf compositions or MAP from castorid data. All Oligocene to Pliocene herbivore $\delta^{13}C$ values measured in this study are within the C_3 consumption range, and may be used to calculate MAP according to the equation:

$$\mathrm{MAP\ (mm)} = 10^{\left[\frac{\Delta(\text{‰,VPDB}) - 2.01 + 0.000198 \times elev - 0.0129 \times Abs(lat)}{5.88}\right]} - 300 \qquad \text{(Eq. 1)}$$

where Δ is given by:

$$\Delta^{13}C(\text{‰, VPDB}) = \frac{\delta^{13}C_{atm} - \delta^{13}C_{leaf}}{1 + {\delta^{13}C_{leaf}}/{1000}} \qquad \text{(Eq. 2)}$$

and $\delta^{13}C_{atm}$ and $\delta^{13}C_{leaf}$ are the average carbon isotope compositions of atmospheric CO_2 and plants, respectively (Table 2). Equation 1 shows how MAP increases with increasing $\Delta^{13}C$ (decreasing $\delta^{13}C$ of enamel and plants). Elevations and latitudes are not thought to have changed significantly for sample sites (Kohn et al., 2002; Orr and Orr, 2012; Retallack et al., 2016), so modern-day elevation and latitudes were used (Table 2).

Uncertainties in MAP may be calculated using numerical error propagation (Kohn and McKay, 2012). A simplified form of this approach, propagating uncertainties in mean $\Delta^{13}C$ alone, uses the following equations:

$$2\sigma(+)_{MAP} = \frac{10^{\left(\Delta^{13}C - +2\sigma_{\Delta} - 2.01 + 0.000198 \times elev - 0.0129 \times lat\right)} - 300 - MAP}{5.88} \qquad \text{(Eq. 3a)}$$

$$2\sigma(+)_{MAP} = \frac{10^{\left(\Delta^{13}C - 2\sigma_{\Delta} - 2.01 + 0.000198 \times elev - 0.0129 \times lat\right)} - 300 - MAP}{5.88} \qquad \text{(Eq. 3b)}$$

Table 2. Times for localities along with estimate MAP (mm/yr) and associated errors. Enamel, plant, and atmospheric $\delta^{13}C$ values, errors, corrected $\Delta^{13}C$ values, latitude, and altitude are also reported. J. Day = John Day, S. Creek = Sucker Creek, Q. Basin = Quartz Basin, R. Basin = Red Basin, Ratt. = Rattlesnake, B. = Birch Creek, T. Ranch = Tyson Ranch.

Time (Ma)	Location or Formation	Source	Mean $\delta^{13}C$ (enamel; ‰; VPDB)	Mean $\delta^{13}C$ (plant; ‰ ; VPDB)	2 s.e.	$\delta^{13}C$ (atm; ‰) 3 Ma	$\delta^{13}C$ (atm; ‰) 0.5 Ma	$\delta^{13}C$ (atm; ‰) high res	$\Delta^{13}C$ (atm-plant; ‰)	Lat. (º)	Alt. (m)	MAP (mm/yr)	σ
~27	J. Day	This study	–11.39	–25.71	0.74	–6.30	–6.18	–6.30	19.92	44	750	644	317
~18*	upper J. Day	Maguire (2015)	–9.77	–23.77	1.04	–5.77	–5.86	–5.91	18.44	44	700	226	264
~16*	lower Mascall	Maguire (2015)	–10.49	–24.49	0.46	–5.31	–5.09	–5.20	19.66	44	700	549	168
15.1	middle Mascall	This study	–11.09	–25.09	0.53	–5.27	–5.29	–5.32	20.42	44	700	784	249
~15.1	middle Mascall	Maguire (2015)	–10.47	–24.47	0.33	–5.27	–5.29	–5.32	19.77	44	700	541	116
14.9	S. Creek	This study	–9.55	–23.64	0.38	–5.31	–5.52	–5.57	18.51	43	950	254	89
14.3-14.8	Q. Basin	This study	–9.40	–23.40	0.23	–5.44	–5.52	–5.03	18.31	42	1150	223	49
12.5-14.8	R. Basin	This study	–10.16	–24.66	0.21	–5.82	–5.54	–5.76	19.32	43	1300	481	66
9.8	Drewsey	This study	–9.38	–23.51	0.73	–5.99	–5.95	–6.02	17.91	43	1150	145	147
~7.1	Ratt.	This study	–11.36	–25.36	0.54	–6.56	–6.54	–6.60	19.25	44	750	425	171

Time (Ma)	Location or Formation	Source	Mean $\delta^{13}C$ (enamel; ‰; VPDB)	Mean $\delta^{13}C$ (plant; ‰ ; VPDB)	2 s.e.	$\delta^{13}C$ (atm; ‰) 3 Ma	$\delta^{13}C$ (atm; ‰) 0.5 Ma	$\delta^{13}C$ (atm; ‰) high res	$\Delta^{13}C$ (atm-plant; ‰)	Lat. (º)	Alt. (m)	MAP (mm/ yr)	σ
3.2	Hagerman	This study	–9.37	–23.81	0.45	–6.38	–6.21	–6.03	18.21	42	940	196	96
2.4	B. Creek	This study	–10.77	–24.77	0.28	–6.46	–6.45	–6.44	18.86	45	1060	348	60
1.9	T. Ranch	This study	–9.92	–23.92	0.14	–6.56	–6.44	–6.89	17.79	44	1158	123	24

where the 2σ uncertainty in mean $\Delta^{13}C$ (=2σ) is added (eq 3a) and subtracted (eq 3b) from $\Delta^{13}C$. The absolute value of each $2\sigma_{MAP}$ is then averaged. Such error propagation represents the uncertainty in MAP due to the reproducibility of the mean $\Delta^{13}C$. Similar kinds of calculations cannot be made so easily for the original regression parameters because of correlation coefficients, but in general, 2σ. Similar kinds of calculations cannot be made so easily for the original regression parameters because of correlation value above c. 500 mm/yr and are never lower than ~120 mm/yr. It is important that propagated errors in the regression parameters are systematic, i.e. if the true MAP value for one-time interval is higher than calculated from Equation 1, all MAP values for all time intervals are also higher.

Statistical Comparison

We cannot apply simple statistical tests (e.g. t-tests) to raw $\delta^{13}C$ values because atmospheric $\delta^{13}C$ values vary throughout geological time, shifting $\delta^{13}C$ values of plants and their consumers. For example, fossil fuel burning has lowered biosphere $\delta^{13}C$ values by c. 1.5 ‰ (Trudinger et al., 1999), so mean $\delta^{13}C$ values for modern vs. pre-industrial animals consuming the same diet in the same environment now differ by c. 1.5 ‰. Because we were interested in comparing environments among different time periods, not atmospheric $\delta^{13}C$ values, calculations and comparisons (e.g. t-tests) to $\Delta^{13}C$ values were made. We assign significance at $p<0.05$, after applying the Bonferroni correction for multiple comparisons.

Results

Herbivore Carbon and Oxygen Isotope Compositions

Specimens from the John Day (~27 Ma), Mascall (~15.1 Ma), and Rattlesnake (~7.15 Ma) Formations, have relatively low mean $\delta^{13}C$ values, respectively of –11.4±0.7 ‰, (2s.e.; VPDB), –11.1±0.5 ‰, and –11.4 ‰±0.5 (Fig 3; Table 2). However, during these time periods, atmospheric CO_2 $\delta^{13}C$ values differed (John Day = –6.2 ‰, Mascall = –5.3 ‰, Rattlesnake = –6.6 ‰; Tipple et al., 2010; Drury et al., 2016). Consequently, although $\delta^{13}C$ values are higher for Mascall specimens (implying small $\Delta^{13}C$), $\Delta^{13}C$ values are actually largest for this time (Mascall $\Delta^{13}C$ = +20.4 ‰ vs. John Day $\Delta^{13}C$ = +19.9 ‰ and Rattlesnake = +19.25 ‰). Data from Maguire (2015) imply somewhat smaller $\Delta^{13}C$ values of ~+19.7 ‰ for the middle and lower Mascall Formation. $\delta^{13}C$ values from other stratigraphic units are higher compared to the John Day, Mascall, and Rattlesnake Formations, ranging from –9.4 ‰ to –10.8 ‰ (Tables 1-2; Fig 3), and $\Delta^{13}C$ values are consistently smaller, typically between +18.0 and +18.5 ‰. Red Basin *Dromomeryx* sp. data imply $\Delta^{13}C$ ~+19.3 ‰, but this single species has anomalous $\delta^{18}O$ values, and we do not interpret its $\delta^{13}C$ values in terms of MAP. John Day and Mascall Formation specimens have comparable $\delta^{18}O$ values of +21.8±1.0 ‰ and +21.4±0.8 ‰ respectively (VSMOW; Fig 3; Table 1). Excluding John Day and Mascall Formations, younger stratigraphic units generally have lower $\delta^{18}O$ values (+17.7 ‰ to +20.6 ‰), with the exception of *Dromomeryx* sp. specimens from Red Basin (+27.4±0.2 ‰).

Because of secular changes to atmospheric $\delta^{13}C$, and because of large systematic calibration errors associated with MAP estimates using Eq. 1, t-tests were applied to $\Delta^{13}C$

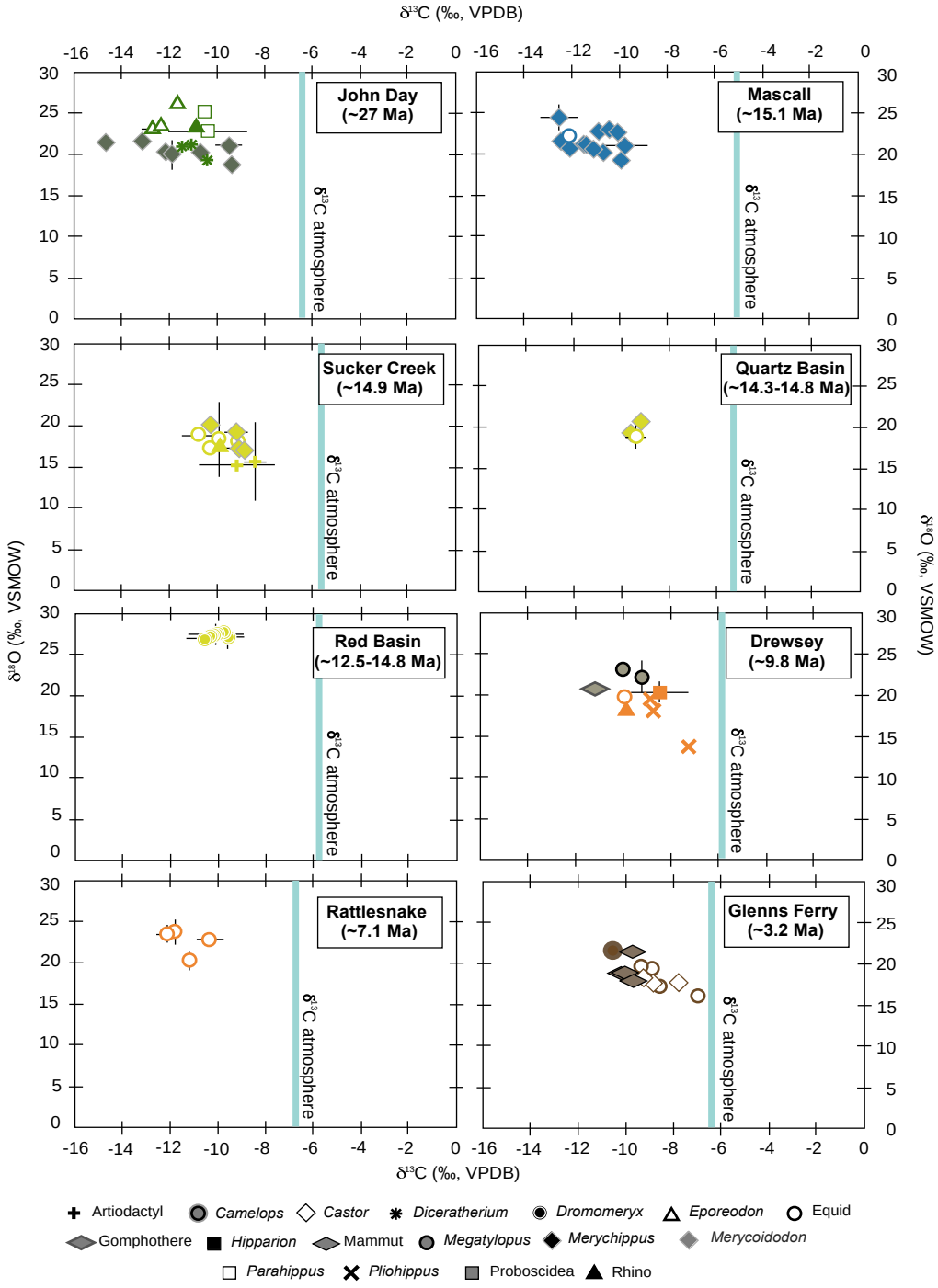

Figure 3. $\delta^{18}O$ values (VSMOW) vs. $\delta^{13}C$ values (VPDB) of herbivore tooth enamel. Different colors represent different localities. The blue bars on each graph indicate the $\delta^{13}C$ of atmospheric CO_2 for each time period (Tipple et al., 2010; Drury et al., 2016). $\delta^{13}C$ values for the Mascall, John Day, and Rattlesnake Formations are lower relative to the $\delta^{13}C$ of atmospheric CO_2 than other formations. $\delta^{18}O$ values for the John Day and Mascall Formations are higher than younger formations, excepting Dromomeryx data from Red Basin.

values to evaluate whether significant differences occur among the middle Mascall, John Day, Rattlesnake and other localities. A significant difference would imply that MAP was indeed different, even if formal propagation of all errors, especially systematic calibration errors, shows overlap. $\Delta^{13}C$ values for the lower and middle Mascall Formation ($\Delta^{13}C$ = +20.4 ‰) and John Day Formation (+19.9 ‰) are not significantly different, implying that differences in MAP are not significant (Table 2). However, because the $\Delta^{13}C$ values for the Mascall and John Day Formations far exceed those of any other site (Table 3), MAP must have been significantly higher (Fig 4).

MAP Estimates

Calculated $\delta^{13}C$ values for plant material consumed by herbivores and $\Delta^{13}C$ values relative to atmospheric $\delta^{13}C$ imply that MAP was highest during deposition of the lower John Day and Mascall Formations (c. 550 to 850 mm/yr) and lowest during deposition of all other units (c. 150-400 mm/yr), including the upper John Day Formation, but excluding anomalous *Dromomeryx* sp. data from Red Basin (Fig 4). The highest MAP estimates derive from our data from the middle Mascall Formation and are precisely dated at 15.1 Ma. Other data from the lower and middle Mascall Formation (Maguire, 2015) imply moderate MAP (550-600 mm/yr), and arguably MAP at 15.1 Ma represents a spike. In general, periods with the highest and lowest pCO_2 show the highest and lowest MAP.

Table 3. t-test for $\Delta^{13}C$ values (‰) for all localities compared to Mascall specimens.

Formations	*p* values when compared to Mascall Formation
John Day	3.60E−03
Quartz Basin	9.30E−018
Sucker Creek	1.50E−17
Red Basin	6.50E−10
Drewsey	1.50E−17
Rattlesnake	3.20E−05
Glenns Ferry	8.90E−13
Birch Creek	8.50E−05
Tyson Ranch	2.20E−17

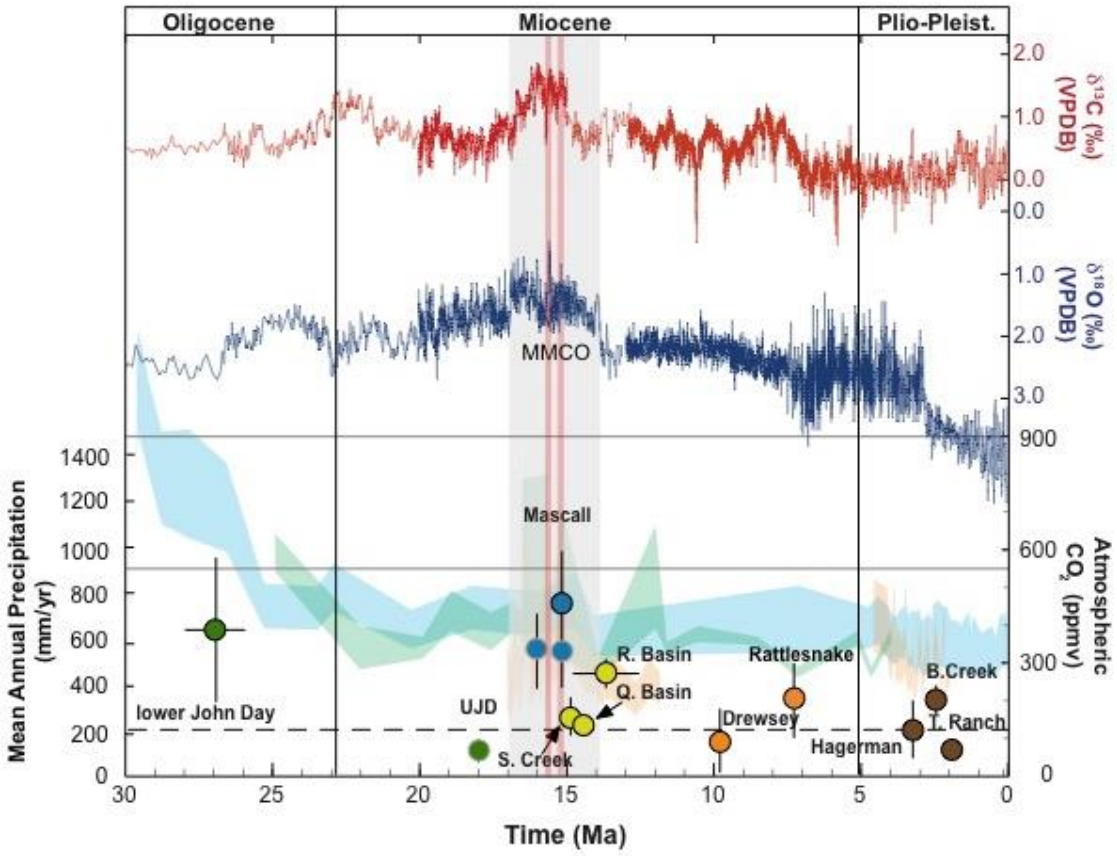

Figure 4. Changes in MAP (symbols) and atmospheric CO_2 levels vs. time. Grey-outline data are basin on published $\delta^{13}C$ values for perissodactyls (Maguire, 2015). MAP inferred from Maguire (2015) is c. 200 mm/yr lower than estimates from this data. However, MAP estimates are much higher than modern day precipitation rates in the Pacific Northwest. $\delta^{13}C$ and $\delta^{18}O$ values for benthic foraminifera are also displayed (Zachos et al., 2001; Holbourn et al., 2013; Drury et al., 2016). Red bars show a major warming event at 15.6 Ma (Holbourn et al., 2015) and an inferred warm/wet cycle from this data at 15.1 Ma. Data show a distinct spike in MAP at c. 15.1 Ma that corresponds precisely with a brief warming event associated with increased pCO_2. The dashed line represent the atmospheric CO_2 concentration threshold needed for plant photosynthesis (Dippery et al., 1995; Campbell et al., 2005).

Discussion

Stable Carbon Isotopes, MAP and pCO_2

Several climate and ecological drivers might influence $\delta^{13}C$ and $\delta^{18}O$ values of herbivore tooth enamel, and each must be considered in interpreting our data. A global increase in C_4 biomass occurred between 8 and 6 Ma, which could in principle affect interpretation of $\delta^{13}C$ data (Cerling et al., 1994; Cerling and Harris, 1999). However, the worldwide expansion of C_4 plants postdates most localities analyzed in this study, with the exception of the Hagerman, Tyson Ranch, and Birch Creek localities. Modern southern and southwestern Idaho contains no native C_4 grasses, and $\delta^{13}C$ values from localities <4 Ma are similar to those of Sucker Creek, Quartz Basin, Red Basin, and Drewsey. Thus, we do not think C_4 consumption biases any of our data, including at Hagerman, Tyson Ranch, and Birch Creek.

Tectonic uplift of the Cascade Range upwind of our sample localities is not likely to have caused a decrease in MAP and a corresponding increase in plant $\delta^{13}C$ for specimens from the John Day through Rattlesnake Formations. Although volcanism has been active in the Cascades since the Eocene, the modern high Cascades are relatively recent, and increases in upwind elevation are thought to have commenced no earlier than ca. 7 Ma (Kohn et al., 2002; Kohn and Fremd, 2007). Thus, excepting the Hagerman, Tyson Ranch, and Birch Creek localities, all our other data should reflect global influences rather than regional tectonic influences.

Several studies attribute warmer temperatures and higher precipitation rates in the middle Miocene to high pCO_2 (Royer et al., 2001; Kürschner et al., 2008; Retallack, 2009). A link between pCO_2 and MAP does explain our data most simply – some of our

highest MAP values correspond with the middle Oligocene John Day and the MMCO Mascall intervals, when pCO_2 values were plausibly highest. During times when pCO_2 was lowest, MAP was markedly lower.

A pCO_2-MAP link makes sense from an oceanographic perspective. Mid-Miocene marine records (Fig 1) show distinct correspondence between perturbations to the C-cycle (as manifested in $\delta^{13}C$ values) and warming and cooling events (as manifested in $\delta^{18}O$ values; Holbourn et al., 2007). For example, a large warming event at 15.6 Ma shows an abrupt shift in benthic foraminiferal $\delta^{13}C$ and $\delta^{18}O$ values, corresponding with deep-water warming of ~5ºC (Holbourn et al., 2013; 2014; 2015). Boron isotopes indicate an increase in pCO_2 at the same time (Greenop et al., 2014). These $\delta^{18}O$, $\delta^{13}C$ and $\delta^{11}B$ records further reveal a strong 100 ka eccentricity signal between 14.7 and 17 Ma, suggesting insolation helped catalyze evenly spaced simultaneous warming and increased pCO_2 (Holbourn et al., 2013; 2014; 2015; Greenop et al., 2014). Increased temperature and pCO_2 at 15.1 Ma conforms with the 100 kyr pattern, and plausibly warmer and wetter conditions in central Oregon can be explained by warmer ocean water temperatures along the Pacific coast in the context of higher pCO_2. Although sea surface temperatures are not well quantified at this latitude during these events, essentially all general circulation models predict that higher pCO_2 during the mid-Miocene causes an increase in temperature and precipitation in the Pacific Northwest (e.g. Krapp and Jungclaus, 2011; Hamon et al., 2012; Goldner et al., 2014; Henrot et al., 2017). Previous work on Mascall Formation paleosols has also proposed cycles of warmer-wetter vs. cooler-drier climates with a 100-kyr periodicity (Bestland et al., 2008). The levels

immediately above the Mascall tuff bed, which are an important source for the specimens analyzed, were interpreted to reflect warmer-wetter conditions (Bestland et al., 2008).

A possible problem with the pCO_2-MAP interpretation is that several intervals from the MMCO, especially Sucker Creek and Quartz Basin show low MAP. Part of the discrepancy may simply reflect poor age constraints for many intervals. With uncertainties of several hundreds of thousands of years, the upper John Day, lower Mascall, Quartz Basin, and Red Basin intervals cannot be pinned accurately to the marine record. In the case of Red Basin, it is even unknown whether the interval corresponds with the late MMCO or post-MMCO cooling. And, while the lowermost Mascall horizons are bracketed precisely between 16.26±0.02 and 16.44±0.05 Ma (McLaughlin et al., 2016), that age range encompasses two warm and three cool events in the marine record (Holbourn et al., 2015). An apparent exception to our hypothesis is the Sucker Creek locality, which ostensibly falls on a warming spike at ~14.95 Ma (Fig 1), but has relatively low calculated MAP of c. 250 mm/yr. Such low MAP is consistent with previous work on floral assemblages, which also suggest cool-dry conditions (e.g. Taggart and Cross, 1980). Besides the fact that the ±100 kyr precision of the age of this interval could allow the Sucker Creek data to fall instead on a cool interval, we note that $^{40}Ar/^{39}Ar$ ages may be subject to significant systematic errors. For example, the original published $^{40}Ar/^{39}Ar$ age for the Mascall tuff was precise (15.98±0.04 Ma; Swisher, 1992); corrected for recalibration of the Fish Canyon sanidine standard: Kuiper et al., 2008), but new U-Pb zircon data place the age about 800 ka later. In general, U-Pb ages are viewed as more accurate than $^{40}Ar/^{39}Ar$ ages. Both ages (~16.0 and ~15.1) happen to correlate with warming spikes, but clearly if accuracy is poorer than 100 ka for $^{40}Ar/^{39}Ar$ ages,

such correspondence cannot be assured. Until the Sucker Creek strata are re-dated using more accurate methods, we do not feel confident in ascribing our isotope data from that locality to either a warming or cooling interval.

Regardless of absolute age uncertainties, a link between oscillations in pCO_2-MAP is illustrated in the pollen record at Sucker Creek. Frequencies of broad-leaved dicots and montane conifers were analyzed in the Whiskey Creek section of the Sucker Creek Formation (Taggart and Cross, 1980; Cross and Taggart, 1982). Cyclical successions between the two tree-types show 4 distinct frequency peaks for both montane conifers and broad-leaved dicots (Cross and Taggart, 1982). Cross and Taggart (1982) suggested that vegetation oscillations might reflect increases in pCO_2 resulting from Milankovitch cycles, but without firm chronologic control. Cross and Taggart (1982) later suggested that fires resulting from volcanic activity may have driven cyclical changes in vegetation. Using the precise (but not necessarily accurate) ages of Fields (1996), estimated sedimentation rates for the Sucker Creek Formation vary from ~250 to ~500 m Myr^{-1} (Cross and Taggart, 1982; Fields, 1996). The Whiskey Creek section is approximately 100 m thick, so the cycles illustrated in the pollen record would occur either every ~40 kyr or 100 kyr. Consequently, the initial interpretation of Cross and Taggart (1982) that floral assemblages responded to Milankovitch cyclicity may have been valid, and may well have been driven by changes in precipitation.

Climate cycles may also be captured in specimens from the late Oligocene and Miocene. Scatter in data from ~27 Ma exceeds scatter at other time periods and suggests both high and low MAP. In contrast, continuous paleosol records from the John Day Formation (~28 to ~19 Ma) show a rhythmic pattern in paleosol physical character, depth

to calcic horizon, inferred MAP (~600 to ~400 mm/yr), and C- and O-isotopes (Retallack, 2004; Retallack et al., 2004). Although our data taken alone are not definitive, taken together with paleosols these observations suggest precipitation cyclicity (Retallack, 2004; Retallack et al., 2004). These characteristics in turn may reflect cyclical variations in pCO_2, much as has been proposed for the mid-Miocene (Holbourn et al., 2013; Greenop et al., 2014; Kochhann et al., 2016). In this instance, our poorly time-constrained specimens may again prove problematic when attempting to correlate MAP with cyclical events. However, this problem may be circumvented in future studies by ensuring that specimens are collected in the context of paleosol character, so that C-isotopes can be linked to warm-wet vs. cool-dry conditions, even if the absolute age is not known accurately.

Stable Oxygen Isotopes

Oxygen isotope values from herbivore teeth have been used to infer uplift of the Cascade Range commencing c. 7 Ma (Kohn et al., 2002; Kohn and Fremd, 2007). Within that context, high $\delta^{18}O$ values measured from John Day and Mascall Formation specimens in this study likely result both from a topographically low volcanic arc to the west and from their proximity to the Pacific coast relative to other localities. Teeth from Sucker Creek, Quartz Basin, and Drewsey were collected from further east than the John Day and Mascall localities, and have consistently lower $\delta^{18}O$ values. As air masses move inland from oceanic reservoirs (e.g., the Pacific Ocean), ^{18}O is preferentially removed, decreasing precipitation $\delta^{18}O$ values. Of Miocene localities, Sucker Creek is the furthest from the Pacific Ocean, and has the lowest $\delta^{18}O$ values, suggesting that geography may have contributed to different $\delta^{18}O$ values among sites. Low $\delta^{18}O$ values for Hagerman

teeth likely reflect the combined effects of topographic rise of the Cascade Range and greatest distance from Pacific Ocean moisture sources.

Red Basin $\delta^{18}O$ values are much higher than any other locality, which may result from the measurement of only *Dromomeryx* teeth. *Dromomeryx* may have been water independent, causing higher $\delta^{18}O$ values than expected for water dependent ungulates such as equids. Alternatively, high aridity at Red Basin might have caused evaporative enrichment of water ^{18}O, generating higher $\delta^{18}O$ values during whatever specific time is represented.

Comparisons to Other MMCO Paleoclimate Studies

Globally, evidence for high MMCO temperatures and precipitation is well-established through studies of paleosols and paleoflora. We restrict comparisons to mid-latitudinal studies because specimens from our study were collected at paleolatitudes ranging from 42°-44°. For reference, modern conditions in central Oregon are roughly MAP = 250-300 mm/yr, and mean annual temperature (MAT) = 9-10°C. Leaf morphology of plant fossils found in the Mascall Formation indicate growing season precipitation of ~620 mm/yr (Yang et al., 2011), or twice the entire yearly precipitation for central and eastern Oregon today. Formation of alfisols in the middle member of the Mascall Formation also indicates high MAP of ca. 1000 mm/yr and MAT of ca. 11 °C (Bestland and Krull, 1997; Sheldon et al., 2002; Bestland et al., 2008). Carbonate-free paleosols from the Columbia River Basalts, ca. 16 Ma (Barry et al., 2010), imply MAP > 500 mm/yr (Sheldon, 2003). On a more global basis, European fossil floras indicative of warm and wet environments expanded to higher latitudes during the MMCO (Mosbrugger et al., 2005b; Bruch et al., 2011). Lateritic weathering of rocks generally

occurs in equatorial regions, but 17-15 Ma laterites and bauxites are found at a paleolatitude of 45° in Germany and are attributed to higher atmospheric CO_2 levels and increased precipitation (Schwarz, 1997). Herpetological assemblages and floral observations in western Europe suggest higher MAP and MAT at 14-16 Ma than before or after (Mosbrugger et al., 2005a; Bohme et al., 2011; Bruch et al., 2011; Pound et al., 2012). As with many of our sites, age resolution is generally too coarse to allow proxy records to be correlated precisely to the marine record. Thus, although the MMCO represents a generally warmer and wetter interval, these other datasets do not allow us to evaluate how terrestrial climates might have responded to 100 ka climate cycles.

Implications for Stratigraphic and Paleontological Successions

The climate cyclicity evident in marine records should be reflected in sedimentary sequences. For example, Retallack et al. (2004) argued that paleosols in Oligocene sediments of the John Day Formation, central Oregon, developed cyclically in response to obliquity (ca. 41 ka) cycles, likely abetted by changes to greenhouse gas levels. Considering the clear evidence from mid-Miocene marine records for 100- kyr climate cycles, one might expect 100-kyr cycles in floras and sediment transport, which should drive cyclic changes in the record of paleosols and fossil floras. Fossil floras and paleosols are rarely so well dated or so continuous over a long temporal interval to test this hypothesis directly. However, the Mascall and Sucker Creek Formations do span a significant period of the middle Miocene, and contain numerous dateable ash beds. Both also reportedly contain cycles of coarse-grained sediment (Bestland et al., 2008) and floral successions (Taggart and Cross, 1980). These strata represent excellent sections in

the Pacific Northwest to test our cyclic climate change model hypothesis for the MMCO. Finding the 15.6 Ma warm spike would be an obvious target for future research.

Although marked changes in the physical morphology of faunas is evident through the middle Miocene (e.g. Webb, 1977; Damuth and Janis, 2011), it seems unlikely that these records would encode climate cycles. Certainly, if MAP changed cyclically, so too should $\delta^{13}C$ values of plants and teeth, and we believe this is responsible for the unusual isotope compositions of middle Mascall faunas. But besides the fact that faunas are rarely found continuously through a section, physical attributes of faunas such as cursoriality and hypsodonty are not expected to be so plastic as to oscillate with changing ecological conditions. Rather, a Ratchet effect (West-Eberhard, 2003; Kohn et al., 2015) might be expected, in which oscillations to cool-dry conditions generate open, dustier habitats that drive ever increasing cursoriality and hypsodonty. As long as these characteristics do not confer an evolutionary disadvantage during oscillations to warm-wet conditions, cursoriality and hypsodonty should increase through time, although with periods of stasis during warm-wet periods. This model explains the increases in hypsodonty observed during the MMCO for the merychippine and equine horse lineages of North America (e.g. Damuth and Janis, 2011) despite evidence for warm and wet conditions. While numerous warm-wet (high pCO_2) periods during the MMCO could well have stalled increases in hypsodonty, intervening cool-dry (low pCO_2) periods could have steadily promoted increases in hypsodonty. The resulting record would show increasing hypsodonty (as observed), not hypsodonty oscillations.

Implications for Future Climate Change

If pCO_2 was a catalyst for increased MAP in the Pacific Northwest, our data may help inform future climate predictions. By the year 2100, global atmospheric CO_2 is predicted to be 550-900 ppmv (Meehl et al., 2005; Meehl et al., 2007; Jones et al., 2013). Insofar as several pCO_2 proxies suggest levels of 600-850 ppmv during the MMCO, this time in Earth's history may provide a useful analogue for evaluating future high pCO_2 climates. Most GCM's suggest that rising atmospheric CO_2 to 800 ppmv over the next century will increase temperature and precipitation in the Pacific Northwest by c. 2 °C and 5 % respectively (Mote and Salathe, 2010). Studies from the mid-Miocene suggest that increasing pCO_2 levels indeed corresponded with higher precipitation and temperature (e.g. Schwarz, 1997; Retallack, 2010; Yang et al., 2011). However, although MAT estimates for the MMCO are within ~2°C of modern MAT, MMCO MAP estimates are typically 2-3 times either modern levels or low-MAP intervals of the Miocene. Overall most GCM's do not reproduce precipitation records for the interior Northwest well during the MMCO, even when high pCO_2 is assumed (e.g. Henrot et al., 2010; Herold et al., 2011; although see Krapp and Jungclaus, 2011). Thus, model refinements may be necessary to match past MMCO precipitation and predict future precipitation better for western North America.

Conclusion

Herbivore tooth enamel $\delta^{13}C$ and $\delta^{18}O$ values spanning the late Oligocene through the Pliocene provide insights into past environments and climates of the Pacific Northwest. Isotopic fractionation as a result of air masses migrating inland and topographic rise of the Cascade Range was recorded in high $\delta^{18}O$ values in John Day and Mascall teeth, and lower $\delta^{18}O$ values recorded in younger tooth enamel. At ~15.1 Ma a

dramatic spike in MAP occurred during the MMCO (supporting some previous work), with precipitation rates immediately decreasing and remaining low to the present. Some of our data from the MMCO suggest comparable MAP as today. A climate oscillation model best explains data, such that warm-wet conditions during high pCO_2 events alternated with cool-dry conditions during low pCO_2 events on timescales of 100-kyr. Because of poor age constraints for many of the specimens, we are able to speculate only that high pCO_2 contributed to higher MAP for Mascall Formation strata at 15.1 Ma, and lower pCO_2 contributed to lower MAP for other localities. Terrestrial climates during the MMCO were likely more dynamic than typically considered, with wet-warm and cool-dry cycles reflecting Milankovitch cycles. Climate models predict that as global atmospheric CO_2 levels continue to increase, the Pacific Northwest will become wetter and warmer. Data collected in this study are from time periods geologically close to our own, and may aid in better understanding how we will transition into the greenhouse climate of the next century.

CHAPTER TWO: SEASONAL PRECIPITATION PATTERNS IN THE AMERICAN SOUTHWEST DURING THE LATE PLEISTOCENE INFERRED FROM STABLE ISOTOPES IN TOOTH ENAMEL AND TUFA

Introduction

At times, during the late Pleistocene, the American Southwest was much wetter than modern-day conditions (e.g. Eardley and Gvosdetsky, 1960; Galloway, 1970; Woodcock, 1986; Quade et al., 1998; Betancourt et al., 2001; Oviatt et al., 2003; Springer et al., 2015; 2017). The largest and most well-known examples of increased net precipitation are the massive late Pleistocene lakes, such as Lake Bonneville, which dwarfed its modern vestige, the Great Salt Lake (Gilbert, 1890). Increased precipitation and lower evaporation rates and temperatures in the American Southwest have been inferred from diverse climate proxies such as lake levels and sediment cores (Allen and Anderson, 1993; Benson et al., 1990; Menking et al., 2004), speleothems (Asmerom et al., 2010; Wagner et al., 2010), packrat middens (Swetnam et al., 1999; Betancourt et al., 2000; Holmgren et al., 2009), and groundwater discharge (GWD) deposits (Quade et al., 1998; Pigati et al., 2009; Springer et al., 2015; 2017).

Strata at Tule Springs Fossil Beds National Monument, located in the upper Las Vegas Wash (LVW), Nevada, are extraordinarily well-dated and contain well preserved GWD deposits (Springer et al., 2015, 2017), fossils, and tufas (low temperature calcium carbonate precipitate). Thus, these deposits provide an exceptional setting for

understanding paleoclimate in the southwest United States through the late Pleistocene. GWD deposits form in arid regions and result from increases in net precipitation (total precipitation minus evapotranspiration), which is discharged along valley edges and floors as springs. Resulting deposits preserve the timing and magnitude of past changes in hydrologic and climate fluctuations. The paleohydrologic record of the upper LVW shows that Pleistocene wetlands were sensitive to past episodes of rapid climate change (Pigati et al., 2009; 2014; Springer et al., 2015; 2017). The records of expansion and contraction of the LVW paleowetlands are well preserved for the last c. 100 ka, and especially well for the last c. 35 ka (Fig 5), when abrupt climate oscillations are evident in ice core and marine records (Alley et al., 1993; Bond et al., 1993). Paleowetland deposits in the upper LVW are of particular interest because they generally correlate with Greenland ice core and North Atlantic climate proxy data (Fig 5; Springer et al., 2015; 2017). Generally, during cool intervals or Heinrich cycles, LVW paleowetlands increased due to increased GWD resulting from increased net precipitation. In contrast, during warm Dansgaard-Oeschger (D-O) events, paleowetland ecosystems almost completely collapsed because of reduced regional discharge (Pigati et al., 2009; 2014; Springer et al., 2015; 2017).

Although the overall mechanics for the formation of GWD deposits are well understood, we do not know the seasonality of the precipitation during the late Pleistocene, which created for an expansion in paleowetlands. Many general circulation models (GCM's) attribute the wetter conditions of the late Pleistocene Southwest deserts to a southward shift of the westerlies (SOW model), which increased seasonal proportions of winter precipitation sourced from the eastern Pacific (e.g. COHMAP

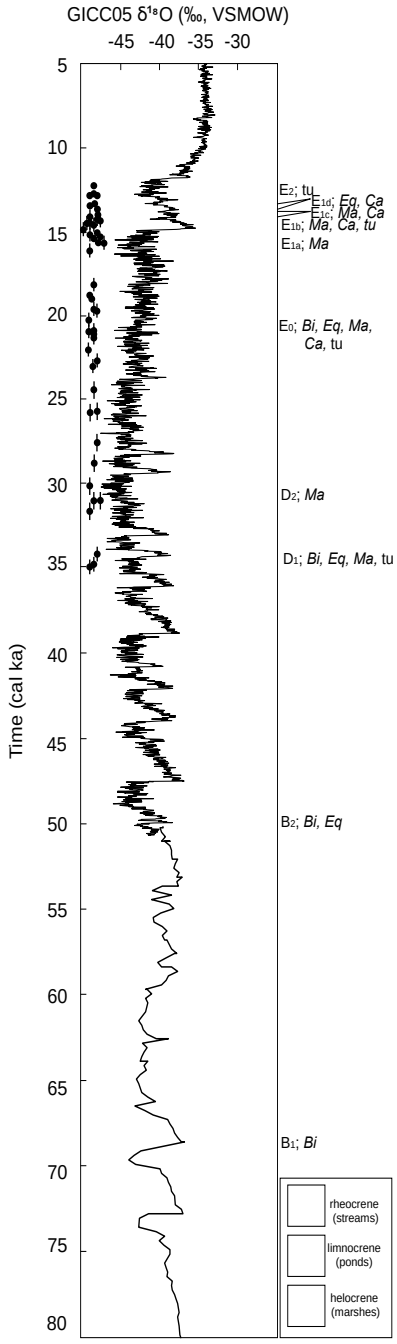

Figure 5. Chronologic record of GWD deposits in the upper LVW (Springer et al. 2015, 2017) compared to Greenland ice core records using CICC05 chronology from 0 to 40 ka (Svensson et al., 2008) and GISP2 chronology from 40 to 80 ka (Grootes and Stuiver, 1997). Filled circles are where calibrated radiocarbon ages were measured, and correspond with GWD deposits. Deposits > 35 ka were dated using OSL dating. Wetland discharge is noted in graduated shades of green. Bi (Bison), Eq (Equus), Ma (Mammuthus), Ca (Camelops), and tu (tufa) specimens and samples were collected.

members, 1988; Toggweiler et al., 2006; Fig. 6). These models predict Cordilleran-Laurentide ice sheets spilt the jet stream into a weak northward (sub)stream and a much stronger southward (sub)stream. The southern jet stream would deliver winter (but not summer) storms inland more efficiently to the Great Basin and American Southwest, aiding in the expansions of late Pleistocene lakes and wetlands (Fig 6). In contrast, Lyle et al. (2012) proposed that increases in late Pleistocene precipitation in the American Southwest resulted from enhanced summer (but not winter) precipitation sourced out of the tropics of the Pacific Ocean or Gulf of Mexico (OOT model; Fig 6).

Past climates are not direct analogs for future climate change, but understanding previous climatic responses, such as changes to seasonal precipitation, can help better inform policy on modern ecosystems and water management. While previous studies of GWD deposits in the desert Southwest have attributed late Pleistocene paleowetland expansion to an increase in net precipitation (Pigati et al., 2011), they do not definitively address the two main SOW vs. OOT hypothesis.

In this study, we collected stable isotope compositions of carbon ($\delta^{13}C$ values) and oxygen ($\delta^{18}O$ values) from fossil herbivore tooth enamel, and $\delta^{18}O$ values from fossil and modern tufa to illuminate the source of increased precipitation, which triggered paleowetland expansion in the upper LVW during the late Pleistocene. Specifically, the consideration of the implications of how either winter or summer precipitation would vary types of vegetation and their $\delta^{13}C$ values and associated water $\delta^{18}O$ values. Data are interpreted to indicate that enhanced winter precipitation increased GWD and stabilized paleowetlands in southern Nevada during the late Pleistocene. These precipitation

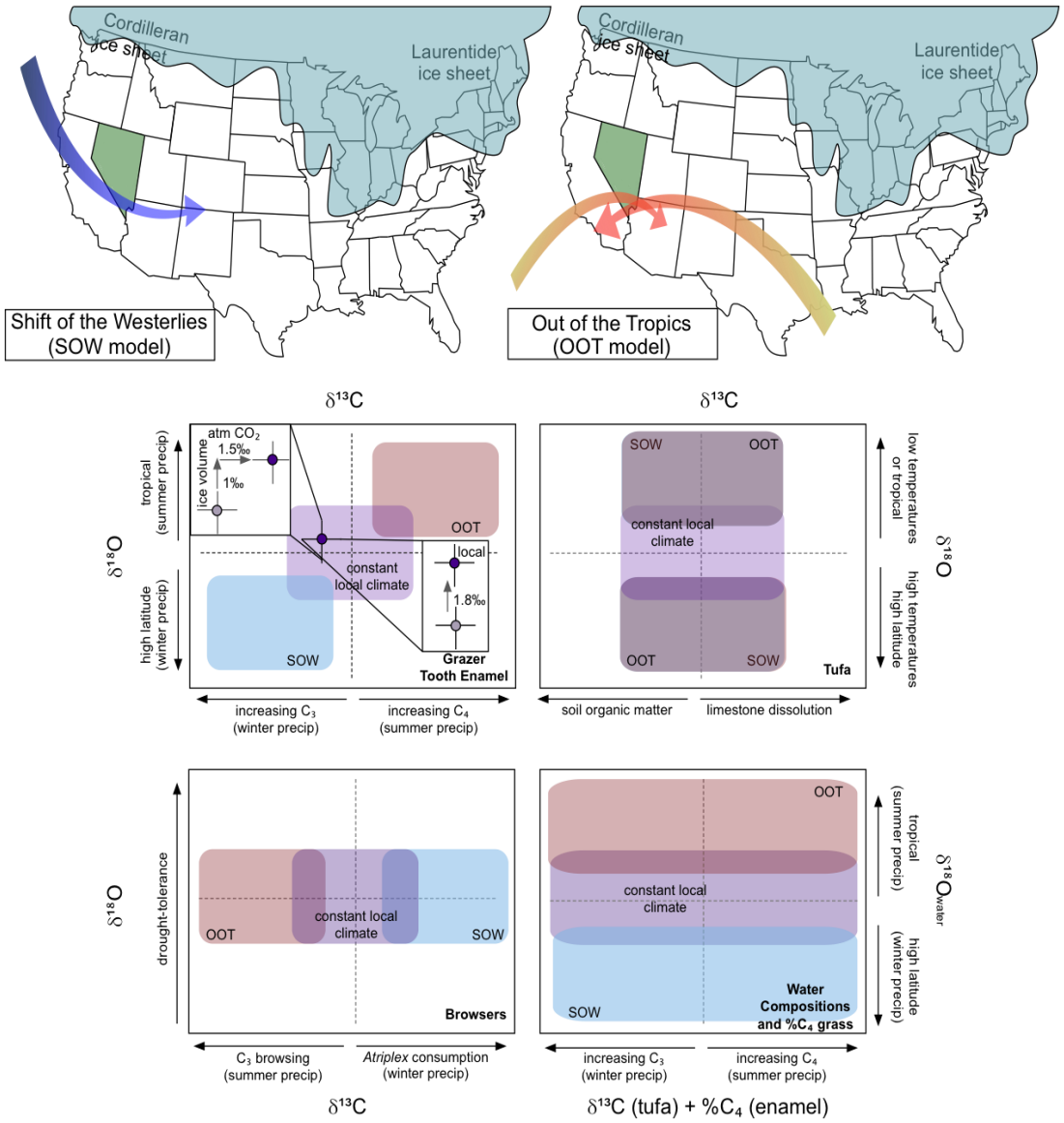

Figure 6. Contrasting seasonality model for southwest US precipitation during the late Pleistocene. Nevada is green and the Laurentide and Cordilleran ice sheet are blue. The Shift of the Westerlies model (SOW; left) transports winter precipitation from the northern Pacific Ocean to the American Southwest (blue arrow). The Out-of-the-Tropics model (OOT; right) transports summer precipitation from the southern Pacific or Gulf of Mexico to the LVW (red arrows). Purple regions indicate modern constant local climate conditions. Lower grazer tooth enamel $\delta^{18}O$ and $\delta^{13}C$ values are indicate of a SOW, while higher values suggest the OOT model. High browser tooth enamel $\delta^{13}C$ values suggest increased winter precipitation. High or low tufa $\delta^{18}O$ values could either indicate enhanced winter or summer precipitation. An increase in $\%C_4$ grass abundance would result from increased summer precipitation, while lower predicted water $\delta^{18}O$ values indicate enhanced winter precipitation.

patterns deviate from modern-day conditions in southern Nevada, which receives almost equal proportion of winter and summer precipitation ("WRCC," 2018).

Upper Las Vegas Wash Deposits

The upper LVW GWD deposits are assigned to distinct temporal units that correlate with widespread deposits throughout the southern Great Basin and American Southwest (Haynes et al., 1967; Quade, 1986; Quade and Pratt, 1989). Primary divisions are denoted A-E, with some strata further subdivided (e.g. E_1, E_2, etc; Haynes et al., 1967; see Fig 5 for some of these units, but not units A). Correlation of strata and sequences with GWD depositional environments is based on Springer and Stevens (2008). The oldest fossil-bearing units, B_1 (c. 100 to c. 55 ka) and B_2 (c. 55 to c. 45 ka) in the upper LVW, reflect spring-fed ponds (limnocrene discharge; Fig 5; all ages from Springer et al., 2015, 2017; Tables 4-7). Units D_1 (36.07 - 34.18 ka) and D_2 (31.68 - 24.45 ka), reflect the wettest conditions and were formed from expansive marshes and black mats (helocrene discharge; Fig 5). The youngest units E_0 (23.04 - 18.16 ka), E_1 (14.59 - 13.37 ka), and E_2 (12.35 - 10.63 ka) reflect tufa-bearing streams (rheocrene discharge; Fig 5).

Stable Isotopes in Teeth and Tufa

Isotope Geochemistry of Tooth Enamel

Mineralogically, teeth consist of hydroxylapatite with major substitutions of CO_3 for PO_4 and OH groups. Enamel is commonly selected for stable isotope analysis because of its resistance to diagenetic alteration, thus preserving biogenic isotope compositions (Kohn and Cerling, 2002). The following discussion of tooth enamel isotope composition is derived from reviews of Koch (1998); 2007; MacFadden (2000); Kohn and Cerling

(2002); Kohn and Dettman (2007); Clementz (2012). Tooth enamel stable carbon and oxygen isotope compositions capture a timestamp of ecological and climatic conditions, and are commonly used for paleoclimatology, paleoecology, and paleoenvironmental reconstructions. Because teeth grow progressively, tooth enamel can also encode sub-annual isotopic variations that in turn reflect sub-annual variation in, among other things, climate and diet.

Oxygen isotopes in water-dependent herbivores strongly correlate with ambient water compositions, and are modulated by differences in physiology. Drought-tolerant herbivores show a much poorer correlation or even no correlation at all (Kohn and Cerling, 2002). Isotope compositions in an environment and in an animal vary on both inter-annual and longer timescales. Water $\delta^{18}O$ values reflect precipitation sources and regional climate, as well as changes in temperature and evaporation. In general, low $\delta^{18}O$ values reflect cooler-wetter conditions, whereas higher $\delta^{18}O$ values reflect warmer-drier conditions.

Carbon isotope compositions of herbivore tooth enamel depend on the isotope compositions of the plant material they consume (DeNiro and Epstein, 1978). Different plants use different photosynthetic pathways - primarily C_3 or C_4 - with relatively high $\delta^{13}C$ values for C_4 plants (between –13 and –11‰ for modern plants, VPDB) and low $\delta^{13}C$ values for C_3 plants (mostly between –31 and –26‰ for global C_3 biomass, but more typically –24 to –26‰ for dry ecosystems; see Kohn, 2010). C_4 plants are dominated by warm climate grasses and sedges that require high temperatures, significant warm-season precipitation, and high light levels (Kohn and Cerling, 2002). Consequently, high $\delta^{13}C$ values in C_4 plants are abundance in open environments that

experience warm and wet summers. C_3 plants are represented by trees, shrubs, herbs, and cool-climate grasses. Consequently, low $\delta^{13}C$ values found in C_3 grasses are abundant in environments with cool or dry summers (Kohn and Cerling, 2002). Of relevance to this study, the shrub saltbush (*Atriplex* sp.) figures as a nearly unique exception to these rules. Unlike other shrubs, many species of saltbush use C_4 photosynthesis and flourish in regions with alkaline soils and dry summers. However, the genus has high salt content (hence the common name) and is unpalatable for most herbivores, but is preferentially consumed by modern camels. Modern ecosystems in the desert Southwest contain trees, shrubs, and herbs as well as C_3 and C_4 grasses, and the proportion of C_3 vs. C_4 vegetation depends primarily on the amount of summer precipitation.

Tooth enamel is enriched in $\delta^{13}C$ compared to consumed vegetation by 14.0‰ (for hind-gut fermenters, e.g. equids/horses; Cerling and Harris, 1999) to 14.5‰ (for fore-gut fermenters, e.g. bovids/bison; Passey et al., 2005). Elephants have an intermediate digestive physiology and are expected to have an intermediate isotopic offset between diet and tooth enamel $\delta^{13}C$ values (i.e., 14.25‰; Kohn and McKay, 2010). Higher $\delta^{13}C$ values in the teeth of grazers (grass consumers) indicates a larger proportion of C_4 grasses in their diets, while lower $\delta^{13}C$ values indicate a greater consumption of C_3 grasses. Normally, browsers (consumers of herbs and woody plants) have low $\delta^{13}C$ values in all environments. However, camels exhibit a singular predilection for *Atriplex*, which can affect their $\delta^{13}C$ values differently from other browsers.

Isotope Geochemistry of Tufa

Tufa is a cold freshwater precipitation of calcium carbonate that provides another avenue for investigating water compositions and environmental conditions, both annually and seasonally (Chaftez, Henry et al., 1991; Ford and Pedley, 1996; Andrews et al., 1997; Ihlenfeld et al., 2003). Tufas are porous and consist of microgranular calcite, which encrusts filamentous microbes (Pazdur et al., 1988; Andrews et al., 1994; 1997). Microbial tufa generally forms laminations whose morphology is controlled by seasonal differences in biotic activity (Andrews and Brasier, 2005), with dense tufa generally forming during spring and early summer and porous tufa forming in late summer and autumn (Pentecost, 1988; Andrews et al., 1997; Kano and Fujii, 2000; Andrews and Brasier, 2005; Brasier et al., 2010). Consequently, summer- vs. winter-precipitated tufas may be distinguished texturally and analyzed preferentially.

Tufa $\delta^{18}O$ values are generally controlled by water composition and by stream temperature variations, usually driven by solar insolation. For a fixed water composition, summer-season tufas have lower $\delta^{18}O$ values by 1-2‰ than winter-seasoned tufas (Chaftez et al., 1991; Andrews et al., 1994; 1997; Matsuoka et al., 2001). This behavior follows the temperature-dependence of carbonate-water isotope fractionation (Kim and O 'Neil, 1997), whereby carbonate $\delta^{18}O$ values decrease with increasing temperature at constant water compositions. However, in arid climates, seasonal evaporation enriches waters in ^{18}O, such that summer tufa could have higher $\delta^{18}O$ values than winter tufa.

Tufa $\delta^{13}C$ values generally do not relate to regional climatic trends, but more-so environmental conditions. $\delta^{13}C$ values close to zero reflect limestone dissolution, while

lower tufa $\delta^{13}C$ values are suggestive of the presence of soil organic materials (Pedley, 1990).

Tooth Enamel and Tufa Geochemistry and Changes in Precipitation Seasonality

A greater proportion of winter precipitation (SOW model) would impart lower $\delta^{18}O$ values for water and herbivore tooth enamel, whereas a greater proportion of summer precipitation (OOT model) would impart higher values compared to modern-day conditions (Fig 6). For carbon isotopes, increased summer precipitation (OOT) would increase the proportion of C_4 grasses, and consequently increase $\delta^{13}C$ values captured within grazer tooth enamel (bison, mammoth, horse). In contrast, increased winter precipitation (SOW) would increase the abundance of C_3 grasses. If enhanced winter precipitation stabilized paleowetlands there would be a higher abundance of C_3 grasses, and thus a decrease in $\delta^{13}C$ values preserved within grazer tooth enamel (Fig 6). Increases in $\delta^{13}C$ values within *Camelops* likely results from the consumption of *Atriplex*, which would indicate diminished proportions of summer precipitation (SOW).

For tufas, a greater proportion of winter precipitation (lower water $\delta^{18}O$ values) would be offset by a larger fractionation at lower temperature (higher carbonate $\delta^{18}O$ values). Similarly, higher water $\delta^{18}O$ in the summer would be offset by a smaller fractionation. Recognizing these potential ambiguities in interpretation, we simply averaged laminae to make a bulk comparison between modern and fossil tufas (Lojen et al., 2008). Both source-dependent compositions and temperature-dependent fractionations govern $\delta^{18}O$ values in tufas, which complicate interpretations. Ignoring evaporative effects, lower $\delta^{18}O$ values in tufa could indicate a smaller fractionation between water and carbonate (OOT; temperature-dependent fractionation), decreased

$\delta^{18}O$ values in precipitation (SOW; source-dependent composition), or a combination of both (Fig 6).

All comparisons between modern and fossil isotope compositions require corrections for modern conditions relative to the late Pleistocene. For carbon isotopes, an upward correction of modern $\delta^{13}C$ values of c. 1.5‰ is needed to offset the effects of fossil fuel burning (Freyer and Belacy, 1983). For oxygen isotopes, an upward correction to modern $\delta^{18}O$ values of c. 1‰ is needed to offset the isotopic effect of ice volume (Edwards et al., 2014).

Methods

Specimens and Research Area

Strata from the upper LVW represent an extraordinary, quasi-continuous sequence of late Pleistocene paleowetland deposits whose precise age control allows for direct comparison to long-term climate records, such as the Greenland ice core. See Springer et al. (2015, 2017) for details on stratigraphy, sedimentology, age constraints, and temporal correlation of strata with global climate records. Of special relevance to this study, analyzed specimens all derive from well-characterized levels, with typical calibrated age uncertainties of ~1% (100-300 yrs) from strata <35 ka dated by ^{14}C dating. Strata that are ≥50 ka were dated using luminescence and have uncertainties of ≥10% (Springer et al., 2015).

Thirty-six fossil teeth were analyzed from the upper LVW, with most effort focused on the younger, more precisely dated levels E_0 to E_{1d} (22 teeth), but also emphasizing older levels, B_1, B_2, D_2, and D_1 (12 teeth). Specifically, we analyzed a single *Bison* tooth from B_1; 6 teeth of *Bison* and *Equus* from B_2; 2 teeth of *Mammuthus* from

D_1; 6 teeth of *Mammuthus columbi*, *Bison*, and *Equus* from D_2; 11 teeth of *Camelops*, *Mammuthus*, and *Bison* from unit E_0; 4 teeth of *Mammuthus* from E_{1a}; 4 teeth from *Mammuthus* and *Camelops* from E_{1b}; 1 *Equus* tooth from E_{1c}; and 2 teeth of *Equus* and *Camelops* from unit E_{1d} (Fig 5; Table 4). Because we desired to evaluate changes between summer vs. winter precipitation based on changes to C_4 grass abundances, we focused most analyses on grazers (*Mammuthus*, *Equus*, and *Bison*). These taxa are also obligate-drinkers - all members of the Bovinae, Equidae, and Elephantidae are water-dependent - potentially allowing us to assess changes in winter (low $\delta^{18}O$ values) vs. summer (high $\delta^{18}O$ values) precipitation. *Camelops*, a drought-tolerant browser, was also analyzed, but primarily to evaluate changes in abundance of the C_4 shrub, *Atriplex* (Vetter et al., 2007; Semprebon and Rivals, 2010). However, the water-dependence of *Camelops* is unclear. Modern camelids vary in their water-dependence. Larger camel and dromedary are very drought-tolerant, whereas the smaller vicuña is quite water-dependent. Some *Camelops* $\delta^{18}O$ values overlap with *Bison*, *Equus*, and *Mammuthus* compositions, suggesting substantial consumption of free- standing waters, but commonly, slightly higher *Camelops* tooth enamel $\delta^{18}O$ values suggest a greater drought-tolerance (see data from Connin et al., 1998; Higgins and MacFadden, 2009; Kohn and McKay, 2012; Perez-Crespo et al., 2012; Kita et al., 2014; Trayler et al., 2015; Bravo-Cuevas et al., 2017).

Table 4. Mean $\delta^{13}C$ and $\delta^{18}O$ values for all browsers and grazers. Identification number, unit, taxa, error, tooth, dating technique, and ages are also included. * are data from Crowley et al (2008) from Reno, NV. P = premolar, M = molar, I = incisor, Frag. = fragment.

ID Number	Unit	Taxa	mean $\delta^{13}C$ (‰, VPDB)	2 s.e.	mean $\delta^{18}O$ (‰, VSMOW)	Tooth	Dating Technique	Age (cal ka BP)	±
		*Equus**			24.7			0	
		*Equus**			23.3			0	
		*Equus**			24			0	
03KS9-23.1a	E_{1d}	*Camelops*	−8.60	0.27	31.79	I	^{14}C	13.69	0.143
03KS-23.1b	E_{1d}	*Equus*	−7.05	0.24	23.28	Frag.	^{14}C	13.69	0.143
03MRR 10-1.2	E_{1c}	*Equus*	−6.85	0.37	24.70	M/X	^{14}C	14.118	0.213
10CM3-18.1a	E_{1b}	*Mammuthus*	−11.99	0.96	16.71	M/X	^{14}C	14.59	0.5
10CM6-17.1	E_{1b}	*Camelops*	−9.47	1.27	22.99	M/X	^{14}C	14.5615	0.3755
10CM6-17.2	E_{1b}	*Camelops*	−1.46	0.53	23.56	M3	^{14}C	14.5615	0.3755
03MJS 10-1.2	E_{1b}	*Camelops*	−6.64	1.01	23.12	M/X	^{14}C	14.5615	0.3755
03GAM10-15.1.1	E_{1a}	*Mammuthus*	−7.30	0.30	19.77	M/X	^{14}C	16.0965	0.2065
03GAM10-15.1.2	E_{1a}	*Mammuthus*	−7.20	1.38	19.78	M/X	^{14}C	16.0965	0.2065
03GAM10-15.1.3	E_{1a}	*Mammuthus*	−8.52	0.95	20.47	M/X	^{14}C	16.0965	0.2065
03GAM10-15.1.4	E_{1a}	*Mammuthus*	−7.75	0.29	19.65	M/X	^{14}C	16.0965	0.2065

ID Number	Unit	Taxa	mean $\delta^{13}C$ (‰, VPDB)	2 s.e.	mean $\delta^{18}O$ (‰, VSMOW)	Tooth	Dating Technique	Age (cal ka BP)	±
L3160-207.1	E_0	*Equus*	−5.46	0.44	23.06	M/X	^{14}C	19.803	0.22
L3160-207.2	E_0	*Equus*	−5.60	0.56	22.21	M/X	^{14}C	19.803	0.22
L3088-390a	E_0	*Bison*	−7.87	0.78	20.71	M3	^{14}C	19.803	0.22
L3088-459	E_0	*Camelops*	−6.06	0.45	22.31	P4	^{14}C	19.803	0.22
L3160-953	E_0	*Camelops*	−10.41	0.53	25.67	M2	^{14}C	19.803	0.22
L3160-773.1	E_0	*Camelops*	−7.62	0.46	22.71	I1	^{14}C	19.803	0.22
L3160-773.2	E_0	*Camelops*	−7.20	0.06	20.88	I2	^{14}C	19.803	0.22
L3160-773.3	E_0	*Camelops*	−7.77	1.23	20.95	Incisor	^{14}C	19.803	0.22
L3088-391	E_0	*Camelops*	−6.79	0.28	23.04	M2	^{14}C	19.803	0.22
L3088-520	E_0	*Camelops*	−5.89	0.40	24.18	I/X	^{14}C	19.803	0.22
L3160-875	E_0	*Mammuthus*	−8.00		20.74	Frag.	^{14}C	21.04	0.5
L3160-39a	D_2	*Mammuthus*	−4.14	0.48	20.24	Frag	^{14}C	29.63	0.52
L3160-6	D_2	*Mammuthus*	−4.34	0.18	20.84	P1	^{14}C	29.63	0.52
L3160-654.1	D_1	*Equus*	−8.90	0.01	32.51	M/X	^{14}C	35.0435	0.5
L3160-654.2	D_1	*Equus*	−2.88	0.34	22.58	M/X	^{14}C	35.0435	0.4985
L3160-779	D_1	*Equus*	−5.96	0.41	22.59	M/X	^{14}C	35.0435	0.4985
L3160-917	D_1	*Bison*	−2.31	0.30	21.88	PX/MX	^{14}C	35.0435	0.4985
L3160-781	D_1	*Bison*	−2.77	0.47	20.93	Frag.	^{14}C	35.0435	0.4985

ID Number	Unit	Taxa	mean $\delta^{13}C$ (‰, VPDB)	2 s.e.	mean $\delta^{18}O$ (‰, VSMOW)	Tooth	Dating Technique	Age (cal ka BP)	±
L3160-647	D_1	*Mammuthus columbi*	−8.16	0.14	19.44	M3	^{14}C	35.0435	0.4985
L3160-748	B_2	*Equus*	−4.07	0.27	19.74	Frag.	OSL luminescence	47.5	2.5
L3160-751	B_2	*Bison*	−7.73	0.49	23.76	M2	OSL luminescence	47.5	2.5
L3160-946	B_2	*Bison*	−4.89	0.61	19.85	M/X	OSL luminescence	47.5	2.5
L3160-230.2	B_2	*Equus*	−4.73	0.18	20.73	M/X	OSL luminescence	47.5	2.5
L3160-230.4	B_2	*Bison*	−5.10	0.18	22.84	M/X	OSL luminescence	47.5	2.5
L3160-818.2	B_2	*Bison*	−3.82	0.34	21.29	M/X	OSL luminescence	47.5	2.5
04MRR1-28.1	B_1	*Bison*	−2.52	0.24	23.75	M/X	OSL luminescence	75	5

Fourteen tufa samples were analyzed, including, 2 modern tufas from the adjacent Cold Creek locality, Nevada, and 12 fossil tufas from units D_1, E_0, E_{1b}, and E_2 (Table 5).

Analytical Methods

Enamel slices were cut along the length of each tooth, with a typical length of 10-40 mm, and subsampled every 1-2mm, using a slow-speed microsaw. This approach retrieves sub-annual isotope variations (Kohn, 2004), while preserving tooth mineralization geometry (Trayler and Kohn, 2017). Enamel was purified and chemically cleaned following the procedures of Koch et al. (1997), which involved removing enamel from dentine, grinding enamel to a fine powder, and pre-treating samples with H_2O_2 and an acetic acid-Ca acetate buffer to remove organics and diagenetic carbonates. Seasonal laminations within tufas were average for each year of growth. Tufas were subsamples every ~0.5 cm (depending on yearly growth width) using Dremel^{TM} rotary tool and 0.5 mm drill bit. Samples were then pre-treated with H_2O_2 to remove any organic materials.

Powdered enamel (1.5-2.0 mg) and tufa (0.2 mg) were dissolved in supersaturated H_3PO_4 in a GasBench II, in-line with a Thermo Delta V Plus Mass Spectrometer, housed in the Stable Isotope Laboratory at Boise State University. Five to six NIST-120c ($\delta^{18}O$ = +28.5‰, VSMOW, $\delta^{13}C$ = –6.55‰, VPDB; Kohn et al., 2015) aliquots were prepared using the same cleaning techniques, pre-treatment methods, and were analyzed with each sample set. Eight to nine NBS-18 ($\delta^{13}C$ = –5.014‰ VPDB and $\delta^{18}O$ = –23.2‰ VPDB) and NBS-19 ($\delta^{13}C$ = +1.95‰ VPDB and $\delta^{18}O$ = –2.2‰ VPDB) calcite standards were also analyzed with each sample set to verify mass spectrometer operation and to calibrate the reference gas. Analytical reproducibility (2 s.e.) for oxygen isotopes was: NIST-120c

Table 5. Mean $\delta^{18}O$ and $\delta^{13}C$ values from tufa samples. Identification number, unit, error, dating technique, and ages are included. Modern tufa samples were collected just west of the upper LVW.

ID Number	Unit	mean $\delta^{18}O$ (‰, VSMOW)	2 s.e.	mean $\delta^{13}C$ (‰, VPBD)	2 s.e.	Dating Technique	Age (cal ka BP)	±
CC-004	Modern Cold Creek	20.66	0.16	−5.84	0.48		0	21.56
CC-005	Modern Cold Creek	21.12	0.29	−5.46	0.35		0	22.02
10CM8-25.1	E_2	18.36	0.10	−5.68	0.76	^{14}C	10.63	0.12
TS-E2−1	E_2	19.36	0.10	−4.99	0.91	^{14}C	12.35	0.23
10CM3-11.1	E_2	21.55	0.07	−0.84	0.65	^{14}C	12.35	0.23
10CM3-11.1b	E_2	20.62	0.09	−2.23	0.59	^{14}C	12.35	0.23
10CM4-22.1	E_{1b}	18.57	0.22	−5.22	1.20	^{14}C	15.35	0.22
10CM4-22.1b	E_{1b}	18.68	0.09	−5.73	0.28	^{14}C	15.35	0.22
10CM3-18.1a	E_{1b}	18.16	0.09	−4.81	0.33	^{14}C	16.10	0.21
09CM9-2.1c	E_0	17.50	0.03	−5.35	0.24	^{14}C	20.28	0.22
03CM11-13.1	E_0	18.66	0.15	−4.23	0.40	^{14}C	20.96	0.24
10CM7-20.1	E_0	23.06	0.17	−0.36	0.88	^{14}C	20.96	0.24
09KS2-12−1	D_1	18.26	0.20	−5.19	0.95	^{14}C	35.04	0.50

= ±0.86‰; NBS-18 = ±0.60‰; and NBS-19 = ±0.67‰. For carbon isotopes, reproducibility (2σ) was: NIST-120c = ±0.53‰; NBS-18 = ±0.48‰, and NBS-19 = ±0.49‰. All further tooth and tufa $\delta^{13}C$ and $\delta^{18}O$ values are reported to VPDB and VSMOW, respectively.

Inferred Water $\delta^{18}O$ Values

Stable oxygen isotope compositions of tooth enamel and tufa were converted to apparent $\delta^{18}O$ values of water ($\delta^{18}O_{water}$) to compare with modern water compositions and to evaluate any secular changes to water $\delta^{18}O$ values. For reference, recent interpolations of isotope compositions from late Glacial precipitation imply $\delta^{18}O$ values were ~2‰ lower for Las Vegas compared to modern $\delta^{18}O$ values (Jasechko, 2016). For tooth enamel, we restricted consideration to water-dependent genera (*Equus*, *Bison*, and *Mammuthus*), and did not attempt to calculate water compositions for *Camelops*, because we are unsure whether they were water-dependent or drought-tolerant.

While $\delta^{18}O_{water}$ values may be estimated in principle from global trends of equine and bovine tooth and bone $\delta^{18}O$ values vs local $\delta^{18}O_{water}$ values (Kohn and Dettman, 2007; Kohn and Fremd, 2007;Hoppe et al., 2004) showed that large errors attend such estimates for horses in the interior Western US. Ideally, we would base calculations on modern equine or bovine compositions from the LVW area where local $\delta^{18}O_{water}$ is known (mean and median are −12.9‰; Friedman et al., 1992; Friedman et al., 2002). From measured Pleistocene equine and bovine compositions, we would then use modern correlations to infer Pleistocene $\delta^{18}O_{water}$ values. However, we know of no measured $\delta^{18}O$ values for modern horses or cattle from the LVW region. Consequently, we instead base calculations on modern horse tooth enamel compositions from the Reno, Nevada area

(~24‰; Crowley et al., 2008), where the spring and well $\delta^{18}O_{water}$ value is also known (−14.7‰; Friedman et al., 2002). Because modern equines, bovines, and elephants have virtually indistinguishable $\delta^{18}O$ values, we regress all modern data together to form a composite calibration applicable to all three groups, but then shift the intercept to anchor the equation to the Reno area:

$$\delta^{18}O_{water}(‰, VSMOW) = 1.12 \cdot \delta^{18}O_{tooth\ enamel}(‰, VSMOW) - 39.9$$

(Eq. 4)

We caution that this calibration has no validity outside the interior Western US, and possibly not outside western Nevada. It should also be mentioned that previous work has found that reconstructed $\delta^{18}O_{water}$ values from modern *Equus* tooth enamel were 2-3‰ higher than predicted from corresponding mean precipitation $\delta^{18}O$ values (Hoppe et al., 2004). The more positive inferred $\delta^{18}O_{water}$ values likely result from modern *Equus* consuming evaporatively enriched waters. Although, increased GWD in the LVW is thought to have occurred during periods of increased precipitation and decreased evapotranspiration, herbivore tooth enamel may overestimate precipitation $\delta^{18}O$ values in interior basins such as in Nevada.

Water $\delta^{18}O$ values derived from tufa were determined by calculating the oxygen isotope fractionation factor for calcite-water using the following equation for calcite precipitation at Devil's Hole, Nevada (Coplen, 2007):

$$1000 \ln \alpha_{\text{tufa}-\text{water}} = 17.4\left(\frac{1000}{\text{T}}\right) - 28.6 \qquad \text{(Eq. 5)}$$

where $\boldsymbol{\alpha}_{\text{tufa-water}}$ is the oxygen fractionation factor for tufa (calcite)-water, and T is the temperature in Kelvins. In general, faster (disequilibrium) precipitation of calcite produces higher $\delta^{18}O$ values (Kim and O 'Neil, 1997). Calcite precipitation rates at

Devil's Hole range from <1 μm/a to 30 μm/a (Coplen, 2007). Because tufa precipitation rates in the LVW area are over an order of magnitude faster (100 to ~1000 μm/a), we anticipate that $\delta^{18}O$ values in calcite are higher than estimated from existing calibrations, and that $\delta^{18}O_{water}$ will be similarly overestimated using Eq. 5.

Modern tufas were collected at Cold Creek, which is ca. 60 km west-northwest of Las Vegas at an elevation of 6300 m. For tufa formation to occur, macrophytes, cyanobacteria, heterotrophic bacteria, and algae are required, and therefore, temperatures <20 °C are ideal for tufa precipitation (Pentecost, 2005). Previous work has measured a spring water temperature of 10 °C on March 31, 1987 (Thomas et al., 1991). Peak snowmelt discharge at Cold Creek occurs during spring months (Winograd et al., 1998; Winograd and Friedman, 1972), and therefore, we assume this measurement represents winter spring-water temperatures. Well logs from the Las Vegas area, taken during the summer months at elevations >5000 m and <7000 m, have an average temperature of 14±6 °C (2σ). Though summer spring water may be as high as 20 °C, it would be unlikely that summer temperatures would be lower than 10 °C. Assuming 10 °C represents winter temperatures and 14±6 °C represent summer temperatures, we assign a modern Cold Creek Spring averaged water temperature of 12±6 °C. Modern well water from Tule Springs taken during summer months is 21 °C (Friedman et al., 2002). However, tufas generally precipitate in waters <20 °C and general circulation models (GCM's) suggest that the late Pleistocene was much cooler than modern-day conditions Braconnot et al., 2007, 2012). We therefore, assign a late Pleistocene spring water temperature of 15±5 °C for LVW waters. For modern tufas we use an oxygen $\alpha_{\text{tufa-water}}$

value of 1.033±0.001 and for fossil tufas we use an oxygen $\alpha_{\text{tufa-water}}$ value of 1.032±0.001. Water $\delta^{18}O$ values are then derived using Eq. 6:

$$\delta^{18}O_{water} = \frac{(1000+\delta^{18}O_{tufa})}{\alpha_{tufa-water}} - 1000 \quad \text{(Eq. 6)}$$

where $\delta^{18}O_{tufa}$ and $\delta^{18}O_{water}$ are, respectively, the stable oxygen isotopic compositions of tufa and water in which tufa precipitates.

Estimated C_4 Grass Abundance

We estimated C_4 vegetation abundance using $\delta^{13}C$ values from tooth enamel, which were converted to vegetation $\delta^{13}C$ values using known isotopic offsets between diet and tooth enamel: 14‰ for *Equus* (Cerling and Harris, 1999) and 14.5‰ for *Bison* (Passey et al., 2005). Considering digestive physiologies, an offset of 14.5‰ was assumed for *Camelops* and 14.25‰ for *Mammuthus.* The proportions of C_4 vegetation in herbivore diets was then estimated using the following expression:

$$X_{C_4} = \frac{(\delta^{13}C_{diet}-\delta^{13}C_{C_3})}{(\delta^{13}C_{C_4}-\delta^{13}C_{C_3})} * 100 \quad \text{(Eq. 7)}$$

For comparison to Pleistocene carbon isotope compositions, we first assumed typical AD2000 $\delta^{13}C$ values of–25±1‰ for C_3 vegetation in dry ecosystems (Kohn, 2010) and –12±1‰ for C_4 vegetation (Cerling et al., 1997), then corrected modern compositions upward by 1.25‰ for 12-16 ka, and 1.5‰ for 17-75 ka. These corrections reflect a typical $\delta^{13}C$ value of –6.75‰ for late Pleistocene CO_2 recovered from ice cores (Lourantou et al., 2010) vs. a reference values of –8.0‰ at AD2000 (e.g. McCarroll and Loader, 2004). These assumptions yield Pleistocene mean $\delta^{13}C$ values of –23.75±1‰ for C_3 vegetation and –10.75±1‰ for C_4 vegetation.

Because grazers do not generally discriminate among the grasses they consume, Eq. 7 is applied to *Mammuthus*, *Equus*, and *Bison* and provides an estimate of the fraction of C_4 grass to total grass. In principle, an estimate of the fraction of C_4 *Atriplex* to total browse might be possible for *Camelops*, but because camels preferentially feed on *Atriplex*, we instead use the $\delta^{13}C$ values in *Camelops* as a measure of *Atriplex* presence/absence during the late Pleistocene. Propagated uncertainties in $\%C_4$ are approximately ±10%, assuming typical uncertainties in the $\delta^{13}C$ values of mean tooth enamel, endmember C_3, and endmember C_4 vegetation. Variabilities in the compositions of mean tooth enamel and endmember C_3 vegetation contribute to the largest sources of error.

Results

Oxygen and Carbon Isotopes in Tooth Enamel

Mean grazer tooth enamel $\delta^{18}O$ values from unit E_0 and E_1 were +21.68±1.15‰ (2 s.e.) and +20.62±1.99‰, respectively, and do not differ considerably from grazer tooth enamel from unit B and D (with mean B = +21.71±1.31‰ and mean D = +21.21±0.90‰, omitting one outlier at +32.51‰; Fig 7; Table 4). *Camelops* tooth enamel $\delta^{18}O$ values from E_0 and E_1 had mean values of +22.82±1.29‰ and + 23.22±0.34‰, respectively (omitting one outlier at +31.79‰), and generally exceed grazer values by ~2‰ (Fig 7; Table 4).

Mean tooth enamel $\delta^{13}C$ values from grazers from unit E_0 and E_1 were –6.73±1.39‰ and –8.10±1.36‰, respectively, and were generally lower than mean grazer $\delta^{13}C$ values from unit B and D (mean B = –4.69±1.21‰ and mean D = –4.93±1.77‰).

Camelops from E_0 and E_1 had mean $\delta^{13}C$ values of –7.39±1.14‰ and –6.54±3.59‰, respectively.

Oxygen and Carbon Isotopes in Tufas

The mean $\delta^{18}O$ value for modern tufas was +20.89±0.46‰ (2 s.e.) and was higher than mean $\delta^{18}O$ values from fossil tufas (D = +18.26, E_0 = +19.74±3.39‰, E_{1b} = +18.47±0.32‰ and E_2 = +19.97±1.40‰; Fig 8; Table 5). Mean $\delta^{13}C$ values from fossil

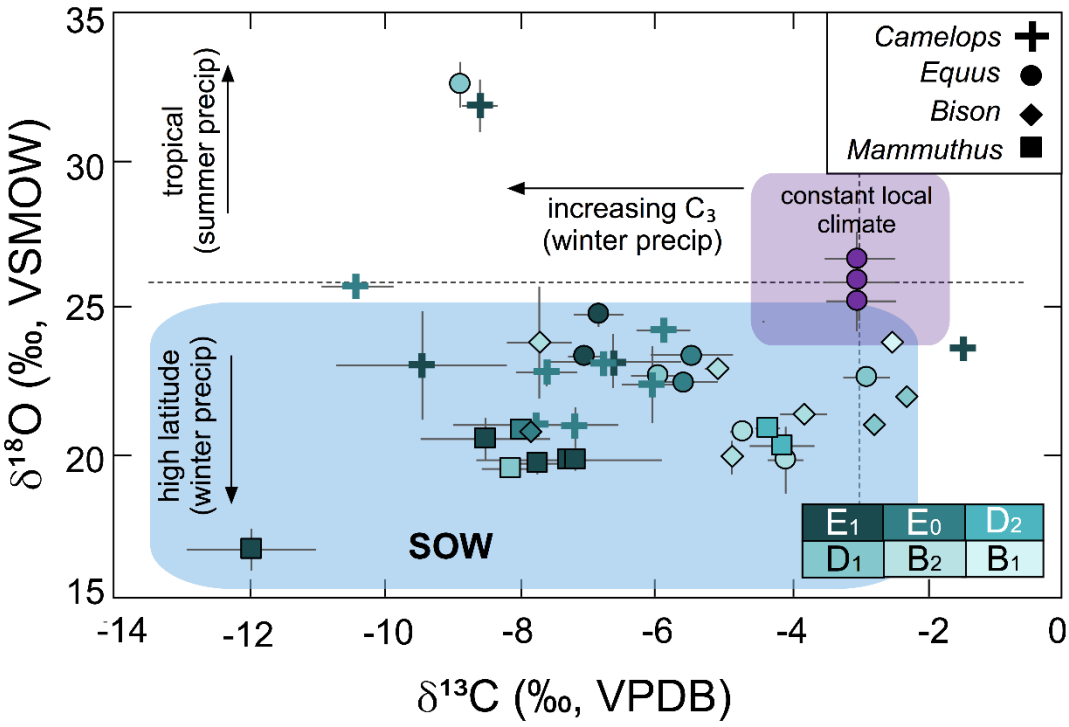

Figure 7. Tooth enamel $\delta^{13}C$ and $\delta^{18}O$ values for grazers (*Bison* = diamonds, *Mammuthus* = squares, and *Equus* = circles) and browsers (*Camelops* = crosses). Modern tooth enamel $\delta^{18}O$ values are from Crowley et al. (2008) and originate from Reno, Nevada, which has a lower water $\delta^{18}O$ values of –14.7‰ when compared to the modern LVW (–12.9‰; Friedman et al., 2002). A modern tooth enamel $\delta^{13}C$ value of c. –3‰ was inferred from modern $\%C_4$ grass abundances (55 to 60% C_4 grass) for the LVW ("National Park Service - Mojave Desert Network," 2018). Differing symbols represent different taxa, and differing colors represent distinct LVW deposits.

tufas were typically lower or comparable (D = –5.19, E_0 = –3.32±3.02‰, E_{1b} = –5.25±0.53‰, E_2 = –3.44±2.28‰) to modern tufas (–5.65±0.79‰).

C_3/C_4 Grass Abundance

Grazer tooth enamel compositions from younger unit E_0 and E_1 (~21 to 13 ka), suggest C_4 grass proportions of 16±6% (2 s.e.; range = 0 to 31%) in the total grass biomass. Grazer tooth enamel from older unit B and D (~80 to 29 ka) have higher C_4 grass proportions of 26±8% (2 s.e.; range = 0 to 44%; Fig 9a Table 6). *Camelops* were consuming 17±10% (range = 0 to 60%) C_4 vegetation (Fig 9c; Table 6).

Inferred Oxygen Water Compositions

Present-day spring water $\delta^{18}O$ values predicted from modern tufa (mean = –11.68±0.45‰ 2 s.e.) from the Cold Creek locality are ~2‰ higher than direct measurements (–13.8‰; Thomas et al., 1991). This disparity likely reflects greater disequilibrium for fast-precipitated tufa compared to the more slowly precipitated calcite (Kim and O 'Neil, 1997). Late Pleistocene $\delta^{18}O_{water}$ values predicted from fossil tufa average –12.74±0.89‰ (Fig 9b; Table 7), or about ~1‰ lower than $\delta^{18}O_{water}$ values predicted from modern tufa and ~0.2‰ higher than measured $\delta^{18}O_{water}$ values from

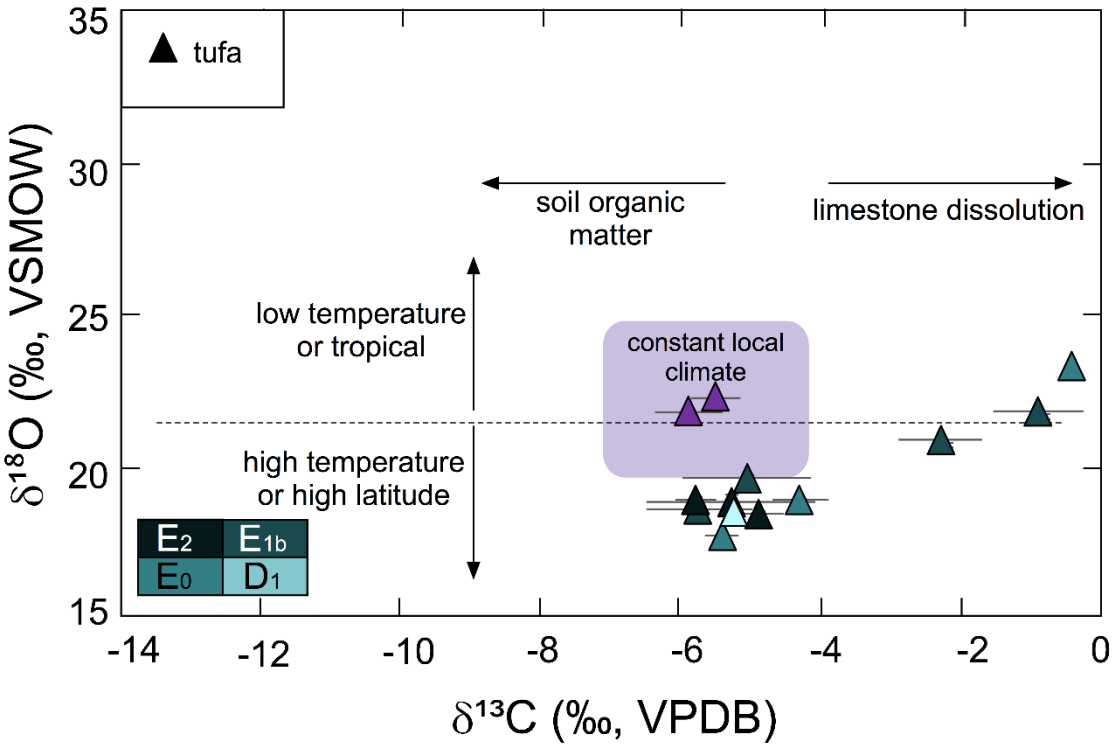

Figure 8. Modern and fossil tufa $\delta^{13}C$ values and $\delta^{18}O$ values from the upper LVW. Triangles outlined in black represent tufa isotope compositions and differing colors represent different GWD deposits in the LVW. High $\delta^{13}C$ values result from limestone dissolution, while low $\delta^{13}C$ values result from the presence of soil organic matter. Modern tufas, from Cold Creek ($\delta^{18}O_{water}$ = –13.8‰), have higher $\delta^{18}O$ values than fossil tufa.

Table 6. Estimated %C_4 grasses (from grazers) and shrubs (from browsers) from the late Pleistocene LVW. Identification number, unit, $\delta^{13}C$ vegetation values, %C_4 grass, high and low estimates, ages, and errors.

ID Number	Unit	Taxa	mean $\delta^{13}C$diet (‰, VPDB)	%C_4	low %	high %	Age (cal ka BP)	±
03KS9−23.1	E_{1d}	*Camelops*	−23.10	5	0	13	13.69	0.14
03KS9−23.1b	E_{1d}	*Equus*	−21.05	21	13	28	13.69	0.14
03MRR 10−1.2	E_{1c}	*Equus*	−20.85	22	15	30	14.12	0.21
10CM3−18.1a	E_{1b}	*Mammuthus*	−26.24	0	0	0	14.59	0.50
10CM6−17.1	E_{1b}	*Camelops*	−23.97	0	0	6	14.59	0.50
10CM6−17.2	E_{1b}	*Camelops*	−15.96	60	52	68	14.59	0.50
03MJS 10−1.2	E_{1b}	*Camelops*	−21.14	20	12	28	14.59	0.50
03GAM10−10.5.1.1	E_{1a}	*Mammuthus*	−21.55	17	9	25	16.10	0.21
03GAM10−15.1.2	E_{1a}	*Mammuthus*	−21.45	18	10	25	16.10	0.21
03GAM10−15.1.3	E_{1a}	*Mammuthus*	−22.77	8	0	15	16.10	0.21
03GAM10−15.1.4	E_{1a}	*Mammuthus*	−22.00	13	6	21	16.10	0.21
L3160−207.1	E_0	*Equus*	−19.46	31	23	39	19.80	0.22
L3160−207.2	E_0	*Equus*	−19.60	30	22	38	19.80	0.22
L3088−390a	E_0	*Bison*	−22.37	9	1	16	19.80	0.22
L3088−459	E_0	*Camelops*	−20.56	23	15	30	19.80	0.22
L3160−953	E_0	*Camelops*	−24.90	0	0	0	19.80	0.22
L3160−773.1	E_0	*Camelops*	−22.13	11	3	18	19.80	0.22
L3160−773.2	E_0	*Camelops*	−21.70	14	6	22	19.80	0.22

ID Number	Unit	Taxa	mean $\delta^{13}C_{diet}$ (‰, VPDB)	$\%C_4$	low %	high %	Age (cal ka BP)	±
L3160−773.3	E_0	*Camelops*	−21.67	14	6	22	19.80	0.22
L3088−391	E_0	*Camelops*	−21.29	17	9	25	19.80	0.22
L3088−520	E_0	*Camelops*	−20.39	24	16	32	19.80	0.22
L3160−875	E_0	*Mammuthus*	−22.25	10	2	17	21.04	0.52
L3160−39a	D_2	*Mammuthus*	−18.39	39	32	47	29.63	2.05
L3160−6	D_2	*Mammuthus*	−18.60	38	30	45	29.63	2.05
L3160−654.1	D_1	*Equus*	−22.90	5	0	12	35.04	0.50
L3160−654.2	D_1	*Equus*	−16.88	51	43	59	35.04	0.50
L3160−779	D_1	*Equus*	−19.96	27	20	35	35.04	0.50
L3160−917	D_1	*Bison*	−16.81	51	44	59	35.04	0.50
L3160−781	D_1	*Bison*	−17.27	48	40	56	35.04	0.50
L3160−647	D_1	*Mammuthus*	−22.42	8	1	16	35.04	0.50
L3160−748	B_2	*Equus*	−18	42	34	49	47.50	2.50
L3160−751	B_2	*Bison*	−22	10	2	17	47.50	2.50
L3160−946	B_2	*Bison*	−19	32	24	39	47.50	2.50
L3160−230.2	B_2	*Bison*	−19	37	29	44	47.50	2.50
L3160−230.4	B_2	*Bison*	−20	30	22	38	47.50	2.50
L3160−818.2	B_2	*Bison*	−18	40	32	48	47.50	2.50
04MRR1−28.1	B_1	*Bison*	−17	49	41	57	75.00	5.00

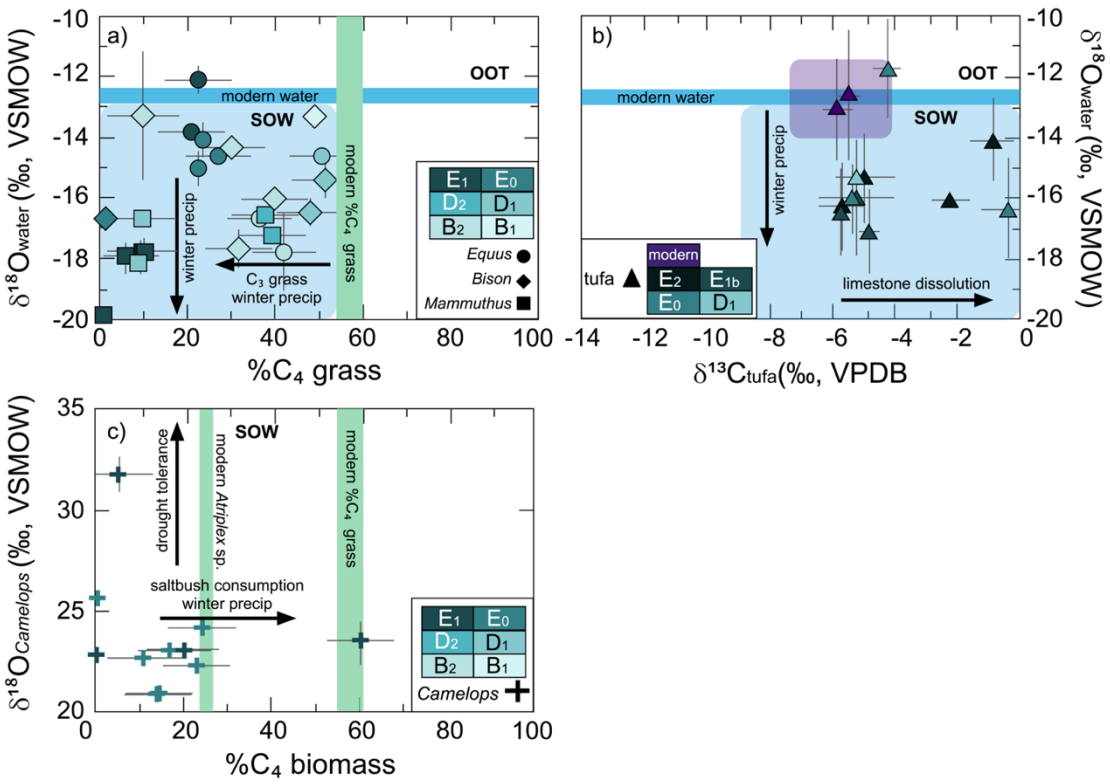

Figure 9. Inferred water $\delta^{18}O$ values (Bison = diamonds, Mammuthus = squares, Equus = squares, tufa = triangles), Camelops $\delta^{18}O$ values (crosses), tufa $\delta^{13}C$ values (triangles), and inferred $\%C_4$ biomass. a) Water $\delta^{18}O$ values from water-dependent herbivores vs. $\%C_4$ grass. The blue bar represents modern water compositions (Friedman et al., 2000), while the green bar represent modern proportions of C_4 grass in the LVW ("National Park Service - Mojave Desert Network," 2018). b) Water $\delta^{18}O$ values from tufas and tufa $\delta^{13}C$ values. Modern tufas (purple) were collected from Cold Creek, and the blue bar reflects modern water $\delta^{18}O$ values from the LVW (Friedman et al., 2000). c) $\%C_4$ biomass inferred from Camelops as well as Camelops tooth enamel $\delta^{18}O$ values. Modern LVW consists of c. 26 % Atriplex (Shanahan et al., 2008).

Table 7. Inferred water compositions of tufa and tooth enamel for the late Pleistocene LVW. Identification number, unit, type of specimen (tooth enamel) or samples (tufa), 2 s.e., age, dating technique, and error.

ID Number	Unit	Type	Taxa	mean $\delta^{18}O_{water}$ (‰, VSMOW)	Corrected mean $\delta^{18}O_{water}$ (‰, VSMOW)	Dating Technique	Age (cal ka BP)	±
CC-004	Modern Cold Creek	tufa		−11.90	−13.90		0	
CC-005	Modern Cold Creek	tufa		−11.45	−13.45		0	
10CM8-25.1	E_2	tufa		−13.50	−15.50		0	
TS-E2-1	E_2	tufa		−12.54	−14.54	^{14}C	12.35	0.23
10CM3-11.1	E_2	tufa		−11.31	−13.31	^{14}C	12.35	0.23
10CM3-11.1b	E_2	tufa		−13.29	−15.29	^{14}C	12.35	0.23
03KS9-23.1b	E_{1d}	enamel	*Equus*	−13.82		^{14}C	13.69	0.14
03MRR10-1.2	E_{1c}	enamel	*Equus*	−12.11		^{14}C	14.12	0.21
10CM3−18.1a	E_{1b}	enamel	*Mammuthus*	−21.19		^{14}C	14.59	0.50
10CM4-22.1	E_{1b}	tufa		−13.19	−15.19	^{14}C	15.35	0.22
10CM4-22.1b	E_{1b}	tufa		−13.70	−15.70	^{14}C	15.35	0.22
10CM3-18.1b	E_{1b}	tufa		−14.33	−16.33	^{14}C	16.10	0.21
03GAM10-10.5.1	E_{1a}	enamel	*Mammuthus*	−17.76		^{14}C	16.10	0.21
03GAM10-10.5.2	E_{1a}	enamel	*Mammuthus*	−17.75		^{14}C	16.10	0.21

ID Number	Unit	Type	Taxa	mean $\delta^{18}O_{water}$ (‰, VSMOW)	Corrected mean $\delta^{18}O_{water}$ (‰, VSMOW)	Dating Technique	Age (cal ka BP)	±
03GAM10-10.5.3	E_{1a}	enamel	*Mammuthus*	−16.97		^{14}C	16.10	0.21
03GAM10-10.5.4	E_{1a}	enamel	*Mammuthus*	−17.89		^{14}C	16.10	0.21
L3160-207.1	E_0	enamel	*Equus*	−14.08		^{14}C	19.80	0.22
L3160-207.2	E_0	enamel	*Equus*	−15.02		^{14}C	19.80	0.22
L3088-390a	E_0	enamel	*Bison*	−16.71		^{14}C	19.80	0.22
09CM9-2.1C	E_0	tufa		−13.21	−15.21	^{14}C	20.28	0.22
03CM11-13.1	E_0	tufa		−8.94	−10.94	^{14}C	20.96	0.24
10CM7-20.1	E_0	tufa		−13.59	−15.59	^{14}C	20.96	0.24
L3160-875	E_0	enamel	*Mammuthus*	−16.67		^{14}C	21.04	0.5
L3160-39a	D_2	enamel	*Mammuthus*	−17.23		^{14}C	29.63	0.52
L3160-6	D_2	enamel	*Mammuthus*	−16.55		^{14}C	29.63	0.52
L3160-654.2	D_1	enamel	*Equus*	−14.62		^{14}C	35.04	0.50
L3160-779	D_1	enamel	*Equus*	−14.60		^{14}C	35.04	0.50
L3160-917	D_1	enamel	*Bison*	−15.40		^{14}C	35.04	0.50
L3160-781	D_1	enamel	*Bison*	−16.46		^{14}C	35.04	0.50
L3160-647	D_1	enamel	*Mammuthus columbi*	−18.13		^{14}C	35.04	0.50
09KS2-12−1	D_1	tufa		−12.55	−14.55	^{14}C	35.04	0.50

ID Number	Unit	Type	Taxa	mean $\delta^{18}O_{water}$ (‰, VSMOW)	Corrected mean $\delta^{18}O_{water}$ (‰, VSMOW)	Dating Technique	Age (cal ka BP)	±
L3160-748	B_2	enamel	*Equus*	−17.79		OSL luminescence	47.50	2.50
L3160-751	B_2	enamel	*Bison*	−13.28		OSL luminescence	47.50	2.50
L3160-946	B_2	enamel	*Bison*	−17.66		OSL luminescence	47.50	2.50
L3160-230.2	B_2	enamel	*Equus*	−16.69		OSL luminescence	47.50	2.50
L3160-230.4	B_2	enamel	*Bison*	−14.32		OSL luminescence	47.50	2.50
L3160-818.2	B_2	enamel	*Bison*	−16.05		OSL luminescence	47.50	2.50
04MRR1-28.1	B_1	enamel	*Bison*	−13.30		OSL luminescence	75.00	5.00

regional springs and wells (–12.9‰; Friedman et al., 2002). If the same tufa-water offset observed in modern tufas is applied to fossil tufas, late Pleistocene water compositions would have been approximately c. –15‰ (Fig 9a and b; Table 7). Excluding anomalous *Equus*, a mean $\delta^{18}O_{water}$ value of –16.08±0.81‰ was inferred from water-dependent herbivore tooth enamel (Fig 9a; Table 7).

Discussion

Carbon Isotopes, C_3/C_4 Grass Abundances, and Seasonal Precipitation

Based on modern species counts, present-day southern Nevada consists of 55-60% C_4 grass and 40-45% C_3 ("National Park Service - Mojave Desert Network," 2018). These proportions reflect a dry climate that receives almost equal amounts of winter and summer precipitation ("WRCC," 2018). In contrast, low tooth enamel $\delta^{13}C$ values from grazers throughout the LVW sections indicate that C_4 grass abundances must have increased markedly from the late Pleistocene to today (Fig 7 and 9a; Table 4 and 6). Relative abundances of C_3 vs. C_4 vegetation generally correlate with several physical parameters, such that C_4 grass competitiveness increases with higher mean annual temperature (MAT), increased proportion of summer precipitation, and low pCO_2 levels (Paruelo and Lauenroth, 1996; Collatz et al., 1998). Decreasing pCO_2 is especially important because it lowers the crossover temperature, which is the temperature at which C_3 and C_4 plants have equivalent light use efficiencies. For example, relative to a reference of 350 ppmv, a pCO_2 of 200 ppmv at 18 ka would lower the crossover temperature by 10 °C (Collatz et al., 1998). Thus, at the LVW, where temperatures at 18 ka (Pedro et al., 2012) were only ~3 °C lower than modern−day (Braconnot et al., 2007), the pCO_2 effect would outweigh MAT (Koch et al., 2004; Kohn and McKay, 2012). If we

consider changes only to temperature and pCO_2, lower pCO_2 during the late Pleistocene should result in higher C_4 grass abundances. Considering how low precipitation is today in the Las Vegas area, and that the late Pleistocene was a time of increased precipitation, the most likely mechanism for increasing C_3 grass abundances is through increased winter precipitation (SOW).

It is unclear why older units B and D have higher $\%C_4$ grass abundance (26±8%) than younger E units (16±6%; $p \sim 6x10^{-6}$). The youngest fossil-bearing strata (E_1) were deposited during periods with somewhat higher pCO_2 levels (230-240 ppmv) compared to other times during the late Pleistocene, for example E_0 (195 ppmv; Pedro et al., 2012) and during the deposition of unit B and D (200-220 ppmv; Indermühle et al., 2010; Bereiter et al., 2012). Although these differences alone might suggest that higher pCO_2 induces greater precipitation seasonality, the greatest expansion of glacial lakes and increased GWD occurred during time periods of reduced pCO_2.

To further evaluate the fraction of C_4 grasses (X_{C4}) in southern Nevada during the late Pleistocene, we used the approach of Kohn and McKay (2012) (see Paruelo and Lauenroth, 1996; Connin et al., 1998; Koch et al., 2004), which is based on changes in pCO_2, MAT, precipitation (MAP), the ratio of June-July-August precipitation to MAP (JJA/MAP), and the change in photosynthetic cross-over temperature (ΔT_x) associated with changes to pCO_2:

$$X_{C_4} = -0.9837 + 0.000594\left(\mathrm{MAP}, {}^{\mathrm{mm}}/_{\mathrm{yr}}\right) + 1.3528\left({}^{\mathrm{JJA}}/_{\mathrm{MAP}}\right) + 0.2710 \ln(MAT - \Delta T_x) \quad \text{(Eq. 8)}$$

Changes to pCO_2 heavily influence the cross-over temperature and consequently the $\%C_4$ grass, because C_4 plants generally outcompete C_3 plants with decreased pCO_2.

Equation 5 is not intended to be fully quantitative, but rather to indicate direction of C_4 grass abundance, i.e. increasing vs. decreasing. In modern southern Nevada, MAT = 19.5 °C, MAP = 105 mm/yr, and JJA/MAP = 0.23 ("WRCC," 2018). During the Last Glacial Maximum (LGM) in southern Nevada, the PMIP2 model predicts higher MAP (~265 mm/yr), a decrease of 3 °C in MAT (16.5 °C), and no change for JJA/MAP (0.23; Braconnot et al., 2007; 2012; Niu et al., 2017). Relative to a modern reference pCO_2 was lower at ~185 ppmv, which decreases the C_3-C_4 crossover temperature by 11-12 °C. The resulting MAT-ΔT_x is ~28 °C (=19.5°C – 3 °C + 11.5 °C). Using Equation 8 we calculated a value of 36% C_4 vegetation, which is similar to the %C_4 grass inferred from herbivore tooth enamel from unit B and D. However, modeled C_4 grass abundances for modern southern Nevada (21%) dramatically underestimate known values (55-60%; Table 6). Calculations are most sensitive to the fraction of summer precipitation. To increase calculate %C_4 to modern observations, JJA/MAP would have to approximately doubled, i.e. plant distributions are more sensitive to summer precipitation in southern Nevada by a factor of ~2. If a similar overrepresentation of summer precipitation applies to Pleistocene %C_4 calculations, accurate JJA/MAP must have been ~0.1, meaning that JJA precipitation in the late Pleistocene was similar to today (~20-25 $mmyr^{-1}$).

Some *Camelops* have high $\delta^{13}C$ values, which reflect consumption of the C_4 plant *Atriplex* (saltbush). *Atriplex* constitutes ~26% of land cover in the modern-day LVW (Shanahan et al., 2008). Saltbush typically thrives in environments with high low summer rains, and therefore high $\delta^{13}C$ values suggest that increased precipitation in southern Nevada during the late Pleistocene occurred primarily through increases to winter precipitation. However, some *Atriplex* species germinate during summer months if MAP

increases (Osmond et al., 1980), and the Late Pleistocene LVW was notably wetter than modern-day climes. Some *Camelops* have low $\delta^{13}C$ values that predict a $\%C_4$ biomass lower than modern saltbush species counts (<26%), which may be interpreted as increased summer precipitation. Previous work has found taxa consuming a pure *Atriplex* diet must offset the increased salt intake by consuming more water (Gihad, 1993). Although the late Pleistocene LVW was wetter than modern conditions, it was still an arid environment that hosted wetland formation. Therefore, it is unlikely *Camelops* diets consisted of purely saltbush, and lower $\delta^{13}C$ most likely reflect a more balanced diet of C_3 shrubs and *Atriplex*.

Oxygen Isotopes and Water Compositions

From our measured tooth enamel compositions, and using our calibration for large, water-dependent herbivores in western Nevada, we estimate a mean $\delta^{18}O_{water}$ of –16.1‰ for the late Pleistocene LVW (Fig 9a; Table 7). This low value makes computational sense in that late Pleistocene tooth enamel from the LVW has a $\delta^{18}O$ value ~2‰ lower than modern enamel near Reno, where local water is –14.7‰ (Friedman et al., 2002). Consequently, $\delta^{18}O_{water}$ values should be ~2‰ lower than modern Reno, or c. –16 to –17‰. The low value also makes sense in the context of lower temperatures during the late Pleistocene (the temperature effect of Dansgaard, 1964; see also Rozanski et al., 1992).

Using Equation 6, predicted $\delta^{18}O_{water}$ values during the late Pleistocene would have been –12.7‰ or ~3.5‰ higher than inferred fossil tooth enamel. However, there is a ~2‰ inconsistency between modern $\delta^{18}O_{water}$ values for modern tufas collected from Cold Creek as determined by direct measurements (–13.8% from Thomas et al. (1991) vs.

estimated from modern tufas of –11.6‰; Fig 9b; Table 7). That is, calculations based on published equations for calcite-water as applied to tufas may overestimate $\delta^{18}O_{water}$ values by as much as ~3‰, probably as a result of increased disequilibrium for rapid calcite precipitation (Kim and O 'Neil, 1997). If a 2‰ downward correction is made to account for a modern disequilibrium offset, $\delta^{18}O_{water}$ values estimated using tooth enamel and tufa are more similar at c. –16.1‰ and –14.7‰, respectively.

In comparison with modern $\delta^{18}O_{water}$ values from the LVW (–12.9‰; Friedman et al., 1992; Friedman et al., 2002), fossil tooth enamel and (corrected) tufa suggest that $\delta^{18}O_{water}$ values were significantly lower in the late Pleistocene by ~3‰. This difference is broadly compatible and even more pronounced then previous regional complications of $\delta^{18}O_{water}$ values for the late Pleistocene (~2‰ lower; Jasechko, 2016), although our data are much more defined in age than most other datasets. Low latitude moisture and summer precipitation have higher $\delta^{18}O_{water}$ values than high latitude moisture of winter precipitation. Consequently, the decrease in $\delta^{18}O_{water}$ values is inconsistent with increased summer precipitation sourced from low latitudes, so does not support the OOT hypothesis. Instead, lower $\delta^{18}O_{water}$ values are consistent with an increase in winter precipitation or a decrease in temperature (or both). These observations support the SOW hypothesis, in which increased winter precipitation was sourced from higher latitudes (colder conditions) and falls across a generally colder landscape.

Comparison to Other American Southwest Studies

Some GCM's and paleoproxy studies have attributed increased late Pleistocene precipitation in the Great Basin and American Southwest to a SOW (COHMAP members, 1988; Toggweiler et al., 2006; Asmerom et al., 2010; Wagner et al., 2010).

However, many observational studies that reconstructed precipitation seasonality in the late Pleistocene American Southwest found that wetter conditions were accompanied by both increased summer (OOT) and winter (SOW) precipitation (Connin et al., 1998; Holmgren et al., 2007; 2009). Both our carbon and oxygen isotope data instead point to enhanced winter precipitation (SOW), which increased GWD and established late Pleistocene wetlands in southern Nevada.

Connin et al. (1998) reported $\delta^{13}C$ and $\delta^{18}O$ values from *Mammuthus*, *Bison*, *Equus*, and *Camelops* (~50 to ~10 ka), from the southeastern Mojave Desert (Nevada, California), northern Sonoran (Arizona) and Chihuahaun (New Mexico) deserts, and Southern High Plains (New Mexico. Their study, as well as Crowley et al. (2008) are of special interest, because stable isotope compositions are reported for fossil from Tule Springs (upper LVW). These older data broadly commensurate with ours, for example grazer $\delta^{18}O$ values from their studies mostly range between 21 and 25‰, while ours mostly range between 20 and 25%. Similarly, Connin et al. (1998) report grazer $\delta^{13}C$ values for level E of c. –8‰, whereas our average –7 to –8‰. Despite these similarities, Connin et al. (1998) proposed that the late Pleistocene isotope record supports enhanced summer and winter moisture, whereas we propose a decrease in summer precipitation. This difference in interpretation reflects the assumed abundance of modern C_4 grasses in the region. We based modern C_4 abundances (c. 50%) on modern species counts. Connin et al. (1998) instead estimated modern C_4 abundances (c. 25%) using an equation from Paruelo and Lauenroth (1996), which in the same as our Equation 5 excluding the crossover temperature correlation. We both estimate a C_4 abundance during the late Pleistocene of c. 35%, but our assumption implies a decrease relative to today, whereas

their assumption implies an increase. In our view, direct species counts are preferable to continental-scale extrapolations, and for the late Pleistocene indicate a decrease in C_4 vegetation and in the proportion of summer rainfall to mean annual precipitation. Although some summer precipitation source from mid-Pacific or Gulf of Mexico may have reached southern Nevada, low Pleistocene tooth enamel $\delta^{13}C$ and $\delta^{18}O$ values from Tule Springs do not favor an increase in more tropical precipitation. Low isotope trends seen in Connin et al. (1998) are also captured within herbivore tooth enamel are established in other Mojave Desert localities (Nevada and California). These low tooth enamel $\delta^{13}C$ and $\delta^{18}O$ values suggest increased moisture sourced into the Mojave Desert during the late Pleistocene resulted from an increased proportion of winter precipitation. Contrasting published tooth enamel $\delta^{13}C$ and $\delta^{18}O$ values from lower latitudinal American Southwest deserts (i.e. Sonoran and Chihuahuan Deserts) illustrate regional complexities when interpreting late Pleistocene precipitation seasonality. To the south and southeast of the LVW, tooth enamel $\delta^{13}C$ values from the late Pleistocene Sonoran and Chihuahuan Deserts of Arizona and New Mexico range from c. –7 to 2‰, and –12 to –2‰, respectively (Connin et al., 1998). These areas may record a strengthened Pleistocene summer monsoon, diverging from increased winter precipitation in the Mojave Desert. Though it is likely the Pleistocene Chihuahuan Desert received a significant proportion of summer rains, high and low $\delta^{13}C$ values may reflect lateral seasonality variations in the American Southwest, further complicating Pleistocene storm track reconstructions.

Other paleoproxies from the American Southwest, such as paleosols, pollen record, and speleothems, also support increased winter precipitation at higher latitudes

and more disparate and possibly dynamic moisture sources at lower latitudes (Monger et al., 1998; Brook et al., 2006; Holmgren et al., 2007; 2009; Asmerom et al., 2010; Wagner et al., 2010). During the Pleistocene-Holocene transitions, paleosol carbonate $\delta^{13}C$ values and pollen assemblages indicate a transition to more C_3-dominated ecosystems that likely received a greater proportion of winter precipitation (Monger et al., 1998). Conversely, speleothem $\delta^{18}O$ values from the Cave of the Bells, Arizona, and Fort Stanton Cave, New Mexico indicate a greater proportion of winter precipitation (Asmerom et al., 2010; Wagner et al., 2010). Although resolving Pleistocene atmospheric circulation for the American Southwest deserts has proved difficult, in part because of conflicting paleoproxy interpretations, mid-latitude effects likely impeded the transport of summer precipitation to higher latitude deserts, north of 35° N (Holmgren et al., 2007). This is evident at Tule Springs (36° N), where low $\delta^{13}C$ and $\delta^{18}O$ values in fossil tooth enamel (Connin et al., 1998; Crowley et al., 2008; this study) likely reflect enhanced winter precipitation, which was transported to the late Pleistocene LVW through southward shift of the westerly winds.

As we advance into the next century's greenhouse climate, climate change models should inform policy surrounding the preservation of modern desert wetlands. Both enhanced summer and winter precipitation may have contributed precipitation to differing regions in the late Pleistocene American Southwest. Dynamic storm tracks are illustrated by conflicting yet regionally compatible climate records, such that, the Mojave Desert likely received increased winter moisture and the Chihuahuan Desert received a summer/winter combination. GCM's for the late Pleistocene Great Basin and American Southwest generalize regional climate trends, specifically seasonality of precipitation,

which is captured within herbivore tooth enamel. As GCM's improve spatial resolution, comparison to temporally precise records should promote more accurate projects for past and future climate changes.

Conclusion

At times, in the late Pleistocene American Southwest, there was an increase in net precipitation that stabilized paleo-lakes and -wetlands. The driver of this increased net precipitation and the seasonality (winter vs. summer) of precipitation transported to the American Southwest are both still debated. A southward shift of the westerlies (SOW) would increase winter precipitation derived from higher latitudes. Alternatively, if precipitation was sourced out of the tropics (OOT), either from the southern Pacific Ocean of Gulf of Mexico, increased summer rains would have stabilized paleo-lakes and -wetlands. Low tooth enamel $\delta^{13}C$ and $\delta^{18}O$ values, as well as low tufa $\delta^{18}O$ values, indicate that paleowetland expansion in the LVW most likely occurred because of an increased proportion of winter precipitation (supporting the SOW hypothesis), coupled with commensurate increases in C_3 grass abundances. Geographical differences in the seasonality of precipitation in the American Southwest during the late Pleistocene (high winter precipitation at ≥36 °N latitude; high summer precipitation at ≤35 °N latitude) provide a useful benchmark for testing GCM accuracy.

CHAPTER THREE: THE INTERPRETABILITY OF STABLE HYDROGEN ISOTOPES IN MODERN HERBIVORE TOOTH ENAMEL

Introduction

Stable hydrogen isotopes (δD values) from animal organic tissues (e.g. keratin, chitin, and collagen) have been used to track migratory patterns, diet type, trophic level, and climate (Estep and Dabrowski, 1980a; Cormie et al., 1994; Hobson et al., 1999; Bearhop et al., 2003; Cryan et al., 2004; Bowen et al., 2005b; Leyden et al., 2006; Ehleringer et al., 2008; Reynard and Hedges, 2008; Hobson and Wassenaar, 2018). Although stable hydrogen isotope compositions of organic materials are desirable for ecological and environmental studies, readily exchangeable, labile hydrogen can complicate interpretations. Ambient hydrogen (H) from water vapor can either exchange with structural H or adsorb onto surfaces, diluting biogenic δD values. Of the total H in modern hair (keratin), approximately 31% is derived from ingested drinking water, and at ambient temperatures, up to 9% is derived from exchangeable water vapor (Sharp et al., 2003). Non-exchangeable hydrogen in bone collagen accounts for 80% of the total H, but 20% of H within collagen is exchangeable with atmospheric water vapor (Cormie et al., 1994; Leyden et al., 2006). For substrates such as chitin, exchangeable structural hydrogen is removed using nitration, but these chemical techniques are applicable only for certain organic tissues (Epstein et al., 1976; Miller et al., 1988; Schimmelmann, 1991).

The compositions of stable hydrogen and oxygen isotopes ($\delta^{18}O$ values) in meteoric waters strongly correlate, depend primarily on precipitation source and temperature, and define the Global Meteoric Water Line (GMWL; $\delta D = \delta^{18}O \times 8 + 10‰$; e.g. Craig, 1961; Dansgaard, 1964; Rozanski et al., 1992). In vertebrates, measured δD and $\delta^{18}O$ values frequently correlate with meteoric and plant leaf waters, but can be affected by relative humidity and (for carnivores) prey compositions (Ayliffe and Chivas, 1990a; Luz et al., 1990; Cormie et al., 1994; Koch, 1998; Kohn and Cerling, 2002; Sharp et al., 2003; Cryan et al., 2004; Leyden et al., 2006; Kohn and Dettman, 2007; O 'Brien and Wooller, 2007; Ehleringer et al., 2008; Pietsch et al., 2011; Clementz, 2012). Because δD and $\delta^{18}O$ values correlate in both meteoric waters and biological materials, reconstructions of climate and ecology might in principle employ enamel δD values. However, it is unclear whether stable hydrogen isotopes preserved within inorganic substrates reflect biogenic ambient waters and/or vegetation signals.

A preliminary study of 3 archeological and 2 modern human teeth showed a weak correlation between tooth enamel δD and $\delta^{18}O$ values (Holobinko et al., 2011). In their study, Holobinko et al (2011), tested whether δD values could be exchanged or otherwise altered by equilibrating sample aliquots for a single tooth with evaporatively enriched- and depleted-waters over a 4-day timespan. Tooth enamel compositions from enriched- and depleted-water equilibrations were similar, which was interpreted to mean that tooth enamel H isotopes are essentially immune to re-equilibration.

Initially, we aimed to characterize and better understand any correlations among herbivore tooth enamel δD, $\delta^{18}O$, and $\delta^{13}C$ values. There is virtually no correlation between δD or $\delta^{18}O$ with respect to $\delta^{13}C$ (which might have reflected an effect of C_3 vs.

C_4 grass consumption; Appendix Fig 3), so the scope of this study was narrowed to focus on the correlations between δD and $\delta^{18}O$ and between δD values of enamel and source water. Because oxygen and hydrogen in animals are derived almost solely from local water, including plant water (see Kohn, 1996), we would expect to find a correlation similar in slope to the meteoric water line, but with an offset and difference in slope that depends on physiology, climate, plant fractionations, and equilibration fractionation between enamel and body water. For example, $\delta^{18}O$ values derived from the phosphate (PO_4) and carbonate (CO_3) components of tooth enamel show systematic offsets with respect to body water compositions, which in turn show systematic offsets relative to meteoric water compositions (see review of Kohn and Cerling, 2002). Holobinko et al. (2011) found a resolvable correlation between human teeth δD and $\delta^{18}O$ values, but the slope of the correlation is quite different from the GMWL. Therefore, in this study we addressed the following questions:

1) Does an expanded tooth enamel dataset over a larger isotopic range for local water compositions and for different herbivore taxa show a different correlation than observed for human tooth enamel?
2) Does labile water contribute a significant amount of H to tooth enamel analyses?
3) What are the timescales of any labile water uptake?
4) Can heating remove any labile water and resolve original biogenic tooth enamel compositions?

To answer these questions, we 1) measured δD values from purified tooth enamel. Such values represent the combined contributions of hydrogen-phosphate (HPO_4) and hydroxyl (OH) components of tooth enamel, plus any labile (likely adsorbed) water; 2)

compared measured H contents of tooth enamel (calibrated against H contents of geological biotite and H_2 signal intensities) with expected H contents for tooth enamel (based on published chemical compositions of tooth enamel; Driessen and Verbeeck, 1990); 3) conducted time-series experiments of enamel that had been equilibrated with anomalously high and low δD values to determine time-scales of labile water equilibration; and 4) conducted heating experiments to determine whether we could remove labile hydrogen from tooth enamel.

Oxygen and Hydrogen Isotopes in Consumed Water and Plants

Water consumption contributes the largest amount of oxygen (O) and H in an animal, both through direct ingestion (drinking) of local water, and consumption of plants or animal, which have high water contents. Because animal O derives so closely from local water (both directly through drinking and indirectly through consumption of plant water and tissues), a strong correlation is observed between $\delta^{18}O$ values of bioapatite and local water (see summary of Kohn, 1996). Likewise, because animals derive most of their H from local water both through ingestion of water and direct consumption through plants, we expect a strong correlation between local water δD and tooth enamel δD values. Such a correlation has been demonstrated for dentine collagen (Kirsanow et al., 2008). Although, for a small number of samples a very weak correlation has been observed between δD values of tooth enamel vs. local water, it is as yet uncertain whether a correlation might occur for a larger dataset.

Tooth Enamel Formation and Isotopes

Tooth enamel is composed of ~98% bioapatite ($Ca_{4.5}[(PO_4)_{2.7}(HPO_4)_{0.2}(CO_3)_{0.3}](OH)_{0.5}$); (Driessens and Verbeeck, 1990). Teeth

progressively mineralize from the occlusal surface towards the root (Passey and Cerling, 2002). Because enamel is not remodeled after its formation, and because the temperature of precipitation is constant in mammals, enamel and other bioaptites preserve an isotopic record of an animal's body water compositions over its period of growth. Differences in mineralization rate and overall tooth size between taxa result in wide variations in the amount of time recorded within a single tooth (Passey and Cerling, 2002; Kohn, 2004; Trayler and Kohn, 2017), typically ranging from a few months to 1-2 years. Enamel $\delta^{18}O$ values correlate with local water compositions (Koch, 1998; MacFadden, 2000; Kohn and Cerling, 2002; Kohn and Dettman, 2007; Clementz, 2012), which are controlled by precipitation sources and temperature (Dansgaard, 1964; Rozanski et al., 1992). Because local water compositions vary seasonally (generally low $\delta^{18}O$ in winter and high $\delta^{18}O$ values in summer), O isotopic zoning within enamel provides a possible avenue for recovering a measure of climate seasonality. In principle, climate and ecology reconstructions might employ enamel δD values, but it is unclear whether stable hydrogen isotopes correlate with local ambient waters and/or vegetation signals.

Methods

Analytical Methods

We selected 12 modern herbivore teeth for analysis (Tables 8 and 9) to avoid possible alteration that occurs in fossils as F exchanges for structural OH in the hydroxyl site in bioapatite (e.g. see Trueman and Tuross, 2002). We collected sub-samples along the growth axis of each tooth, typically every 1-2 mm using a Dremel™ rotary tool and a 0.5 mm dental drill bit. Samples were then pretreated as per Koch et al. (1997), with

H_2O_2 to remove organic matter, and then with an acetic acid-Ca acetate buffer to remove any labile carbonates.

Stable oxygen isotopic compositions were measured by dissolving 1.5-2.0 mg of powdered enamel with supersaturated H_3PO_4. The subsequent CO_2 was measured using a

Table 8. Identification number, taxa, tooth, and location for intra-tooth and bulk specimens.

Intra-tooth specimens		
ID Number	Taxa/Tooth/Sample type	Location
BTM	*Castor canadensis*/I	Canyon City, CO
O2120	*Oryx sp.*/M2	Sibiloi National Park, Kenya
GGK	*Nanger granti*/M2	Sibiloi National Park, Kenya
BC	*Bison bison*/M3	Catalina, CA
EEC	*Equus ferus caballus* /M3	El Criado, Argentina
GBM2	*Equus ferus caballus* /M2	Gran Barranca, Argentina
NEPGO	*Capra hircus*/Mxt	Nepal
COW2	*Bos taurus*/M2	Juntura, OR
DREW	*Equus ferus caballus*/M2	Drewsey, OR
UWB-1	*Bos taurus*/M3	Uni. of Wisconsin, WI
M-00-59	*Cervus elaphus*/M2	Yellowstone, WY
M-00-49	*Cervus elaphus*/M3	Yellowstone, WY
Bulk specimens		
ID Number	Taxa/Tooth/Sample type	Location
BM1-Y	*Bison bison*/M1	Yellowstone, WY
BM3-C	*Bison bison*/M3	Catalina, CA
BOSM2-B	*Bos taurus*/M2	Brazil
UWB-2	*Bos taurus*/M3	Uni. of Wisconsin, WI
KBS	bone standard	-
NIST 2910	hydroxyapatite standard	-

Table 9. Identifier of fossil specimens, taxa, mean, maximum, and minimum δD and $\delta^{18}O$ values for all formations and specimens. Water δD values for each locality are also displayed ("OIPC," 2018; Johnson et al., 1991)

ID Number	mean δD (‰, VSMOW)	2 s.e.	max δD	min δD	mean $\delta^{18}O$ (‰, VSMOW)	2 s.e.	max $\delta^{18}O$	min $\delta^{18}O$	δD_{water}
BTM	−131.61	1.75	−123.64	−139.20	19.20	0.34	20.46	17.46	−52
O2120	−129.48	1.28	−117.54	−133.99	35.61	0.22	36.34	34.64	22
GGK	−130.73	1.57	−124.58	−135.15	32.95	0.28	33.77	31.37	22
BC	−131.42	1.53	−120.72	−135.68	28.19	0.27	29.40	26.94	−48
EEC	−130.42	0.99	−123.62	−133.26	24.79	0.54	28.84	23.45	−86
GBM2	−141.96	1.25	−132.10	−148.85	25.07	0.53	30.54	19.19	−86
NEPGO	−149.82	1.00	−137.02	−155.34	21.63	0.24	23.21	19.60	−85
COW2	−150.17	1.28	−144.25	−157.90	21.24	0.71	24.53	19.11	−103
DREW	−152.24	0.80	−145.38	−160.54	20.14	0.43	24.71	16.89	−103
UWB-1	−147.65	0.50	−144.21	−151.38	20.24	0.75	23.34	15.81	−50
M-00-59	−163.72	1.62	−159.42	−173.90	14.50	0.37	16.35	13.47	−140
M-00-49	−164.62	0.41	−162.84	−165.85	15.23	0.31	16.78	14.10	−140

ThermoFisher GasBench II, in-line with a Thermo Delta V Plus mass spectrometer, housed in the Stable Isotope Laboratory at Boise State University. Five to six NIST-120c ($\delta^{18}O$ = +28.5‰, VSMOW and $\delta^{13}C$ = −6.55‰, VPDB; Kohn et al., 2015) aliquots were prepared using the same cleaning pretreatment methods and analyzed with each sample set as a check standard. Each sample set was standardized to VPDB using eight to nine aliquots of the calcite standards NBS-18 (−23.2‰, VPDB) and NBS-19 (−2.2‰, VPDB) calcite standards. Analytical reproducibility for oxygen isotopes was: NIST-120c = ±0.83‰ (2σ); NBS-18 =±0.66‰; and NBS-19 = ±0.46‰. Reproducibility of sample weights was ±0.002 mg.

Stable hydrogen isotope compositions (Tables 2 and 3) were measured by combusting 1-2 mg of powdered enamel in silver capsules using a ThermoFisher TC/EA, coupled with the Thermo Delta V Plus mass spectrometer. For our initial isotope measurements, we included ten aliquots each of biotite standard (NBS-30; δD = −65.7‰, VSMOW) and a caribou hoof standard (CBS; δD = −197‰, VSMOW) with each analytical run. For our equilibration experiments, we included twenty-six analyses of each the biotite and hoof standards. Reproducibility for stable hydrogen isotopes was: NBS-30 = ±4.80‰ (2σ); CBS = ±4.45‰. Importantly this technique cannot distinguish hydrogen from different components (i.e. OH, HPO_4), and our results should be viewed as the bulk H isotope composition of biotite, keratin, and enamel. All further $\delta^{18}O$ and δD values (Table 2 and 3) are reported in VSMOW.

Hydrogen in enamel bioapatite is sourced from two crystallographic sites within the enamel structure, with ~40% bound in the HPO_4 and ~60% bound in the OH component (Driessens and Verbeeck, 1990). We compared sample weights of the 12 sub-

sampled teeth to the hydrogen peak area (Appendix Table 3) to test whether measured δD values reflect solely structural hydrogen, or a combination of structural and labile (adsorbed) hydrogen. If measured H inferred from measurements exceeds the amount expected from published chemical compositions, labile water must contribute to total H. That is, on a plot of measured H content (from peak area) vs. sample weight, the difference in slope between measured vs. expected H contents provides an estimate of the amount of labile water per mg of sample. To determine water contents from mass spectrometer measurements we calibrated the signal intensity of the H_2 peak to NBS-30 (biotite), which has a H_2 content of 0.0041% wt (Qi et al., 2017).

Because we found evidence for significant labile water contamination, we performed equilibration experiments with depleted-water (δD = −300.4±2.2‰; VSMOW) and enriched-water (δD = +62.0±1.7‰) to better understand possible equilibration timescales between labile water and ambient water vapor. Water compositions for depleted- and enriched-waters (Table 10) were measured using a fourth generation Los Gatos Research Liquid Water Isotope Analyzer (LWIA), housed in the Stable Isotope Laboratory at Boise State University. For bulk analyses (Tables 8 and 10), we selected 4 teeth (2 *Bison bison* and 2 *Bos taurus*; BM1-Y, BM3-C, BOSM2-B, and UWB) and 2 phosphate standards (NIST-2910, which is synthetic hydroxylapatite, and KBS, which is an in-house powdered fossil bone). Multiple aliquots of each material were split into open silver capsules and placed in airtight containers with either depleted- or enriched-water for 48 hours. Bulk samples were removed, exposed to ambient laboratory conditions for 0, 1, 2, 4, and 8 hours (which are notated as, respectively: t_0, t_1, t_2, t_4, and t_8) and then δD values were measured. Because silver capsules needed crimping

prior to analysis, each, exposure time must be increased by several minutes. This has no effect on exposure times ≥1 hour, but may be significant for "0" time experiment. We

Depleted−water (δD = −300.42±2.15‰)						
Time (hr)	BM1-Y	BM3-C	BOSM2-B	UWB-2	NIST-2910	KBS
0	−179.84	−203.82	−199.63	−167.78	−228.23	−152.6
1	−169.25	−141.96	−173.68	−167.43	−161.4	−141
2	−160.41	−143.45	−129.61	−164.18	−149.26	−147.33
4	−156.14	−136.15	−154.52	−159.73	−156.93	−140.23
8	−154.53	−135.33	−142.26	−152.8	−155.35	−133.73
Enriched−water (δD = 62.01±1.68‰)						
Time (hr)	BM1-Y	BM3-C	BOSM2-B	UWB-2	NIST-2910	KBS
0	−110.72	−100.09	−66.41	−94.43	61.44	42.26
1	−128.48	−121.91	−120.90	−147.13	−152.83	−132.21
2	−139.11	−116.67	−132.89	−152.98	−162.86	−133.45
4	−136.38	−130.92	−138.97	−146.73	−152.70	−134.12
8	−149.57	−139.69	−145.18	−144.47	−155.61	−130.11
Oven (70 ºC)						
Time (hr)	BM1-Y	BM3-C	BOSM2-B	UWB-2	NIST-2910	KBS
0	−174.99	−159.48	−146.089	−180.41	−168.90	−149.22
1	−166.33	−149.40	−142.85	−169.83	−148.38	−158.18
2	−160.08	−158.21	−138.16	−172.96	−138.60	−159.14
4	−162.11	−147.24	−132.39	−156.03	−147.19	−140.90

Table 10. δD values for bulk specimens equilibrated with enriched− and depleted waters, as well as samples placed in an oven. Samples were then left to equilibrate with ambient water vapor for 1, 2, 4, and 8 hours.

were unable to measure laboratory water vapor compositions directly, but previous work shows a mean precipitation δD value of −111‰ for the Boise region (Tappa et al., 2016), and thus, assume laboratory water vapor is in equilibrium with water of that composition. To test whether labile H could be completely removed, sample aliquots were placed in a 70 ºC oven for 48 hours. Samples were then removed and exposed to laboratory conditions for 0, 1, 2, 4, and 8 hours and δD values were measured.

Results

Stable Hydrogen and Oxygen Isotope Compositions

From the 12 sub-sectioned teeth, two *Cervus elaphus* teeth, M-00-49 and M-00-59, from Yellowstone, WY had the lowest mean δD and $\delta^{18}O$ values of c. −160‰ and +15‰, respectively, whereas *Oryx gazelle* (O2120) and *Nanger granti* (GGK) from Kenya had the highest δD and $\delta^{18}O$ values of c. −135‰ and +34‰, respectively (Fig 10; Table 9). *Castor canadensis* (BTM) from Cañon City, CO, had anomalously high δD

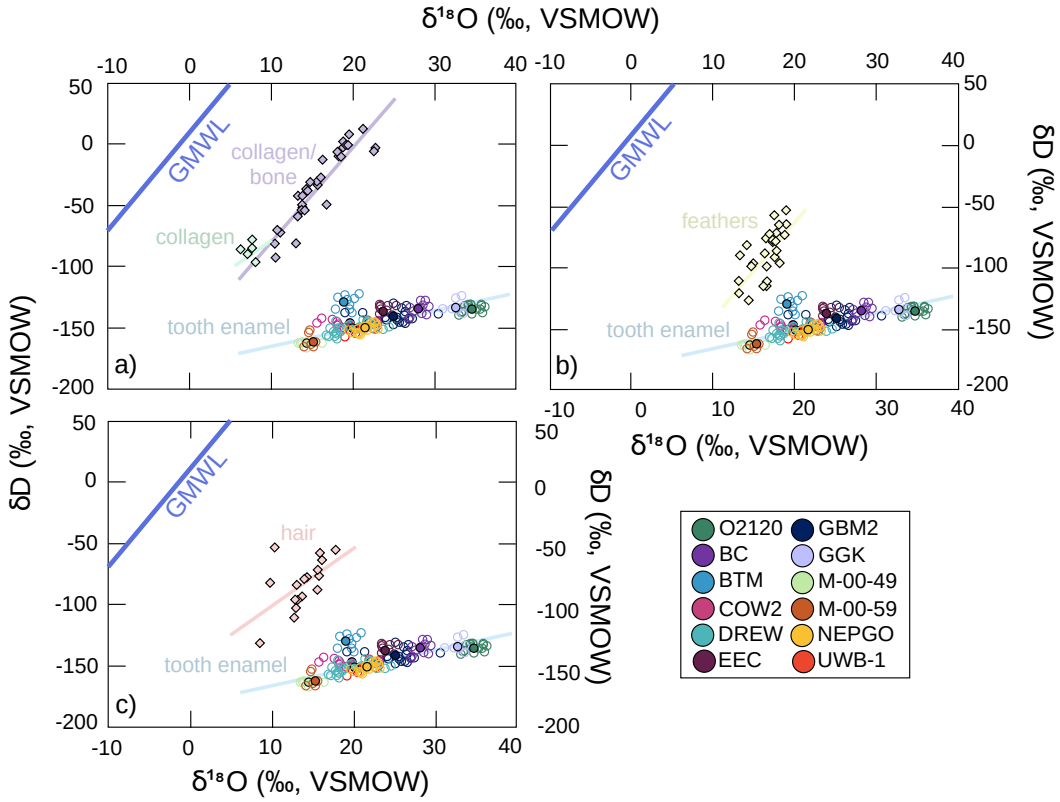

Figure 10. Herbivore tooth enamel δD vs. $\delta^{18}O$ (‰, VSMOW) for this study and previously published data for other organic materials. Opaque symbols represent mean tooth enamel compositions; semi-transparent symbols are intra-tooth δD and $\delta^{18}O$ values. a) Comparison with collagen δD and either collagen or bone $\delta^{18}O$ values (Cormie et al., 1994; Kirsanow and Tuross, 2011); b) comparison with hair δD and $\delta^{18}O$ (Ehleringer et al., 2008). c) Comparison to feather δD and $\delta^{18}O$ (Hobson et al., 2012).

values (c. −132‰), which are comparably to *Oryx gazelle* (O2120) and *Nanger granti* (GGK) values that reflect a warm, equatorial climate (Fig 10; Table 9)

For regressing mean isotope data for δD_{enamel} and $\delta^{18}O_{enamel}$ values, we used all data expect specimen BTM (*Castor canadensis*). This sample was excluded because beaver is semi-aquatic, and also because samples are susceptible to contamination from dentine. The resulting regression is:

$$\delta D\ (‰) = 1.80 \pm 0.26(\delta^{18}O) - 187 \pm 6‰ \qquad (R^2 = 0.84) \qquad \text{(Eq. 9)}$$

A slope of 1.8 is considerably shallower than the GMWL slope (c. 8.0).

Most local water δD values were estimated from the Online Isotope Precipitation Calculator ("OIPC," 2018; Johnson et al., 1991). The lowest tooth enamel δD values from Yellowstone, WY, correlate with the lowest local water δD values (−140‰), while the highest tooth enamel δD values from Kenya correspond with the highest local water δD values (+22‰; Fig 11; Table 9). A regression of δD_{enamel} vs. $\delta D_{local\ water}$ values yields:

$$\delta D_{enamel} = 0.19 \pm 0.05(\delta D_{precipitation}) - 131 \pm 4‰ \quad (R^2 = 0.71) \quad \text{(Eq. 10)}$$

The slope of this expression is considerably less than 1.0, which implies a very small dependence of measures enamel compositions on original source water composition.

Labile Hydrogen

Using NBS-30 biotite as a standard for hydrogen content [H], a regression of tooth enamel [H] vs. sample mass yields an average [H] of 0.93 wt%. A representative [H] for tooth enamel bioapatite (Driessens and Verbeeck, 1990) is 0.16 wt%.Thus, most H in our analyses must be derived from another source. In contrast, similar measurements and calculations for keratin (CBS) show that the measured slope of [H] vs. sample mass for hoof and hair keratin is the same as the predicted slope (Fig 12). That is, any labile

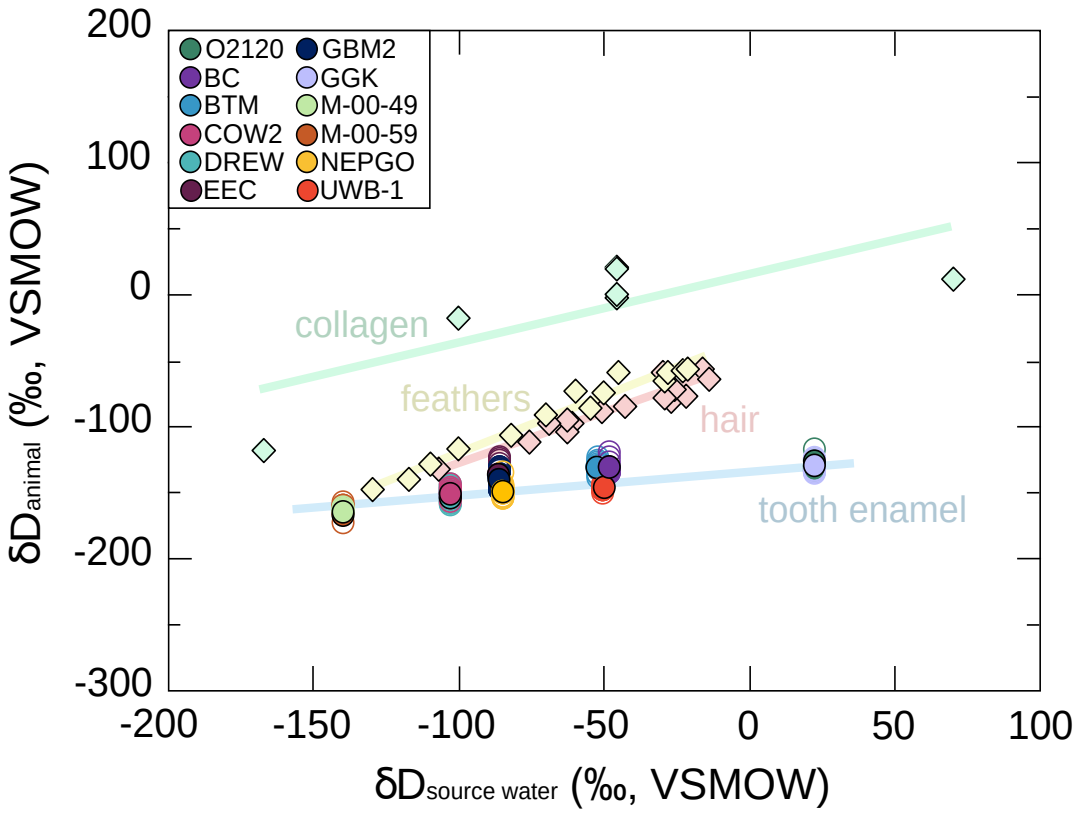

Figure 11. Tooth enamel δD values for serially sectioned samples vs. local water δD (‰, VSMOW; OIPC, 2018; Johnson et al., 1991). Opaque symbols represent mean tooth enamel compositions, while semi-transparent symbols are intra-tooth δD values. Data for collagen, hair and feathers are from Cormie et al. (1994), Ehleringer et al. (2008), and Hobson et al. (2012).

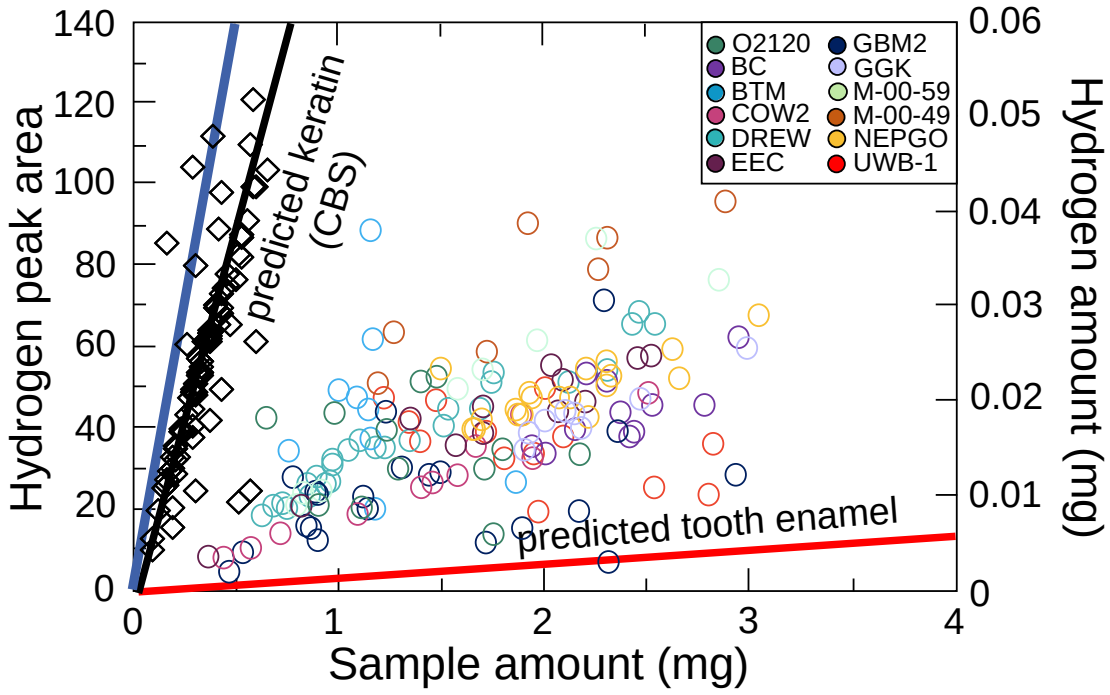

Figure 12. Mass of hydrogen (mg) vs. mass of sample (mg) for intra-tooth enamel (colored symbols) and caribou hoof standard (gray). Enamel data show excess mass (from adsorbed water) compared to predicted mass for enamel hydroxylapatite (red line; Driessens and Verbeeck, 1990). Keratin data show good correspondence between measured and expected masses (black line; Leon, 1972; Samata and Mastsuda, 1988). Blue line represents water.

[H] in keratin does not increase the total H content, but rather exchanges with structural H (Wassenaar and Hobson, 2003).

Equilibration Experiments

All apatite samples show anomalous isotope compositions for the t_0 experiment, with higher δD for samples equilibrated with high water δD values, and lower δD for samples equilibrated with low water δD values. All compositions shift dramatically towards an intermediate composition after 1 hour of exposure to laboratory air, then gradually converge with increasing time to a common, intermediate isotope composition, similar to local water (Fig 13). The absolute values of the t_0 data range widely, perhaps because of small differences in timing of analysis after removal, or differential access of laboratory air to samples after removal. Samples subjected to heating for 48 hours show an increase (equilibration with low δD_{water}) or decrease (high δD_{water}) of 10-30‰ with time and converge on a similar common δD value as for unheated samples.

Discussion

Hydrogen Isotopes in Tooth Enamel

A relatively high R^2 value (0.84) for the tooth enamel stable hydrogen vs. oxygen isotope compositions (Fig 10; Table 9) is expected because of the direct dependence of isotope compositions in animals on meteoric water δD and $\delta^{18}O$ values, which are highly correlated and form the GMWL (Craig, 1961; Dansgaard, 1964). It is well established that tooth enamel $\delta^{18}O$ values are a function of consumed waters, whether directly from surface water or plant material, which generally correlated with meteoric waters (Koch, 1998; MacFadden, 2000; Kohn and Cerling, 2002; Kohn and Dettman, 2007). Many

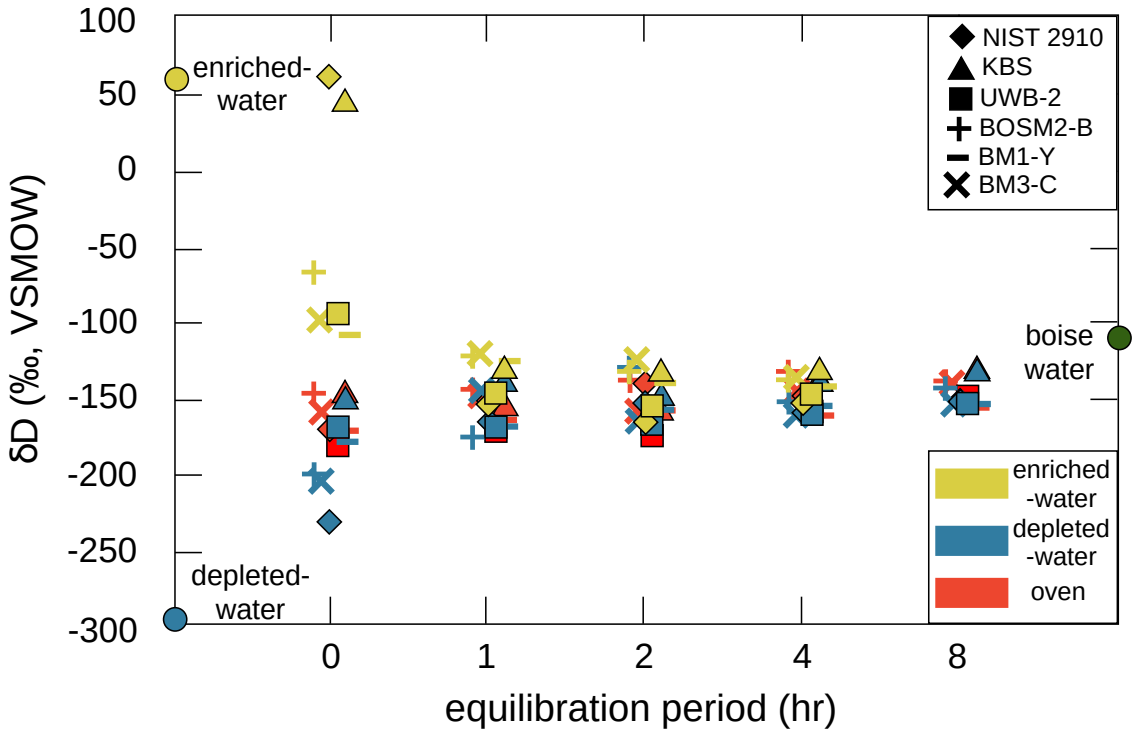

Figure 13. Tooth enamel δD values vs. time, showing rapid exchange of adsorbed water from laboratory air (steady-state compositions by 1-2 hours).

other biological materials also demonstrate a correlation between δD and $\delta^{18}O$ values (e.g. hair; collagen; (Cormie et al., 1994; Reynard and Hedges, 2008; Kirsanow and Tuross, 2011), but many of these regression have slopes more similar to that of the GMWL (i.e. 8.0; Fig 10).

The outlier data for *Castor canadensis* (BTM) may in part reflect its semiaquatic ecology. $\delta^{18}O$ values of aquatic mammals are consistently lower than their terrestrial counterparts (Bocherens et al., 1996; Clementz and Koch, 2001; Matson and Fox, 2010). Sample BTM does have lower tooth enamel $\delta^{18}O$ values than terrestrial specimens from areas with similar local water compositions (i.e. samples BC and UWB). However, the unusually high δD values from BTM probably reflect inadvertent sampling of dentine. *Castor canadensis* has thin enamel, and dentine is rich in collagen, which has higher δD values (Fig 10). A very small amount of collagen contamination (c. 2-4% by weight) would shift compositions towards collagen data (Fig 10). The intra-tooth δD and $\delta^{18}O$ regression for BTM also mirrors that of collagen, suggesting contamination (Fig 10).

The moderate correlation between tooth enamel and local meteoric water δD values (R^2 = 0.71), suggest tooth enamel captures stable hydrogen isotopic variation between specific regions (Fig 11; Table 8). For example, the highest tooth enamel δD values for O2120 and GGK correspond with the highest local water values, while the lowest tooth enamel δD values from M-00-49 and M-00-59 correspond with the lowest meteoric water values. The correlation might improve if direct measurements of local water were gathered. More importantly, the large isotopic range in local water between Kenya (+22‰) and Yellowstone, WY (−140‰) would predict a large range in tooth enamel δD values (~150‰), but specimens from these isotopically disparate localities

differ only ~35‰ (Fig 10 and 11; Table 8). The reason for this low variability is that most of the H analyzed is not from tooth enamel.

Labile Hydrogen

For enamel the predicted vs. measured regression of [H] vs. sample mass show that only ~20% of measure [H] can be ascribed as structural [H]. The difference between δD values for samples that have been exposed to water with either very high or low δD values suggest that the source is adsorbed water. If so, the data of Holobinko et al. (2011) should have been offset to higher δD values than ours because their data were measured in a geographic region with higher local water δD values (c. −48‰; Dundee, UK; "OIPC," 2018), Assuming the same ~80% contribution from local water vapor, their data should plot approximately 50‰ higher than ours ("OIPC," 2018). Relative to our regression, their data plot approximately 30‰ higher, broadly consistent with expectations.

In contrast to enamel, keratin shows no evidence for additional, adsorbed [H], as data for hooves show the expected trend for [H] vs. sample weight (Fig 12). These organic substrates do contain exchangeable H (Epstein et al., 1976; Schimmelmann, 1991; Cormie et al., 1994), but in the context of adsorbed water no reevaluation of isotope compositions is required beyond what has already been published (see Wassenaar and Hobson, 2000).

In comparison to uptake of adsorbed water in other materials, tooth enamel behaves somewhat like clays. Swelling clays, such as smectite, water adsorbs onto clay surfaces and into interlayer sites (i.e. between structural sheets) on the timescales of hours, but heating to >200 ºC removes most adsorbed water (Moum and Rosenqvist,

1958; Savin and Epstein, 1970; Savin and Hsieh, 1998). Like tooth enamel, however, swelling clays will regain adsorbed water if they are exposed to ambient laboratory conditions. For this reason, pretreatment of swelling clays for isotope measurements can include exchange of replacement of adsorbed water with Na^+ (Tabor et al., 2004).

Equilibration Experiments

With increasing duration of exposure, the time-series samples approach a steady-state δD value 30 to 40‰ lower than local water, similar to measured compositions of tooth enamel that were collected 8 hours (this study) to 7 days (Holobinko et al., 2011) after equilibrating with isotopically anomalous waters. The final composition for all analyses is likely governed by sample-specific biogenic and adsorbed water compositions that reflect equilibration partitioning between ambient water vapor and adsorbed water. Because we do not know the compositions of either biogenic or adsorbed components independently, we cannot infer any fractions quantitatively. However, we would except analyses to evolve towards a common composition, rapidly at first, and more slowly later. Zero-time or t_0 experiments show quite different compositions compared to final compositions, while t_1 experiments are more similar, but are still resolvably different (Fig 13; Table 10). Complete equilibration is attained for the t_2, t_4 and t_8 experiments. We interpret the more extreme compositions of synthetic hydroxyl apatite (NIST-2910) and fossil bone (KBS) to reflect slower equilibration of materials that are physically different from modern tooth enamel. Because a) equilibration times are short, b) the amount of H is hosted in the tooth enamel is small, and c) the compositions of water vapor in different laboratories is different, it is virtually impossible to determine original biogenic compositions from powdered tooth enamel with good resolution. Analysis of un-

powdered enamel might show less dependence on adsorbed water, but because of small amounts of included proteins, compositions would not likely reflect tooth enamel apatite.

In some organic substrates, full equilibration between exchangeable (not adsorbed) hydrogen and water vapor also occurs in hours, for example 1 to 2 hours for keratin from butterfly wings and quail eggs (Wassenaar and Hobson, 2000). However, exchangeable hydrogen in horse hair (keratin), that was subjected to isotopically unique water reaches full equilibration only in c. 4 days (Bowen et al., 2005a). In this context, tooth enamel responds more rapidly than other substrates because the dominant exchange component is adsorbed water.

Heating Experiments

Tooth enamel δD values, measure upon immediate removal from the oven, were lower than compositions from samples, which were equilibrated at ambient temperatures (Fig 13; Table 10). However, low tooth enamel δD values at the t_0 experiment do not reflect removal of adsorbed water, but likely result from a larger temperature-dependent partition coefficient. As with depleted- and enriched water experiments, full equilibration with laboratory water vapor is reached with 1 to 2 hours (Fig 13; Table 10).

Conclusion

Tooth enamel δD and $\delta^{18}O$ values display a strong correlation ($R^2 = 0.84$), while tooth enamel δD and local water δD values display a moderate correlation ($R^2 = 0.71$). Comparison of H contents and sample weights indicate a large component of labile hydrogen, likely from adsorbed water. Time series experiment for unheated and heated samples show that full equilibration with ambient water vapor occurs within 1 to 2 hours, but also imply a temperature dependence to the isotope composition of the adsorbed

water. Rapid equilibration, but large amounts of adsorbed hydrogen of different compositions in different laboratories indicate that original biogenic compositions of tooth enamel apatite cannot be recovered precisely.

REFERENCES

Albright, L.B., Woodburne, M.O., Fremd, T.J., Swisher III, C.C., MacFadden, B.J., Scott, G.R., 2008. Revised chronostratigraphy and biostratigraphy of the John Day Formation (Turtle Cove and Kimberly Members), Oregon, with implications for updated calibration of the Arikareean North American Land Mammal Age. J. Geol. 116, 211–237. doi:10.1086/587650

Allen, B.D., Anderson, R.Y., 1993. Evidence from Western North America for rapid shifts in climate during the Last Glacial Maximum. Science 260, 1920–1923. doi:10.1126/science.260.5116.1920

Alley, R.B., Meese, D.A., Shuman, C.A., Gow, A.J., Taylor, K.C., Grootes, P.M., White, J.W.C., Ram, M., Waddington, E.D., Mayewski, P.A., Zielinski, G.A., 1993. Abrupt increase in Greenland snow accumulation at the end of the Younger Dryas event. Nature 362, 527–529. doi:10.1038/362527a0

Andrews, J.E., Brasier, A.T., 2005. Seasonal records of climatic change in annually laminated tufas: short review and future prospects. J. Quat. Sci. 20, 411–421. doi:10.1002/jqs.942

Andrews, J.E., Pedley, H.M., Dennis, P.F., 1994. Stable isotope record of palaeoclimatic change in a British Holocene tufa. The Holocene 4, 349–355. doi:10.1177/095968369400400402

Andrews, J.E., Riding, R., Dennis, P.F., 1997. The stable isotope record of environmental and climatic signals in modern terrestrial microbial carbonates from Europe. Palaeogeogr. Palaeoclimatol. Palaeoecol. 129, 171–189. doi:10.1016/S0031-0182(96)00120-4

Asmerom, Y., Polyak, V.J., Burns, S.J., 2010. Variable winter moisture in the southwestern United States linked to rapid glacial climate shifts. Nat. Geosci. 3,

114–117. doi:10.1038/ngeo754

Ayliffe, L.K., Chivas, A.R., 1990. Oxygen isotope composition of the bone phosphate of Australian kangaroos: Potential as a palaeoenvironmental recorder. Geochim. Cosmochim. Acta 54, 2603–2609. doi:10.1016/0016-7037(90)90246-H

Barreda, V., Palazzesi, L., 2007. Patagonian vegetation turnovers during the Paleogene-early Neogene: origin of arid-adapted floras. Bot. Rev. 73, 31–50. doi:10.1663/0006-8101(2007)73[31:PVTDTP]2.0.CO;2

Barry, T.L., Self, S., Kelley, S.P., Reidel, S., Hooper, P., Widdowson, M., 2010. New $^{40}Ar/^{39}Ar$ dating of the Grande Ronde lavas, Columbia River Basalts, USA: Implications for duration of flood basalt eruption episodes. Lithos 118, 213–222.

Bartoli, G., Hönisch, B., Zeebe, R.E., 2011. Atmospheric CO_2 decline during the Pliocene intensification of Northern Hemisphere glaciations. Paleoceanography 26, PA4213. doi:10.1029/2010PA002055

Bearhop, S., Furness, R.W., Hilton, G.M., Votier, S.C., Waldron, S., 2003. A forensic approach to understanding diet and habitat use from stable isotope analysis of (avian) claw material. Funct. Ecol. 17, 270–275. doi:10.1046/j.1365-2435.2003.00725.x

Beerling, D.J., Royer, D.L., 2011. Convergent Cenozoic CO_2 history. Nat. Geosci. 4, 418–420. doi:10.1038/ngeo1186

Benson, L.V., Currey, D.R., Dorn, D., 1990. Chronology of expansion and contraction of four Great Basin lake systems during the past 35,000 years. Palaeogeogr. Palaeoclimatol. Palaeoecol. 78, 241–286. doi:10.1016/0031-0182(90)90217-U

Bereiter, B., Lüthi, D., Siegrist, M., Schüpbach, S., Stocker, T.F., Fischer, H., 2012. Mode change of millennial CO_2 variability during the last glacial cycle associated with a bipolar marine carbon seesaw. Proc. Natl. Acad. Sci. U. S. A. 109, 9755–60. doi:10.1073/pnas.1204069109

Bestland, E.A., Forbes, M.S., Krull, E.S., Retallack, G.J., Fremd, T., 2008. Stratigraphy, paleopedology, and geochemistry of the middle Miocene Mascall Formation (type area, central Oregon, USA). PaleoBios 28, 41–61.

Bestland, E.A., Krull, E.S., 1997. Mid-Miocene climatic optimum recorded in paleosols from the Mascall Formation (Oregon), in: Geological Society of America. p. 5.

Betancourt, J.L., Aasen Rylander, K., Peñalba, C., McVickar, J.L., 2001. Late Quaternary vegetation history of Rough Canyon, south-central New Mexico, USA. Palaeogeogr. Palaeoclimatol. Palaeoecol. 165, 71–95. doi:10.1016/S0031-0182(00)00154-1

Betancourt, J.L., Latorre, C., Rech, J.A., Quade, J., Rylander, K.A., 2000. A 22,000-year record of monsoonal precipitation from northern Chile's Atacama Desert. Science 289, 1542–1546.

Birchnall, J., O'Connell, T.C., Heaton, T.H.E., Hedges, R.E.M., 2005. Hydrogen isotope ratios in animal body protein reflect trophic level. J. Anim. Ecol. 74, 877–881. doi:10.1111/j.1365-2656.2005.00979.x

Bocherens, H., Koch, P.L., Mariotti, A., Geraads, D., Jaeger, J.-J., 1996. Isotopic biogeochemistry ($\delta^{13}C$, $\delta^{18}O$) of mammalian enamel from African Pleistocene hominid sites. Palaios 11, 306–318. doi:10.2307/3515241

Bohme, M., 2003. The Miocene Climatic Optimum: evidence from ectothermic vertebrates of Central Europe. Palaeogeogr. Palaeoclimatol. Palaeoecol. 195, 389–401. doi:10.1016/S0031-0182(03)00367-5

Bohme, M., Winklhofer, M., Ilg, A., 2011. Miocene precipitation in Europe: temporal trends and spatial gradients. Palaeogeogr. Palaeoclimatol. Palaeoecol. 304, 212–218.

Bond, G., Broecker, W., Johnsen, S., McManus, J., Labeyrie, L., Jouzel, J., Bonani, G., 1993. Correlations between climate records from North Atlantic sediments and Greenland ice. Nature 365, 143–147. doi:10.1038/365143a0

Bowen, G.J., Chesson, L., Nielson, K., Cerling, T.E., Ehleringer, J.R., 2005a. Treatment methods for the determination of $\delta^{2}H$ and $\delta^{18}O$ of hair keratin by continuous-flow isotope-ratio mass spectrometry. Rapid Commun. Mass Spectrom. 19, 2371–2378. doi:10.1002/rcm.2069

Bowen, G.J., Ehleringer, J.R., Chesson, L.A., Thompson, A.H., Podlesak, D.W., Cerling, T.E., 2008. Dietary and Physiological Controls on the Hydrogen and Oxygen Isotope Ratios of Hair from Mid-20th Century Indigenous Populations. Am. J. Phys.

Antropol. 139, 494–504. doi:10.1002/ajpa.21008

Bowen, G.J., Wassenaar, L.I., Hobson, K.A., 2005b. Global application of stable hydrogen and oxygen isotopes to wildlife forensics. Oecologia 143, 337–348. doi:10.2307/20062256

Braconnot, P., Harrison, S.P., Kageyama, M., Bartlein, P.J., Masson-Delmotte, V., Abe-Ouchi, A., Otto-Bliesner, B., Zhao, Y., 2012. Evaluation of climate models using palaeoclimatic data. Nat. Publ. Gr. doi:10.1038/NCLIMATE1456

Braconnot, P., Otto-Bliesner, B., Harrison, S., Joussaume, S., Peterchmitt, J.-Y., Abe-Ouchi, A., Crucifix, M., Driesschaert, E., Fichefet, T., Hewitt, C.D., Kageyama, M., Kitoh, A., Lané, A., Loutre, M.-F., Marti, O., Merkel, U., Ramstein, G., Valdes, P., Weber, S.L., Yu, Y., Zhao, Y., 2007. Results of PMIP2 coupled simulations of the Mid-Holocene and Last Glacial Maximum – Part 1: experiments and large-scale features. Clim. Past 3, 261–277.

Brasier, A.T., Andrews, J.E., Marca-Bell, A.D., Dennis, P.F., 2010. Depositional continuity of seasonally laminated tufas: Implications for $\delta^{18}O$ based palaeotemperatures. Glob. Planet. Change 71, 160–167. doi:10.1016/j.gloplacha.2009.03.022

Bravo-Cuevas, V.M., Morales-García, N.M., Barrón-Ortiz, C.R., Theodor, J.M., Cabral-Perdomo, M.A., 2017. Canid coprolites from the late Pleistocene of Hidalgo, Central Mexico: Importance for the carnivore record of North America. Ichnos 24, 239–249. doi:10.1080/10420940.2016.1270209

Brook, G.A., Ellwood, B.B., Railsback, L.B., Cowart, J.B., 2006. A 164 ka record of environmental change in the American Southwest from a Carlsbad Cavern speleothem. Palaeogeogr. Palaeoclimatol. Palaeoecol. 237, 483–507. doi:10.1016/J.PALAEO.2006.01.001

Bruch, A.A., Utescher, T., Mosbrugger, V., NECLIME members, 2011. Precipitation patterns in the Miocene of Central Europe and the development of continentality. Palaeogeogr. Palaeoclimatol. Palaeoecol. 304, 202–211. doi:10.1016/J.PALAEO.2010.10.002

Campbell, C.D., Sage, R.F., Kocacinar, F., Way, D.A., 2005. Estimation of the whole-plant CO_2 compensation point of tabacco (*Nicotiana tabacum* L.). Glob. Chang. Biol. 11, 1956–1967. doi:10.1111/j.1365-2486.2005.01045.x

Carrasco, M.A., Barnosky, A.D., Kraatz, B.P., Davis, E.B., 2009. The Miocene mammal mapping project (Miomap): An online database of Arikareean through Hemphillian fossil mammals. Bull. Carnegie Museum Nat. Hist. doi:10.2992/0145-9058(2007)39[183:TMMMPM]2.0.CO;2

Cerling, T.E., Harris, J.M., 1999. Carbon isotope fractionation between diet and bioapatite in ungulate mammals and implications for ecological and paleoecological studies. Oecologia 120, 347–363. doi:10.1007/s004420050868

Cerling, T.E., Quade, J., Wang, Y., 1994. Expansion and emergence of C_4 plants. Nature 371, 112–113. doi:10.1038/371112a0

Chaftez, H.S., Utech, N.M., Fitzmaurice, S.P., 1991. Difference in the $\delta^{18}O$ and $\delta^{13}C$ signatures of seasonal laminae comprising travertine stromatolites. J. Sediment. Res. 61, 1015–1028.

Clementz, M.T., 2012. New insights from old bones: Stable isotope analysis of fossil mammals. J. Mammal. 93, 368–380. doi:10.1644/11-MAMM-S-179.1

Clementz, M.T., Koch, P.L., 2001. Differentiating aquatic mammal habitat and foraging ecology with stable isotopes in tooth enamel. Oecologia 129, 461–472. doi:10.1007/s004420100745

COHMAP members, 1988. Climatic changes of the last 18,000 years: observations and model simulations. Science 241, 1043–1052. doi:10.1126/science.241.4869.1043

Collatz, G.J., Berry, J.A., Clark, J.S., 1998. Effects of climate and atmospheric CO_2 partial pressure on the global distribution of C_4 grasses: present, past, and future. Oecologia 114, 441–454. doi:10.1007/s004420050468

Connin, S.L., Betancourt, J., Quade, J., 1998. Late Pleistocene C_4 plant dominance and summer rainfall in the southwestern United States from isotopic study of herbivore teeth. Quat. Res. 50, 179–193.

Coplen, T.B., 2007. Calibration of the calcite–water oxygen-isotope geothermometer at Devils Hole, Nevada, a natural laboratory. Geochim. Cosmochim. Acta 71, 3948–3957. doi:10.1016/J.GCA.2007.05.028

Cormie, A.B., Luz, B., Schwarcz, H.P., 1994. Relationship between the hydrogen and oxygen isotopes of deer bone and their use in the estimation of relative humidity. Geochim. Cosmochim. Acta 58, 3439–3449. doi:10.1016/0016-7037(94)90097-3

Craig, H., 1961. Isotopic variations in meteoric waters. Science 133, 1702–1703.

Cramer, B.S., Miller, K.G., Barrett, P.J., Wright, J.D., 2011. Late Cretaceous–Neogene trends in deep ocean temperature and continental ice volume: Reconciling records of benthic foraminiferal geochemistry ($\delta^{18}O$ and Mg/Ca) with sea level history. J. Geophys. Res. 116, C12023. doi:10.1029/2011JC007255

Cross, T., Taggart, R.E., 1982. Cause of short-term sequential changes in fossil plant assemblages: some considerations based on Miocene flora of the Northwest. Annu. Missouri Bot. Gard. 69, 676–734.

Crowley, B.E., Koch, P.L., Davis, E.B., 2008. Stable isotope constraints on the elevation history of the Sierra Nevada Mountains, California. Geol. Soc. Am. Bull. 120, 588–598. doi:10.1130/B26254.1

Cryan, P.M., Bogan, M.A., Rye, R.O., Landis, G.P., Kester, C.L., 2004. Stable hydrogen isotope analysis of bat hair as evidence for seasonal molt and long-distance migration. J. Mammal. 85, 995–1001. doi:10.1644/BRG-202

Damuth, J., Janis, C.M., 2011. On the relationship between hypsodonty and feeding ecology in ungulate mammals, and its utility in palaeoecology. Biol. Rev. 86, 733–758. doi:10.1111/j.1469-185X.2011.00176.x

Dansgaard, W., 1964. Stable isotopes in precipitation. Tellus 16, 436–468. doi:10.3402/tellusa.v16i4.8993

DeNiro, M.J., Epstein, S., 1978. Influence of diet on the distribution of carbon isotopes in animals. Geochim. Cosmochim. Acta 42, 495–506. doi:DO16-7037/78/0501-0495

Diefendorf, A.F., Mueller, K.E., Wing, S.L., Koch, P.L., Freeman, K.H., 2010. Global

patterns in leaf $\delta^{13}C$ discrimination and implications for studies of past and future climate. Proc. Natl. Acad. Sci. U. S. A. 107, 5738–43. doi:10.1073/pnas.0910513107

Dippery, J.K., Tissue, D.T., Thomas, R.B., Strain, B.R., 1995. Effects of Low and Elevated CO_2 on C_3 and C_4 Annuals. I. Growth and Biomass Allocation. Oecologia. doi:10.2307/4220846

Domingo, L., Prado, J.L., Alberdi, M.T., 2012. The effect of paleoecology and paleobiogeography on stable isotopes of Quaternary mammals from South America. Quat. Sci. Rev. 55, 103–113. doi:10.1016/J.QUASCIREV.2012.08.017

Downing, K.F., 1992. Biostratigraphy, taphonomy, and paleoecology of vertebrates from the Sucker Creek Formation (Miocene) of southeastern Oregon. University of Arizona.

Downs, T., 1956. The Mascall fauna from the Miocene of Oregon. Univ. Calif. Publ. Geol. Sci. 31, 199–354.

Drewicz, A.E., Kohn, M.J., 2018. Stable isotopes in large herbivore tooth enamel capture a mid-Miocene precipitation spike in the interior Pacific Northwest. Palaeogeogr. Palaeoclimatol. Palaeoecol. 495. doi:10.1016/j.palaeo.2017.11.022

Driessens, F.C., Verbeeck, R., 1990. Biominerals. CRC Press.

Drury, A.J., John, C.M., Shevenell, A.E., 2016. Evaluating climatic response to external radiative forcing during the late Miocene to early Pliocene: New perspectives from eastern equatorial Pacific (IODP U1338) and North Atlantic (ODP 982) locations. Paleoceanography 31, 167–184. doi:10.1002/2015PA002881

Eardley, A.J., Gvosdetsky, V., 1960. Analysis of Pleistocene core from Great Salt Lake. Geol. Soc. Am. Bull. 71, 1323–1344.

Edwards, R., Cheng, H., Cutler, K., Richards, D., Edwards, R.L., Cutler, K.B., Gallup, C.D., 2014. Geochemical evidence for Quaternary sea-level changes. Ocean. Mar. Geochemistry 8, 355–372. doi:10.1016/B978-0-08-095975-7.00613-6

Ehleringer, J.R., Bowen, G.J., Chesson, L.A., West, A.G., Podlesak, D.W., Cerling, T.E.,

2008. Hydrogen and oxygen isotope ratios in human hair are related to geography. Proc. Natl. Acad. Sci. U. S. A. 105, 2788–93. doi:10.1073/pnas.0712228105

Epstein, S., Yapp, C.J., Hall, J.H., 1976. The determination of the D/H ratio of non-exchangeable hydrogen in cellulose extracted from aquatic and land plants. Science 30, 241–251. doi:10.1016/0012-821X(76)90251-X

Estep, M.F., Dabrowski, H., 1980. Tracing food webs with stable hydrogen isotopes. Science 209, 1537–1538.

Feranec, R.S., MacFadden, B.J., 2006. Isotopic discrimination of resource partitioning among ungulates in C_3-dominated communities from the Miocene of Florida and California. Paleobiology 32, 191–205. doi:10.1666/05006.1

Fields, P.F., 1996. A Throchodendron infructescence from the 15 Ma Succor Creek flora in Oregon: a geographic and possibly temporal range extension. Am. J. Bot. 83, 531.

Flower, B.P., Kennett, J.P., 1993. Middle Miocene Ocean-Climate Transition - high-resolution oxygen and carbon isotopic records from Deep-Sea Drilling Project Site 588a, Southwest Pacific. Paleoceanography 8, 811–843.

Ford, T.D., Pedley, H.M., 1996. A review of tufa and travertine deposits of the world. Earth-Science Rev. 41, 117–175. doi:10.1016/S0012-8252(96)00030-X

Foster, G.L., Lear, C.H., Rae, J.W., 2012. The evolution of pCO_2, ice volume and climate during the middle Miocene. Earth Planet. Sci. Lett. 341, 243–254.

Fox-Dobbs, K., Leonard, J.A., Koch, P.L., 2008. Pleistocene megafauna from eastern Beringia: Paleoecological and paleoenvironmental interpretations of stable carbon and nitrogen isotope and radiocarbon records. Palaeogeogr. Palaeoclimatol. Palaeoecol. 261, 30–46. doi:10.1016/J.PALAEO.2007.12.011

Fremd, T.J., Bestland, E.A., Retallack, G.J., 1997. John Day Basin paleontology: Field trip guide and road log, 1994 Society of Vertebrate Paleontology Annual Meeting. Northwest Interpret. Assoc. 80.

Fremd, T.J., Bestland, E.A., Retallack, G.J., 1996. John Day Basin paleontology. Northwest Interpret. Assoc. Seattle, WA 1–80.

Freyer, H.D., Belacy, N., 1983. $^{13}C/^{12}C$ records in northern hemispheric trees during the past 500 years—Anthropogenic impact and climatic superpositions. J. Geophys. Res. 88, 6844–6852. doi:10.1029/JC088iC11p06844

Friedman, I., Smith, G.I., Gleason, J.D., Warden, A., Harris, J.M., 1992. Stable isotope composition of waters in southeastern California 1. Modem precipitation. J. Geophys. Res. 97, 5795–5812.

Friedman, I., Smith, G.I., Johnson, C.A., Moscati, R.J., 2002. Stable isotope compositions of waters in the Great Basin, United States 2. Modern precipitation. J. Geophys. Res. 107, 4401. doi:10.1029/2001JD000566

Galloway, R.W., 1970. The full-glacial climate in the southwestern United States. Ann. Assoc. Am. Geogr. 60, 245–256. doi:10.1111/j.1467-8306.1970.tb00719.x

Gihad, E.A., 1993. Utilization of high salinity tolerant plants and saline water by desert animals, in: Towards the Rational Use of High Tolerant Plants. Springer, Dordrecht, pp. 443–447. doi:10.1007/978-94-011-1858-3_45

Gilbert, K.G., 1890. Lake Bonneville, 1st ed. US Government Printing Office.

Goldner, A., Herold, N., Huber, M., 2014. The challenge of simulating the warmth of the mid-Miocene climatic optimum in CESM1. Clim. Past 10, 523–536. doi:10.5194/cp-10-523-2014

Greenop, R., Foster, G.L., Wilson, P.A., Lear, C.H., 2014. Middle Miocene climate instability associated with high-amplitude CO_2 variability. Paleoceanography 29, 845–853. doi:10.1002/2014PA002653

Grootes, P.M., Stuiver, M., 1997. Oxygen$^{18/16}$ variability in Greenland snow and ice with 10^{-3} - to 10^{-5}-year time resolution. J. Geophys. Res. Ocean. 102, 26455–26470. doi:10.1029/97JC00880

Hamon, N., Sepulchre, P., Donnadieu, Y., Henrot, A.-J., Francois, L., Jaeger, J.-J., Ramstein, G., 2012. Growth of subtropical forests in Miocene Europe: The roles of carbon dioxide and Antarctic ice volume. Geology 40, 567–570. doi:10.1130/G32990.1

Haynes, C.V., Wormington, H.M., Ellis, D., 1967. Quaternary geology of the Tule Springs Area Clark County, Nevada. Pleistocene Stud. South. Nevada Nevada State Museum Anthropol. Pap. 13, 1–104.

Henrot, A.-J., François, L., Favre, E., Butzin, M., Ouberdous, M., Munhoven, G., 2010. Effects of CO_2, continental distribution, topography and vegetation changes on the climate at the Middle Miocene: a model study. Clim. Past 6, 675–694. doi:10.5194/cp-6-675-2010

Henrot, A.-J., Utescher, T., Erdei, B., Dury, M., Hamon, N., Ramstein, G., Krapp, M., Herold, N., Goldner, A., Favre, E., Munhoven, G., Francois, L., 2017. Middle Miocene climate and vegetation models and their validation with proxy data. Palaeogeogr. Palaeoclimatol. Palaeoecol. 467, 95–119. doi:10.1016/J.PALAEO.2016.05.026

Herbert, T.D., Lawrence, K.T., Tzanova, A., Peterson, L.C., Caballero-Gill, R., Kelly, C.S., 2016. Late Miocene global cooling and the rise of modern ecosystems. Nat. Geosci. 9, 843–847. doi:10.1038/ngeo2813

Herold, N., Huber, M., Muller, R.D., 2011. Modeling the miocene climatic optimum. Part I: Land and atmosphere. J. Clim. 24, 6353–6373. doi:10.1175/2011JCLI4035.1

Herold, N., Seton, M., Müller, R.D., You, Y., Huber, M., 2008. Middle Miocene tectonic boundary conditions for use in climate models. Geochemistry, Geophys. Geosystems 9, 1–10. doi:10.1029/2008GC002046

Higgins, P., MacFadden, B.J., 2009. Seasonal and geographic climate variabilities during the Last Glacial Maximum in North America: applying isotopic analysis and macrophysical climate models. Palaeogeogr. Palaeoclimatol. Palaeoecol. 283, 15–27. doi:10.1016/J.PALAEO.2009.08.015

Hinojasa, L.F., Villagran, C., 2005. Did South American mixed paleofloras evolve under thermal equability or in the absence of an effective Andean barrier during the Cenozoic? Palaeogeogr. Palaeoclimatol. Palaeoecol. 217, 1–23. doi:10.1016/J.PALAEO.2004.11.013

Hobson, K.A., Van Wilgenburg, S.L., Wassenaar, L.I., Larson, K., 2012. Linking

hydrogen (δ^2H) isotopes in feathers and precipitation: sources of variance and consequences for assignment to isoscapes. PLoS One 7, e35137. doi:10.1371/journal.pone.0035137

Hobson, K.A., Wassenaar, L.I., 2018. Tracking animal migration with stable isotopes. Academic Press.

Hobson, K.A., Wassenaar, L.I., Taylor, O.R., 1999. Stable isotopes (δD and $\delta^{13}C$) are geographic indicators of natal origins of monarch butterflies in eastern North America. Oecologia 20, 397–404.

Holbourn, A., Kuhnt, W., Clemens, S., Prell, W., Andersen, N., 2013. Middle to late Miocene stepwise climate cooling: Evidence from a high-resolution deep water isotope curve spanning 8 million years. Paleoceanography 28, 688–699. doi:10.1002/2013PA002538

Holbourn, A., Kuhnt, W., Kochhann, K.G.D., Andersen, N., Sebastian Meier, K.J., 2015. Global perturbation of the carbon cycle at the onset of the Miocene Climatic Optimum. Geology 43, 123–126. doi:10.1130/G36317.1

Holbourn, A., Kuhnt, W., Lyle, M., Schneider, L., Romero, O., Andersen, N., 2014. Middle Miocene climate cooling linked to intensification of eastern equatorial Pacific upwelling. Geology 42, 19–22. doi:10.1130/G34890.1

Holbourn, A., Kuhnt, W., Schulz, M., Flores, J.-A., Andersen, N., 2007. Orbitally-paced climate evolution during the middle Miocene "Monterey" carbon-isotope excursion. Earth Planet. Sci. Lett. 261, 534–550. doi:10.1016/j.epsl.2007.07.026

Holmgren, C.A., Betancourt, J.L., Rylander, K.A., 2009. A 36,000-yr vegetation history from the Peloncillo Mountains, southeastern Arizona, USA. Palaeo 240, 405–422. doi:10.1016/j.palaeo.2006.02.017

Holmgren, C.A., Norris, J., Betancourt, J.L., 2007. Inferences about winter temperatures and summer rains from the late Quaternary record of C_4 perennial grasses and C_3 desert shrubs in the northern Chihuahuan Desert. J. Quat. Sci. 22, 141–161. doi:10.1002/jqs.1023

Holobinko, A., Meier-augenstein, W., Kemp, H.F., Prowse, T., Ford, S.M., 2011. ^2H

stable isotope analysis of human tooth enamel: a new tool for forensic human provenancing? Rapid Commun. Mass Spectrom. 25, 910–916. doi:10.1002/rcm.4942

Hooper, P.R., Swanson, D.A., 1990. Geology of the Blue Mountains region of Oregon, Idaho, and Washington: Cenozoic geology of the Blue Mountains region. U. S. Geol. Surv. Prof. Pap. 1437, 63–99.

Hoppe, K.A., Amundson, R., Vavra, M., McClaran, M.P., Anderson, D.L., 2004. Isotopic analysis of tooth enamel carbonate from modern North American feral horses: implications for paleoenvironmental reconstructions. Palaeogeogr. Palaeoclimatol. Palaeoecol. 203, 299–311. doi:10.1016/S0031-0182(03)00688-6

Hunt, R.M.J., Stepleton, E., 2004. Geology and paleontology of the Upper John Day Beds, John Day River Valley, Oregon: Lithostratigraphic and biochronologic revision in the Haystack Valley and Kimberly areas (Kimberly and Mt. Misery quadrangles). Bull. Am. Museum Nat. Hist. 282, 1–90. doi:10.1206/0003-0090(2004)282<0001:GAPOTU>2.0.CO;2

Ihlenfeld, C., Norman, M.D., Gagan, M.K., Drysdale, R.N., Maas, R., Webb, J., 2003. Climatic significance of seasonal trace element and stable isotope variations in a modern freshwater tufa. Geochim. Cosmochim. Acta 6, 2341–2357. doi:10.1016/S0016-7037(02)01344-3

Indermühle, A., Monnin, E., Stauffer, B., Stocker, T.F., Wahlen, M., 2010. Atmospheric CO_2 concentration from 60 to 20 kyr BP from the Taylor Dome Ice Core, Antarctica. Geophys. Res. Lett. 27, 735–738. doi:10.1029/1999GL010960

Janis, C.M., 2008. An evolutionary history of browsing and grazing ungulates, The ecology of browsing and grazing. Springer, Berlin, Heidelberg. doi:10.1007/978-3-540-72422-3_2

Janis, C.M., Damuth, J., Theodor, J.M., 2002. The origins and evolution of the North American grassland biome: the story from the hoofed mammals. Palaeogeogr. Palaeoclimatol. Palaeoecol. 177, 183–198. doi:10.1016/S0031-0182(01)00359-5

Jasechko, S., 2016. Late-Pleistocene precipitaiton $\delta^{18}O$ interpolated across the global

landmass. Geochemistry, Geophys. Geosystems 17, 3274–3288. doi:10.1002/2016GC006400

Jefferson, G.T., MacDonald, H.G., Akersten, W.A., Miller, S.J., 2002. Catalogue of late Pleistocene and Holocene fossil vertebrates from Idaho. whereas...papers veterbrate Paleontol. Idaho Honor John A. White 2, 157–192.

Johnson, T.C., Halfman, J.D., Showers, W.J., 1991. Paleoclimate of the past 4000 years at Lake Turkana, Kenya, based on the isotopic composition of authigenic calcite. Palaeogeogr. Palaeoclimatol. Palaeoecol. 85, 189–198. doi:10.1016/0031-0182(91)90158-N

Jones, C., Robertson, E., Arora, V., Friedlingstein, P., Shevliakova, E., Bopp, L., Brovkin, V., Hajima, T., Kato, E., Kawamiya, M., Liddicoat, S., Lindsay, K., Reick, C.H., Roelandt, C., Segschneider, J., Tjiputra, J., 2013. Twenty-first-century compatible CO_2 emissions and airborne fraction simulated by CMIP5 earth system models under four representative concentration pathways. J. Clim. 26, 4398–4413. doi:10.1175/JCLI-D-12-00554.1

Jordan, B.T., Grunder, A.L., Duncan, R.A., Deino, A.L., 2004. Geochronology of age-progressive volcanism of the Oregon High Lava Plains: Implications for the plume interpretation of Yellowstone. J. Geophys. Res. Solid Earth 109, 1–19. doi:10.1029/2003JB002776

Kano, A., Fujii, H., 2000. Origin of the gross morphology and internal texture of tufas of Shirokawa Town, Ehime Prefecture, southwest Japan. J. Geol. Soc. Japan 106, 397–412. doi:10.5575/geosoc.106.397

Keeley, J.E., Rundel, P.W., 2005. Fire and the Miocene expansion of C_4 grasslands. Ecol. Lett. doi:10.1111/j.1461-0248.2005.00767.x

Kelly, T.S., 1998. New middle Miocene equid crania from California and their implcations for the phylogeny of the Equini. Nat. Hist. Museum Los Angeles County, Contrib. Sci. 473, 1–43.

Kim, S.-T., O ’Neil, J.R., 1997. Equilibrium and nonequilibrium oxygen isotope effects in synthetic carbonates. Geochim. Cosmochim. Acta 61, 3461–3475.

Kirsanow, K., Makarewicz, C., Tuross, N., 2008. Stable oxygen ($\delta^{18}O$) and hydrogen (δD) isotopes in ovicaprid dentinal collagen record seasonal variation. J. Archaeol. Sci. 35, 3169–3167. doi:10.1016/j.jas.2008.06.025

Kirsanow, K., Tuross, N., 2011. Oxygen and hydrogen isotopes in rodent tissues: Impact of diet, water and ontogeny. Palaeogeogr. Palaeoclimatol. Palaeoecol. 310, 9–16. doi:10.1016/j.palaeo.2011.03.022

Kita, Z.A., Secord, R., Boardman, G.S., 2014. A new stable isotope record of Neogene paleoenvironments and mammalian paleoecologies in the western Great Plains during the expansion of C_4 grasslands. Palaeogeogr. Palaeoclimatol. Palaeoecol. 399, 160–172. doi:10.1016/J.PALAEO.2014.02.013

Knorr, G., Butzin, M., Micheels, A., Lohmann, G., 2011. A warm Miocene climate at low atmospheric CO_2 levels. Geophys. Res. Lett. 38, 1–5. doi:10.1029/2011GL048873

Koch, P.L., 2007. Isotopic study of the biology of modern and fossil vertebrates. Stable Isot. Ecol. Environ. Sci. 99–154. doi:10.1002/9780470691854.ch5

Koch, P.L., 1998. Isotopic reconstruction of past continental environments. Annu. Rev. Earth Planet. Sci. 26, 573–613. doi:10.1146/annurev.earth.26.1.573

Koch, P.L., Diffenbaugh, N.S., Hoppe, K.A., 2004. The effects of late Quaternary climate and pCO_2 change on C_4 plant abundance in the south-central United States. Palaeogeogr. Palaeoclimatol. Palaeoecol. 207, 331–357. doi:10.1016/j.palaeo.2003.09.034

Koch, P.L., Tuross, N., Fogel, M.L., 1997. The effects of sample treatment and diagenesis on the isotopic integrity of carbonate in biogenic hydroxylapatite. J. Archaeol. Sci. 24, 417–429. doi:10.1006/jasc.1996.0126

Kochhann, K.G.D., Holbourn, A., Kuhnt, W., Channell, J.E.T., Lyle, M., Shackford, J.K., Wilkens, R.H., Andersen, N., 2016. Eccentricity pacing of eastern equatorial Pacific carbonate dissolution cycles during the Miocene Climatic Optimum. Paleoceanography 31, 1176–1192. doi:10.1002/2016PA002988

Kohn, M.J., 2010. Carbon isotope compositions of terrestrial C_3 plants as indicators of

(paleo)ecology and (paleo)climate. Proc. Natl. Acad. Sci. U. S. A. 107, 19691–5. doi:10.1073/pnas.1004933107

Kohn, M.J., 2004. Comment: Tooth enamel mineralization in ungulates: Implications for recovering a primary isotopic time-series, by B. H. Passey and T. E. Cerling (2002). Geochim. Cosmochim. Acta 68, 403–405. doi:10.1016/S0016-7037(03)00443-5

Kohn, M.J., 1996. Predicting animal $\delta^{18}O$: Accounting for diet and physiological adaptation. Geochim. Cosmochim. Acta 60, 4811–4829. doi:10.1016/S0016-7037(96)00240-2

Kohn, M.J., Cerling, T.E., 2002. Stable isotope compositions of biological apatite. Rev. Mineral. Geochemistry 48, 455–488. doi:10.2138/rmg.2002.48.12

Kohn, M.J., Dettman, D.L., 2007. Paleoaltimetry from stable isotope compositions of fossils. Rev. Mineral. Geochemistry 66, 119–154. doi:10.2138/rmg.2007.66.5

Kohn, M.J., Fremd, T.J., 2008. Miocene tectonics and climate forcing of biodiversity, western United States. Geology 36, 783–786. doi:10.1130/G24928A.1

Kohn, M.J., Fremd, T.J., 2007. Tectonic controls on isotope compositions and species diversification, John Day Basin, central Oregon. PaleoBios 27, 48–61.

Kohn, M.J., McKay, M., 2010. Stable isotopes of fossil teeth corroborate key general circulation model predictions for the Last Glacial Maximum in North America. Geophys. Res. Lett. 37, 1–5. doi:10.1029/2010GL045404

Kohn, M.J., McKay, M.P., 2012. Paleoecology of late Pleistocene-Holocene faunas of eastern and central Wyoming, USA, with implications for LGM climate models. Palaeogeogr. Palaeoclimatol. Palaeoecol. 326–328, 42–53. doi:10.1016/j.palaeo.2012.01.037

Kohn, M.J., Miselis, J.L., Fremd, T.J., 2002. Oxygen isotope evidence for progressive uplift of the Cascade Range, Oregon. Earth Planet. Sci. Lett. 204, 151–165. doi:10.1016/S0012-821X(02)00961-5

Kohn, M.J., Strömberg, C.A.E., Madden, R.H., Dunn, R.E., Evans, S., Palacios, A., Carlini, A.A., 2015. Quasi-static Eocene–Oligocene climate in Patagonia promotes

slow faunal evolution and mid-Cenozoic global cooling. Palaeogeogr. Palaeoclimatol. Palaeoecol. 435, 24–37. doi:10.1016/j.palaeo.2015.05.028

Krapp, M., Jungclaus, J.H., 2011. The Middle Miocene climate as modelled in an atmosphere-ocean-biosphere model. Clim. Past 7, 1169–1188. doi:10.5194/cp-7-1169-2011

Kuiper, K.F., Deino, A., Hilgen, F.J., Krijgsman, W., Renne, P.R., Wijbrans, J.R., 2008. Synchronizing rock clocks of Earth history. Science 320, 500–504. doi:10.1126/science.1154339

Kürschner, W.M., Kvacek, Z., Dilcher, D.L., 2008. The impact of Miocene atmospheric carbon dioxide fluctuations on climate and the evolution of terrestrial ecosystems. Proc. Natl. Acad. Sci. U. S. A. 105, 449–53. doi:10.1073/pnas.0708588105

Langebroek, P.M., Paul, A., Schulz, M., 2009. Antarctic ice-sheet response to atmospheric CO_2 and insolation in the Middle Miocene. Clim. Past 5, 633–646. doi:10.5194/cp-5-633-2009

LaRiviere, J.P., Ravelo, C., Crimmins, A., Dekens, P.S., Ford, H., 2012. Late Miocene decoupling of oceanic warmth and atmospheric carbon dioxide forcing. Nature 486, 97–100.

Lear, C.H., Mawbey, E.M., Rosenthal, Y., 2010. Cenozoic benthic foraminiferal Mg/Ca and Li/Ca records: Toward unlocking temperatures and saturation states. Paleoceanography 25, 1–11. doi:10.1029/2009PA001880

Leon, N.H., 1972. Structural aspects of keratin fibres. Soc. Cosmet. Chem. Gt. Britain 23, 427–445.

Leyden, J.J., Wassenaar, L.I., Hobson, K.A., Walker, E.G., 2006. Stable hydrogen isotopes of bison bone collagen as a proxy for Holocene climate on the Northern Great Plains. Palaeogeogr. Palaeoclimatol. Palaeoecol. 239, 87–99. doi:10.1016/j.palaeo.2006.01.009

Lojen, S., Trkov, A., Ščančar, J., Vázquez-Navarro, J.A., Cukrov, N., 2008. Continuous 60-year stable isotopic and earth-alkali element records in a modern laminated tufa (Jaruga, river Krka, Croatia): Implications for climate reconstruction. Chem. Geol.

258, 242–250. doi:10.1016/j.chemgeo.2008.10.013

Long, P.E., Duncan, R.A., 1982. $^{40}Ar/^{39}Ar$ ages of Columbia River basalt from deep boreholes in south-central Washington, in: Joint Pacific Northwest American Geophysical Union and American Advancement of Science Meeting. Fairbanks, p. 13.

Lourantou, A., Chappellaz, J., Barnola, J.-M., Masson-Delmotte, V., Raynaud, D., 2010. Changes in atmospheric CO_2 and its carbon isotopic ratio during the penultimate deglaciation. Quat. Sci. Rev. 29, 1983–1992. doi:10.1016/J.QUASCIREV.2010.05.002

Luz, B., Cormie, A.B., Schwarcz, H.P., 1990. Oxygen isotope variations in phosphate of deer bones. Geochim. Cosmochim. Acta 54, 1723–1728.

Lyle, M., Heusser, L., Ravelo, C., Yamamoto, M., Barron, J., Diffenbaugh, N.S., Herbert, T., Andreasen, D., 2012. Out of the Tropics: The Pacific, Great Basin lakes, and late Pleistocene water cycle in the Western United States. Science 337, 1629–1633. doi:10.1126/science.1218390

MacFadden, B.J., 2000. Cenozoic mammalian herbivores from the Americas: reconstructing ancient diets and terrestrial communities. Annu. Rev. Ecol. Syst. 31, 33–59. doi:10.1146/annurev.ecolsys.31.1.33

MacFadden, B.J., Cerling, T.E., Prado, J., 1996. Cenozoic terrestrial ecosystem evolution in Argentina: evidence from carbon isotopes of fossil mammal teeth. Palaios 11, 319–327. doi:10.2307/3515242

MacFadden, B.J., Higgins, P., 2004. Ancient ecology of 15-million-year-old browsing mammals within C_3 plant communities from Panama. Oecologia. doi:10.2307/40005590

Maguire, K.C., 2015. Dietary niche stability of equids across the mid-Miocene Climatic Optimum in Oregon, USA. Palaeogeogr. Palaeoclimatol. Palaeoecol. 426, 297–307. doi:10.1016/j.palaeo.2015.03.012

Maguire, K.C., Samuels, J.X., Schmitz, M.D., 2018. The fauna and chronostratigraphy of the middle Miocene Mascall type area, John Day Basin, Oregon, USA. PaleoBios

35, 1–51.

Martin, C., Bentaleb, I., Antoine, P.-O., 2011. Pakistan mammal tooth stable isotopes show paleoclimatic and paleoenvironmental changes since the early Oligocene. Palaeogeogr. Palaeoclimatol. Palaeoecol. 311, 19–29. doi:10.1016/J.PALAEO.2011.07.010

Matson, S.D., Fox, D.L., 2010. Stable isotopic evidence for terrestrial latitudinal climate gradients in the Late Miocene of the Iberian Peninsula. Palaeogeogr. Palaeoclimatol. Palaeoecol. 287, 28–44. doi:10.1016/J.PALAEO.2009.12.010

Matsuoka, J., Kano, A., Oba, T., Watanabe, T., Sakai, S., Seto, K., 2001. Seasonal variation of stable isotopic compositions recorded in a laminated tufa, SW Japan. Earth Planet. Sci. Lett. 192, 31–44. doi:10.1016/S0012-821X(01)00435-6

McCarroll, D., Loader, N.J., 2004. Stable isotopes in tree rings. Quat. Sci. Rev. 23, 771–801.

McLaughlin, W.N.F., Hopkins, S.S.B., Schmitz, M.D., 2016. A new late Hemingfordian vertebrate fauna from Hawk Rim, Oregon, with implications for biostratigraphy and geochronology. J. Vertebr. Paleontol. 36, e1201095. doi:10.1080/02724634.2016.1201095

Medina, E., Minchin, P., 1980. Stratification of $\delta^{13}C$ values of leaves in Amazonian Rain Forests. Oecologia 45, 377–378. doi:10.1007/BF00540209

Medina, E., Montes, G., Guevas, E., Rokzandic, Z., 1986. Profiles of CO_2 concentration and $\delta^{13}C$ values in tropical rain forests of the Upper Rio Negro Basin, Venezuela. J. Trop. Ecol. 2, 207–217. doi:10.2307/2559851

Meehl, G.A., Arblaster, J.M., Tebaldi, C., 2005. Understanding future patterns of increased precipitation intensity in climate model simulations. Geophys. Res. Lett. 32, 1–4. doi:10.1029/2005GL023680

Meehl, G.A., Covey, C., Taylor, K.E., Delworth, T., Stouffer, R.J., Latif, M., McAvaney, B., Mitchell, J.F.B., Meehl, G.A., Covey, C., Taylor, K.E., Delworth, T., Stouffer, R.J., Latif, M., McAvaney, B., Mitchell, J.F.B., 2007. THE WCRP CMIP3 Multimodel Dataset: A New Era in Climate Change Research. Bull. Am. Meteorol.

Soc. 88, 1383–1394. doi:10.1175/BAMS-88-9-1383

Menking, K.M., Anderson, R.Y., Shafike, N.G., Syed, K.H., Allen, B.D., 2004. Wetter or colder during the Last Glacial Maximum? Revisiting the pluvial lake question in southwestern North America. Quat. Res. 62, 280–288. doi:10.1016/j.yqres.2004.07.005

Miller, R.F., Fritz, P., Morgan, A.V., 1988. Climatic implications of D/H ratios in beetle chitin. Palaeogeogr. Palaeoclimatol. Palaeoecol. 66, 277–288. doi:10.1016/0031-0182(88)90204-0

Monger, H.C., Cole, D.R., Gish, J.W., Giordano, T.H., 1998. Stable carbon and oxygen isotopes in Quaternary soil carbonates as indicators of ecogeomorphic changes in the northern Chihuahuan Desert, USA. Geoderma 82, 137–172. doi:10.1016/S0016-7061(97)00100-6

Moore, D.M., Reynolds, R.C., 1997. X-ray diffraction and the identification and analysis of clay minerals, 2nd ed. Oxford University Press, New York.

Mosbrugger, V., Utescher, T., Dilcher, D.L., 2005. Cenozoic continental climatic evolution of Central Europe. Proc. Natl. Acad. Sci. U. S. A. 102, 14964–14969. doi:10.1073/pnas.0505267102

Mote, P.W., Salathe, E.P., 2010. Future climate in the Pacific Northwest. Clim. Change 102, 29–50. doi:10.1007/s10584-010-9848-z

Moum, J., Rosenqvist, I.T., 1958. Hydrogen (protium)-deuterium exchange in clays. Geochim. Cosmochim. Acta 14, 250–252.

National Park Service - Mojave Desert Network [WWW Document], 2018. URL https://science.nature.nps.gov/im/units/mojn/ (accessed 1.12.18).

Nelson, S.V., 2013. Chimpanzee fauna isotopes provide new interpretations of fossil ape and hominin ecologies. Proceedings. Biol. Sci. 280, 1–6. doi:10.1098/rspb.2013.2324

Niu, L., Lohmann, G., Hinck, S., Gowan, E.J., 2017. Sensitivity of atmospheric forcing on Northern Hemisphere ice sheets during the last glacial-interglacial cycle using

output from PMIP3. Clim. Past Discuss. 105, 1–30. doi:10.5194/cp-2017-105

O 'Brien, D.M., Wooller, M.J., 2007. Tracking human travel using stable oxygen and hydrogen isotope analyses of hair and urine. Rapid Commun. Mass Spectrom. 21, 2422–2430. doi:10.1002/rcm.3108

OIPC [WWW Document], 2018. URL http://wateriso.utah.edu/waterisotopes/pages/data_access/oipc.html (accessed 5.24.18).

Orr, E.L., Orr, W.N., 2012. Oregon fossil. Oregon State Univ. Press 1–304.

Osmond, C.B., Björkman, O., Anderson, D.J., 1980. Physiological processes in plant ecology: toward a synthesis with Atriplex. Springer Berlin Heidelberg.

Oviatt, C.G., Madsen, D.B., Schmitt, D.N., 2003. Late Pleistocene and early Holocene rivers and wetlands in the Bonneville basin of western North America. Quat. Res. 60, 200–210. doi:10.1016/S0033-5894(03)00084-X

Pagani, M., Freeman, J.C., Arthur, K.H., Tipple, B.J., Bohaty, S., 1999. Late Miocene atmospheric CO_2 concentrations and the expansion of C_4 grasses. Science 285, 876–9. doi:10.1126/science.285.5429.876

Pagani, M., Zachos, J.C., Freeman, K.H., Tipple, B.J., Bohaty, S., 2005. Marked decline in atmospheric carbon dioxide concentration during the Paleogene. Science 309, 600–603. doi:10.1126/science.1110063

Paruelo, J.M., Lauenroth, W.K., 1996. Relative abundance of plant functional types in grasslands and shrublands of North America. Ecol. Appl. 6, 1212–1224. doi:10.2307/2269602

Passey, B.H., Cerling, T.E., 2002. Tooth enamel mineralization in ungulates: implications for recovering a primary isotopic time-series. Geochim. Cosmochim. Acta 66, 3225–3234. doi:10.1016/S0016-7037(02)00933-X

Passey, B.H., Robinson, T.F., Ayliffe, L.K., Cerling, T.E., Sphonheimer, M., Dearing, M.D., Roeder, B.L., Ehleringer, J.R., 2005. Carbon isotope fractionation between diet, breath CO_2, and bioapatite in different mammals. J. Archaeol. Sci. 32, 1459–

1470. doi:10.1016/j.jas.2005.03.015

Pazdur, A., Mieczyslaw, F., Starkel, L., Szulc, J., 1988. Stable isotopes of Holocene calcareous tufa in southern Poland as paleoclimatic indicators. Quat. Res. 30, 177–189. doi:10.1016/0033-5894(88)90022-1

Pearson, P.N., Palmer, M.R., 2000. Atmospheric carbon dioxide concentrations over the past 60 million years. Nature 406, 695–699. doi:10.1038/35021000

Pedley, H.M., 1990. Classification and environmental models of cool freshwater tufas. Sediment. Geol. 68, 143–154. doi:10.1016/0037-0738(90)90124-C

Pedro, J.B., Rasmussen, S.O., van Ommen, T.D., 2012. Tightened constraints on the time-lag between Antarctic temperature and CO_2 during the last deglaciation. Clim. past 8, 1213–1221.

Pekar, S.F., DeConto, R.M., 2006. High-resolution ice-volume estimates for the early Miocene: Evidence for a dynamic ice sheet in Antarctica. Palaeogeogr. Palaeoclimatol. Palaeoecol. 231, 101–109. doi:10.1016/J.PALAEO.2005.07.027

Pentecost, A.N., 2005. Travertine. Springer-Verlag, Berlin.

Pentecost, A.N., 1988. Growth and calcification of the Cyanobacterium Homoeothrix crustaceu. J. Gen. Microbiol. 134, 2665–267.

Perez-Crespo, V.A., Arroyo-Cabrales, J., Alva-Valdivia, L.M., Morales-Puente, P., Cienfuegos-Alvarada, E., 2012. Isotope data ($\delta^{13}C$, $\delta^{18}O$) of the Pleistocene fauna of Laguna de las Cruses, San Luis Potosi, Mexico. Mex. J. Geol. Sci. 29, 299–307.

Pietsch, S.J., Hobson, K.A., Wassenaar, L.I., Tütken, T., Shanas, U., 2011. Tracking cats: Problems with placing feline carnivores on $\delta^{18}O$, δD Isoscapes. PLoS One 6, e24601. doi:10.1371/journal.pone.0024601

Pigati, J.S., Bright, J.E., Shanahan, T.M., Mahan, S.A., 2009. Late Pleistocene paleohydrology near the boundary of the Sonoran and Chihuahuan Deserts, southeastern Arizona, USA. Quat. Sci. Rev. 28, 286–300. doi:10.1016/j.quascirev.2008.09.022

Pigati, J.S., Miller, D.M., Bright, J.E., Mahan, S.A., Nekola, J.C., Paces, J.B., 2011.

Chronology, sedimentology, and microfauna of groundwater discharge deposits in the central Mojave Desert, Valley Wells, California. Geol. Soc. Am. Bull. 123, 2224–2239. doi:10.1130/B30357.1

Pigati, J.S., Rech, J.A., Quade, J., Bright, J., 2014. Desert wetlands in the geologic record. Earth-Science Rev. 132, 67–81. doi:10.1016/J.EARSCIREV.2014.02.001

Pound, M.J., Haywood, A.M., Salzmann, U., Riding, J.B., 2012. Global vegetation dynamics and latitudinal temperature gradients during the mid to late Miocene (15.97–5.33 Ma). Earth-Science Rev. 112, 1–22. doi:10.1016/j.earscirev.2012.02.005

Qi, H., Coplen, T.B., Gehre, M., Vennemann, T.W., Brand, W.A., Geilmann, H., Olack, G., Bindeman, I.N., Palandri, J., Huang, L., Longstaffe, F.J., 2017. New biotite and muscovite isotopic reference materials, USGS57 and USGS58, for δ^2H measurements–A replacement for NBS 30. Chem. Geol. 467, 89–99. doi:10.1016/j.chemgeo.2017.07.027

Quade, J., 1986. Late quaternary environmental changes in the upper Las Vegas Valley, Nevada. Quat. Res. 26, 340–357. doi:10.1016/0033-5894(86)90094-3

Quade, J., Forester, R.M., Pratt, W.L., Carter, C., 1998. Black mats, spring-fed streams, and late-Glacial-Age recharge in the Southern Great Basin. Quat. Res. 49, 129–148. doi:10.1006/qres.1997.1959

Quade, J., Pratt, W.L., 1989. Late Wisconsin groundwater discharge environments of the southwestern Indian Springs Valley, southern Nevada. Quat. Res. 31, 351–370. doi:10.1016/0033-5894(89)90042-2

Retallack, G.J., 2010. Lateritization and bauxitization events. Econ. Geol. 105, 655–667. doi:10.2113/gsecongeo.105.3.655

Retallack, G.J., 2009. Greenhouse crises of the past 300 million years. Bull. Geol. Soc. Am. 121, 1441–1455. doi:10.1130/B26341.1

Retallack, G.J., 2004. Late Oligocene bunch grassland and early Miocene sod grassland paleosols from central Oregon, USA. Palaeogeogr. Palaeoclimatol. Palaeoecol. 207, 203–237. doi:10.1016/J.PALAEO.2003.09.027

Retallack, G.J., 2001. A 300-million-year record of atmospheric carbon dioxide from fossil plant cuticles. Nature 411, 287–290. doi:10.1038/35077041

Retallack, G.J., Gavin, G.D., Davis, E.B., Sheldon, N.D., Erlandson, J.M., Reed, M.H., Bestland, E. a, Roering, J.J., Carson, R.J., Mitchell, R.B., 2016. Oregon 2100: Projected climatic and ecological changes. Bull. Museum Nat. Hist. Univ. Oregon 26.

Retallack, G.J., Wynn, J.G., Fremd, T.J., 2004. Glacial-interglacial-scale paleoclimatic change without large ice sheets in the Oligocene of central Oregon. Geology 32, 297–300. doi:10.1130/G20247.1

Reynard, L.M., Hedges, R.E.M., 2008. Stable hydrogen isotopes of bone collagen in palaeodietary and palaeoenvironmental reconstruction. J. Archaeol. Sci. 35, 1934–1942. doi:10.1016/j.jas.2007.12.004

Royer, D.L., Wing, S.L., Beerling, D.J., Jolley, D.W., Koch, P.L., Hickey, L.J., Berner, R.A., 2001. Paleobotanical evidence for near present-day levels of atmospheric CO_2 during part of the tertiary. Science 292, 2310–2313. doi:10.1126/science.292.5525.2310

Rozanski, K., Araguás-Araguás, L., Gonfiantini, R., 1992. Relation between long-term trends of oxygen-18 isotope composition of precipitation and climate. Science 258, 981–985. doi:10.2307/2881675

Samata, T., Mastsuda, M., 1988. Studies of the amino acid compositions of equine body hair and the hoof. Japanese J. Vet. Sci. 5, 333–340.

Sankey, J.T., 2002. Vertebrate paleontology and magnetostratigraphy of the Glenns Ferry and Bruneau Formations (Plio-Pleistocene), near Murphy, southwestern Idaho. whereas...papers veterbrate Paleontol. Idaho Honor John A. White 37, 52–100.

Savin, S.M., Epstein, S., 1970. The oxygen and hydrogen isotope geochemistry of clay minerals. Geochim. Cosmochim. Acta 34, 25–42.

Savin, S.M., Hsieh, J.C., 1998. The hydrogen and oxygen isotope geochemistry of pedogenic clay minerals: principles and theoretical background. Geoderma 82, 227–253. doi:10.1016/S0016-7061(97)00103-1

Scherler, L., Tütken, T., Becker, D., 2014. Carbon and oxygen stable isotope compositions of late Pleistocene mammal teeth from dolines of Ajoie (Northwestern Switzerland). Quat. Res. 82, 378–387. doi:10.1016/J.YQRES.2014.05.004

Schimmelmann, A., 1991. Determination of the concentration of stable isotopic compositions of nonexchangeable hydrogen in organic matter. Anal. Chem. 62, 2456–2459.

Schwarz, T., 1997. Lateritic bauxite in central Germany and implications for Miocene palaeoclimate. Palaeogeogr. Palaeoclimatol. Palaeoecol. 129, 37–50. doi:10.1016/S0031-0182(96)00065-X

Semprebon, G.M., Rivals, F., 2010. Trends in the paleodietary habits of fossil camels from the Tertiary and Quaternary of North America. Palaeogeogr. Palaeoclimatol. Palaeoecol. 295, 131–145. doi:10.1016/J.PALAEO.2010.05.033

Shanahan, S.A., Silverman, D., Ehrenbreg, A., 2008. Land cover types of Las Vegas Wash, Nevada. Las Vegas.

Sharp, Z.D., Atudorei, V., Panaerllo, H.O., Fernandez, J., Douthitt, C., 2003. Hydrogen isotope systematics of hair: archeological and forensic applications. J. Archaeol. Sci. 30, 1709–1716. doi:10.1016/S0305-4403(03)00071-2

Sheldon, N.D., 2003. Pedogenesis and geochemical alteration of the Pacific Gorge subgroup Columbia River basalt, Oregon. Bull. Geol. Soc. Am. 115, 1377–1387. doi:10.1130/B25223.1

Sheldon, N.D., Retallack, G.J., Tanaka, S., 2002. Geochemical climofunctions from North American soils and application to paleosols across the Eocene-Oligocene boundary in Oregon. J. Geol. 110, 687–696. doi:10.1086/342865

Shevenell, A.E., Kennett, J.P., Lea, D.W., 2001. Middle Miocene Southern Ocean cooling and Antarctic cryosphere expansion. Science 305, 1766–1770. doi:10.1126/science.1100061

Shotwell, J.A., 1968. Miocene mammals of southeast Oregon. Bull. Museum Nat. Hist. Univ. Oregon 21.

Shotwell, J.A., Bowen, R.G., Gray, W.L., Gregory, D.C., Taylor, D.W., Russell, D.E., 1963. The Juntura Basin: Studies in Earth history and paleoecology. Trans. Am. Philos. Soc. 53, 1. doi:10.2307/1005944

Springer, A.E., Stevens, L.E., 2008. Spheres of discharge of springs. Hdrogeology J. 17, 83. doi:10.1007/s10040-008-0341-y

Springer, K.B., Manker, C.R., Pigati, J.S., 2015. Dynamic response of desert wetlands to abrupt climate change. Proc. Natl. Acad. Sci. U. S. A. 112, 14522–15426. doi:10.1073/pnas.1513352112

Springer, K.B., Pigati, J.S., Scott, E., Sprinkel, D.A., Schamel, S., Loughlin, B., Eaton, C., 2017. Tule Spring Fossil Beds National Monument, Nevada (USA) 4.

Strömberg, C.A.E., 2006. Evolution of hypsodonty in equids: testing a hypothesis of adaptation. Paleobiology 32, 236–258. doi:10.1666/0094-8373(2006)32[236:EOHIET]2.0.CO;2

Strömberg, C.A.E., 2005. Decoupled taxonomic radiation and ecological expansion of open-habitat grasses in the Cenozoic of North America. Proc. Natl. Acad. Sci. U. S. A. 102, 11980–11984. doi:10.1073/pnas.0505700102

Svensson, A., Andersen, K.K., Bigler, M., Clausen, H.B., Dahl-Jensen, D., Davies, S.M., Johnsen, S.J., Muscheler, R., Parrenin, F., Rasmussen, S.O., 2008. A 60,000 year Greenland stratigraphic ice core chronology. Clim. past 4, 47–57.

Swetnam, T.W., Allen, C.D., Betancourt, J.L., 1999. Applied historical ecology: Using the past to manage for the future. Ecol. Appl. 9, 1189–1206. doi:10.1890/1051-0761(1999)009[1189:AHEUTP]2.0.CO;2

Swisher, C.C., 1992. $^{40}Ar/^{39}Ar$ dating and its application to the calibration of the North American Land Mammal Ages. University of California, Berkley.

Tabor, N.J., Montanez, I.P., Montanez, M., 2004. Morphology and distribution of fossil soils in the Permo-Pennsylvanian Wichita and Bowie Groups, north-central Texas, USA: implications for western equatorial Pangean palaeoclimate during icehouse-greenhouse transition. Sedimentology 51, 851–884. doi:10.1111/j.1365-3091.2004.00655.x

Taggart, R.E., Cross, A.T., 1980. Vegetation change in the Miocene Succor Creek flora of Oregon and Idaho: a case study of paleosuccession., Biostratigraphy of Fossil Plants-Successional and Paleoecological Analyses. Dowden, Hutchinson & Ross, Inc., Stroudsburg.

Tappa, D.J., Kohn, M.J., Mcnamara, J.P., Benner, S.G., Flores, A.N., 2016. Isotopic composition of precipitation in a topographically steep, seasonally snow-dominated watershed and implications of variations from the global meteoric water line; Isotopic composition of precipitation in a topographically steep, seasonally snow-dom. Hydrol. Process. 30, 4582–4592. doi:10.1002/hyp.10940

Thomas, J.M., Lyles, B.F., Carpenter, L.A., 1991. Chemical and isotopic data for water from wells, springs, and streams in carbonate-rock terrane of southern and eastern Nevada and southeastern California, 1985-88. Denver.

Tipple, B.J., Meyers, S.R., Pagani, M., 2010. Carbon isotope ratio of Cenozoic CO_2 : A comparative evaluation of available geochemical proxies. Paleoceanography 25, 1–11. doi:10.1029/2009PA001851

Toggweiler, J.R., Russell, J.L., Carson, S.R., 2006. Midlatitude westerlies, atmospheric CO_2, and climate change during the ice ages. Paleoceanography 21, 1–15. doi:10.1029/2005PA001154

Trayler, R.B., Dundas, R.G., Fox-Dobbs, K., Van De Water, P.K., 2015. Inland California during the Pleistocene—Megafaunal stable isotope records reveal new paleoecological and paleoenvironmental insights. Palaeogeogr. Palaeoclimatol. Palaeoecol. 437, 132–140. doi:10.1016/J.PALAEO.2015.07.034

Trayler, R.B., Kohn, M.J., 2017. Tooth enamel maturation reequilibrates oxygen isotope compositions and supports simple sampling methods. Geochim. Cosmochim. Acta 198, 32–47. doi:10.1016/j.gca.2016.10.023

Trudinger, C.M., Enting, I.G., Francey, R.J., Etheridge, D.M., Rayner, P.J., 1999. Long-term variability in the global carbon cycle inferred from a high-precision CO_2 and $\delta^{13}C$ ice-core record. Tellus 51B, 233–248. doi:10.1034/j.1600-0889.1999.t01-1-00009.x

Trueman, C.N., Tuross, N., 2002. Trace elements in recent and fossil bone apatite. Rev. Mineral. Geochemistry 48, 489–521. doi:10.2138/rmg.2002.48.13

Vetter, L., Lachniet, M., Rowland, S., 2007. Paleoecology of Pleistocene megafauna in southern Nevada: Isotoptic evidence for browsing on halophytic plants, in: Annual Meeting Abstracts with Programs. p. 402.

Wagner, J.D.M., Cole, J.E., Beck, J.W., Patchett, P.J., Henderson, G.M., Barnett, H.R., 2010. Moisture variability in the southwestern United States linked to abrupt glacial climate change. Nat. Geosci. 3, 110–113. doi:10.1038/ngeo707

Wang, Y., Deng, T., 2005. A 25 m.y. isotopic record of paleodiet and environmental change from fossil mammals and paleosols from the NE margin of the Tibetan Plateau. Earth Planet. Sci. Lett. 236, 322–338. doi:10.1016/J.EPSL.2005.05.006

Wang, Y., Kromhout, E., Zhang, C., Xu, Y., Parker, W., Deng, T., Qui, Z., 2008. Stable isotopic variations in modern herbivore tooth enamel, plants and water on the Tibetan Plateau: Implications for paleoclimate and paleoelevation reconstructions. Palaeogeogr. Palaeoclimatol. Palaeoecol. 260, 359–374. doi:10.1016/J.PALAEO.2007.11.012

Wassenaar, L.I., Hobson, K.A., 2003. Comparative equilibration and online technique for determination of non-exchangeable hydrogen of keratins for use in animal migration studies. Isotopes Environ. Health Stud. 39, 211–217. doi:10.1080/1025601031000096781

Wassenaar, L.I., Hobson, K.A., 2000. Improved methods for determining the stable-hydrogen isotopic compositions (δD) of complex organic materials of environmental interest. Environ. Sci. Technol. 34, 2354–2360.

Webb, S.D., 1977. A history of savanna vertebrates in the New World. Part I: North America. Annu. Rev. Ecol. Syst. 8, 355–380.

West-Eberhard, M.J., 2003. Developmental plasticity and evolution. Oxford University Press.

Winograd, I.J., Friedman, I., 1972. Deuterium as a tracer in regional groundwater flow, southern Great Basin, Nevada and California. Geol. Soc. Am. Bull. 83, 3691–3708.

Winograd, I.J., Riggs, A.C., Coplen, T.B., 1998. The relative contributions of summer and cool-season precipitation to groundwater recharge, Spring Mountains, Nevada, USA. Hydrogeol. J. 6, 77–93.

Wolfe, J.A., 1994. Tertiary climatic changes at middle latitudes of western North America. Palaeogeogr. Palaeoclimatol. Palaeoecol. 108, 195–205. doi:10.1016/0031-0182(94)90233-X

Woodcock, D., 1986. The late Pleistocene of Death Valley: A climatic reconstruction based on macrofossil data. Palaeogeogr. Palaeoclimatol. Palaeoecol. 57, 273–283. doi:10.1016/0031-0182(86)90016-7

WRCC [WWW Document], 2018. URL https://wrcc.dri.edu/ (accessed 1.30.18).

Yang, J., Spicer, R.A., Spicer, T.E. V, Li, C. Sen, 2011. "CLAMP Online": A new web-based palaeoclimate tool and its application to the terrestrial Paleogene and Neogene of North America. Palaeobiodiversity and Palaeoenvironments 91, 163–183. doi:10.1007/s12549-011-0056-2

You, Y., Huber, M., Müller, R.D., Poulsen, C.J., Ribbe, J., 2009. Simulation of the Middle Miocene Climate Optimum. Geophys. Res. Lett. 36, L04702. doi:10.1029/2008GL036571

Zachos, J., Pagani, M., Sloan, L., Thomas, E., Billups, K., 2001. Trends, rhythms, and aberrations in global climate 65 Ma to present. Science 292, 686–693. doi:10.1126/science.1059412

Zanazzi, A., Kohn, M.J., 2008. Ecology and physiology of White River mammals based on stable isotope ratios of teeth. Palaeogeogr. Palaeoclimatol. Palaeoecol. 257, 22–37. doi:10.1016/J.PALAEO.2007.08.007

Zhang, C., Wang, Y., Li, Q., Wang, X., Deng, T., Tseng, Z.J., Takeuchi, G.T., Xie, G., Xu, Y., 2012. Diets and environments of late Cenozoic mammals in the Qaidam Basin, Tibetan Plateau: Evidence from stable isotopes. Earth Planet. Sci. Lett. 333–334, 70–82. doi:10.1016/J.EPSL.2012.04.013

Zhang, Y.G., Pagani, M., Liu, Z., Bohaty, S.M., Deconto, R., 2013. A 40-million-year history of atmospheric CO_2. Philos. Trans. A. Math. Phys. Eng. Sci. 371, 20130096.

doi:10.1098/rsta.2013.0096

APPENDIX A

Stable Isotopes in Large Herbivore Tooth Enamel Capture a Mid-Miocene Precipitation Spike in the Interior Pacific Northwest

ISOTOPIC COMPOSITIONS OF EQUIDS VS. OTHRE HERBIVORES

Equids were abundant during the Oligocene and Miocene leaving a rich paleontological record. During this period, equids began to transition from browsers to grazers (Janis et al., 2002; Strömberg, 2006; Janis, 2008). The expansion of grasslands during the Oligocene created more open drier grazing environments compared to dense forested environments of the past (Retallack, 2001; Keeley and Rundel, 2005; Strömberg, 2005). Dense forested and open grazing environments have distinctly different $\delta^{13}C$ values (Medina and Minchin, 1980; Medina et al., 1986). There is also a negative correlation between $\delta^{13}C$ values of C_3 plants and MAP (Appendix Fig 1; Kohn, 2010). If equids occupied drier ecosystems, or were disproportionately represented in drier ecosystems, our data could be biased towards higher $\delta^{13}C$ values. Here we compared equid stable isotopic carbon compositions ($\delta^{13}C$ values) to other fauna from this study, as well as collagen and tooth enamel from previous studies focusing on C_3 environments (Appendix Table 1). We tested whether equids have preferentially higher $\delta^{13}C$ values, because of open-habit feeding. If equid $\delta^{13}C$ values are systematically higher, MAP estimates acquired from equid tooth enamel would be lower, meaning equid data could potentially underestimate MAP. Equid $\delta^{13}C$ values measured in our study are ~1‰ higher than other herbivores analyzed (Appendix Table 2). Nelson (2013) also analyzed $\delta^{13}C$ values from Miocene herbivores, which have a mean $\delta^{13}C$ value for equid enamel ~3.5‰ higher when compared to other fauna. However, out of 17 studies (including our data), only 6 datasets

suggested equids have higher mean $\delta^{13}C$ values when compared to other taxa. For example, a Pleistocene mammalian study shows nearly 3‰ lower $\delta^{13}C$ values for equids compared to other herbivores (MacFadden et al., 1996). The non-systematic $\delta^{13}C$ values of equids and other herbivores suggest that there is no notable offset between differing faunas. This result implies the MAP estimates from equid tooth enamel from C_3 environments are not steadily offset from MAP estimates basin on all mammalian herbivores from an ecosystem

Table A. 1. Averaged $\delta^{13}C$ values from our study and previous studies focusing on equids and other herbivore (browsers and grazers) tooth enamel and collagen from C_3 environment.

Study	$\delta^{13}C$ (‰; PDB) Equids	$\delta^{13}C$ (‰; PDB) Other Herbivores	Equid-herbivore offset (‰)	Material	Age
Bocherens et al. (1996)	–20.22	–19.73	–0.49	Collagen	Pleistocene
Cerling and Harris (1999)	–11.9	–14.30	2.40	Enamel	Modern
Domingo et al. (2012)	–10.390	–10.39	0.00	Enamel	Pleistocene
Drewicz and Kohn (2018)	–9.51	–10.05	0.54	Enamel	Oligocene-Pliocene
Feranec and MacFadden (2006)	–11.76	–13.53	1.77	Enamel	Miocene
Fox-Dobbs et al. (2008)	–21.13	–20.27	–0.87	Collagen	Pleistocene
Kohn and McKay (2012)	–11.50	–10.43	–1.07	Enamel	Pleistocene-Holocene
Martin et al. (2011)	–8.51	–10.00	1.49	Enamel	Oligocene
MacFadden and Higgins (2004)	–12.10	–12.88	0.78	Enamel	Miocene
MacFadden et al. (1996)	–12.00	–9.2	–2.80	Enamel	Pleistocene
Nelson (2013)	–7.78	–11.25	3.47	Enamel	Miocene
Scherler et al. (2014)	–11.66	–11.50	–0.17	Enamel	Pleistocene
Trayler et al. (2015)	–11.62	–11.11	–0.51	Enamel	Pleistocene
Wang and Deng (2005)	–9.93	–9.89	–0.03	Enamel	Miocene-Pleistocene
Wang et al. (2008)	–11.85	–11.13	–0.72	Enamel	Modern
Zanazzi and Kohn (2008)	–9.75	–8.6	–1.15	Enamel	late Eocene-Oligocene
Zhang et al. (2012)	–10.55	–10.04	–0.51	Enamel	Late Miocene-Pliocene

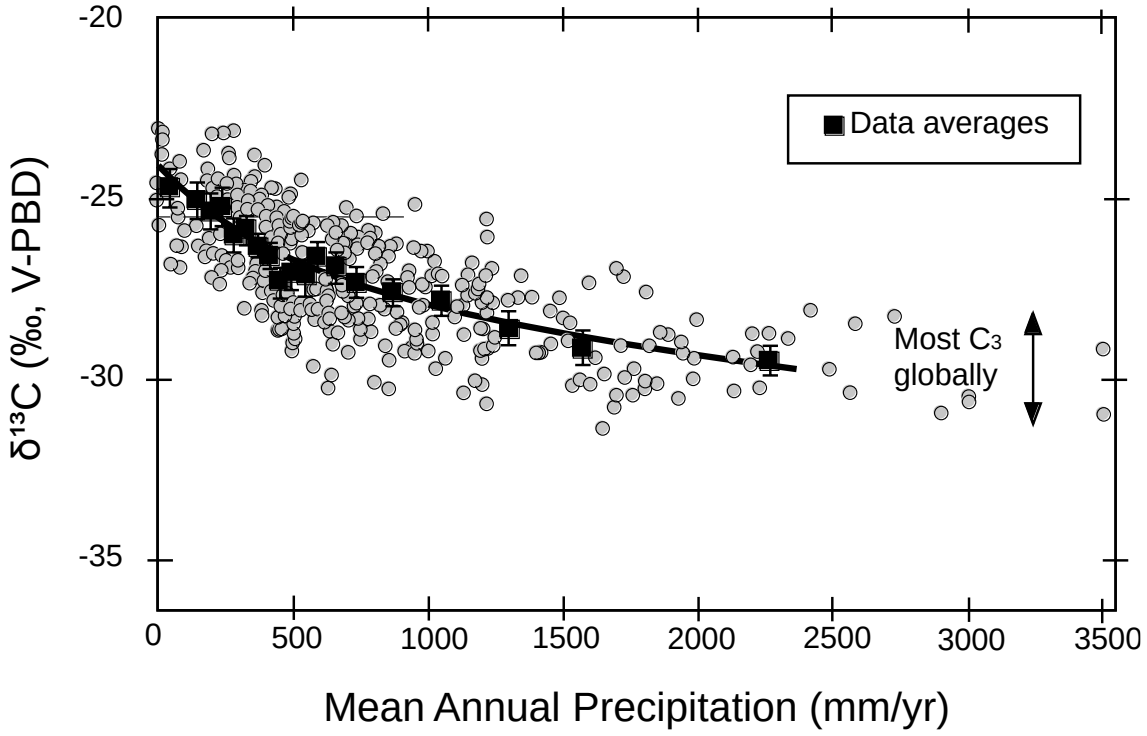

Figure A. 1. Modern C_3 plant $\delta^{13}C$ values vs. MAP. Lower plant $\delta^{13}C$ values reflect higher MAP (Kohn, 2010).

Table A. 2. Identification number of fossil specimens, $\delta^{13}C$ and $\delta^{18}O$ values, taxa, location, and length of tooth sub-sampled.

John Day Formation (~28 Ma)					
Identification number	$\delta^{13}C$ (VPDB)	$\delta^{18}O$ (VSMOW)	Taxon	Location or Formation	Distance from occlusal surface (mm)
JODA 2802(B)-C	–10.76	20.14	Merycoidodont	John Day	3.75
JODA 2802(B)-D	–10.54	20.7	Merycoidodont	John Day	5
JODA 1940(A)-A	–12.04	19.98	Merycoidodont	John Day	1.25
JODA 1940(A)-B	–12.23	20.39	Merycoidodont	John Day	2.5
JODA 7003(B)-C	–14.56	21.49	Merycoidodont	John Day	3.75
JODA 400A+B-A	–12.26	19.07	Merycoidodont	John Day	1.25
JODA 400A+B-B	–11.5	18.92	Merycoidodont	John Day	2.5
JODA 400A+B-C	–11.81	21.7	Merycoidodont	John Day	3.75
JODA 7003(D)-E	–13.38	21.4	Merycoidodont	John Day	6.25
JODA 7003(D)-F	–13	21.69	Merycoidodont	John Day	7.5
JODA 7003(D)-H	–12.99	21.66	Merycoidodont	John Day	8.75
JODA 8472-C	–10.26	20.46	Merycoidodont	John Day	3.75
JODA 8472-D	–9.28	21.97	Merycoidodont	John Day	5
JODA 8472-F	–9.44	21.46	Merycoidodont	John Day	7.5
JODA 8472-I	–8.9	20.61	Merycoidodont	John Day	11.25
JODA 1296-D	–9.34	18.75	Merycoidodont	John Day	5
JODA 5795/1-B	–12.87	21.85	*Parahippus*	John Day	2.5
JODA 5795/1-C	–9.46	23.18	*Parahippus*	John Day	3.75

Identification number	$\delta^{13}C$ (VPDB)	$\delta^{18}O$ (VSMOW)	Taxon	Location or Formation	Distance from occlusal surface (mm)
JODA 5795/1-D	–9.42	23.03	*Parahippus*	John Day	5
JODA 5795/1-E	–9.85	23.07	*Parahippus*	John Day	6.25
JODA 5795/1-F	–10.53	25.07	*Parahippus*	John Day	7.5
JODA 5685(B)-B	–11.63	26.09	*Eporeodon*	John Day	2.5
JODA 5685(A)-D	–12.25	23.44	*Eporeodon*	John Day	5
JODA 5854(A)-F	–12.95	22.84	*Eporedon*	John Day	7.5
JODA 5854(A)-J	–12.47	23.27	*Eporedon*	John Day	8.75
JODA 3408-D	–11.11	20.54	*Diceratherium*	John Day	5
JODA 3408-G	–11.43	21.01	*Diceratherium*	John Day	8.75
JODA 3408-J	–11.54	20.7	*Diceratherium*	John Day	12.5
JODA 1828-G	–11.07	21.48	*Diceratherium*	John Day	8.75
JODA 1828-H	–11.3	22.4	*Diceratherium*	John Day	10
JODA 3408-I	–11.03	20.17	*Diceratherium*	John Day	11.25
JODA 1828-J	–11.2	21.42	*Diceratherium*	John Day	12.5
JODA 1828-M	–11.13	21.07	*Diceratherium*	John Day	15
JODA 1828-N	–10.65	20.52	*Diceratherium*	John Day	17.5
JODA 1828-O	–10.85	21.39	*Diceratherium*	John Day	20
JODA 1296-A	–10.85	18.7	*Diceratherium*	John Day	1.25
JODA 1296-C	–10.28	18.99	*Diceratherium*	John Day	3.75
JODA 1296-F	–10.21	19.44	*Diceratherium*	John Day	6.25
JODA 1296-G	–10.39	19.88	*Diceratherium*	John Day	7.5
JODA 2798-B	–10.76	23.09	Rhino	John Day	2.5
JODA 2798-D	–10.75	23.37	Rhino	John Day	5

Mascall Formation (~15.1 Ma)					
Identification number	$\delta^{13}C$ (VPDB)	$\delta^{18}O$ (VSMOW)	Taxon	Location or Formation	Distance from occlusal surface (mm)
JODA 2004-A	–13.55	20.18	*Merychippus*	Mascall	1.25
JODA 2004-B+C	–13.38	21.32	*Merychippus*	Mascall	3.75
JODA 2004-D	–12.8	21.02	*Merychippus*	Mascall	5
JODA 2004-E	–12.1	22.47	*Merychippus*	Mascall	6.25
JODA 2004-F	–12.07	22.54	*Merychippus*	Mascall	7.5
JODA 2004-G	–12.24	22.44	*Merychippus*	Mascall	8.75
JODA 2004-H	–11.88	22.31	*Merychippus*	Mascall	10
JODA 2004-I	–12.13	23.07	*Merychippus*	Mascall	11.25
JODA 2004-J	–12.28	20.18	*Merychippus*	Mascall	12.5
JODA 2004-K	–12.52	21.39	*Merychippus*	Mascall	13.75
JODA 2004-L	–12.48	20.77	*Merychippus*	Mascall	15
JODA 2004-M	–12.09	20.64	*Merychippus*	Mascall	16.25
JODA 2004-N	–12.29	19.65	*Merychippus*	Mascall	17.5
JODA 2004-O	–12.46	21.13	*Merychippus*	Mascall	18.75
JODA 2004-P	–11.83	21.2	*Merychippus*	Mascall	20
JODA 2004-Q	–12.68	21.57	*Merychippus*	Mascall	21.25
JODA 1999-A	–10.82	22.76	*Merychippus*	Mascall	1.25
JODA 1999-B	–11.02	21.26	*Merychippus*	Mascall	2.5
JODA 1999-C	–11.07	22.1	*Merychippus*	Mascall	3.75
JODA 1999-D	–12.57	21.73	*Merychippus*	Mascall	5
JODA 1999-E	–10.3	22.11	*Merychippus*	Mascall	6.25
JODA 1999-F	–9.78	22.3	*Merychippus*	Mascall	7.5

Identification number	$\delta^{13}C$ (VPDB)	$\delta^{18}O$ (VSMOW)	Taxon	Location or Formation	Distance from occlusal surface (mm)
JODA 1999-G	–10.01	22.62	*Merychippus*	Mascall	8.75
JODA 1999-H	–9.64	23.89	*Merychippus*	Mascall	10
JODA 1999-I	–9.46	24.28	*Merychippus*	Mascall	11.25
JODA 1999-J	–9.86	22.78	*Merychippus*	Mascall	12.5
JODA 1999-K	–10.52	23.53	*Merychippus*	Mascall	13.75
JODA 1999-L	–10.45	23.73	*Merychippus*	Mascall	15
JODA 1999-M	–11.02	23.31	*Merychippus*	Mascall	16.25
JODA 1999-N	–9.37	22.33	*Merychippus*	Mascall	17.5
JODA 2003-B	–10.94	22.39	*Merychippus*	Mascall	2.5
JODA 2003-C	–11.04	22.32	*Merychippus*	Mascall	3.75
JODA 2003-D	–11.11	22.33	*Merychippus*	Mascall	5
JODA 2003-E	–11.49	22.19	*Merychippus*	Mascall	6.25
JODA 2003-F	–11.31	22.2	*Merychippus*	Mascall	7.5
JODA 2003-G	–11.04	22.01	*Merychippus*	Mascall	8.75
JODA 2003-H	–10.89	22.38	*Merychippus*	Mascall	10
JODA 2003-I	–10.07	22.76	*Merychippus*	Mascall	11.25
JODA 2003-J	–10.48	22.32	*Merychippus*	Mascall	12.5
JODA 2003-K	–10.27	22.56	*Merychippus*	Mascall	13.75
JODA 2003-L	–10.57	23.27	*Merychippus*	Mascall	15
JODA 2003-M	–9.96	22.54	*Merychippus*	Mascall	16.25
JODA 2003-N	–10.83	23.83	*Merychippus*	Mascall	17.5
JODA 2026-B	–9.42	20.92	*Merychippus*	Mascall	2.5
JODA 2026-C	–9.58	21.7	*Merychippus*	Mascall	3.75

Identification number	$\delta^{13}C$ (VPDB)	$\delta^{18}O$ (VSMOW)	Taxon	Location or Formation	Distance from occlusal surface (mm)
JODA 2026-D	–9.78	21.2	*Merychippus*	Mascall	5
JODA 2026-E	–9.93	20.83	*Merychippus*	Mascall	6.25
JODA 2026-F	–9.13	22.88	*Merychippus*	Mascall	7.5
JODA 2026-G	–10.13	24.04	*Merychippus*	Mascall	8.75
JODA 2026-H	–10.01	23.89	*Merychippus*	Mascall	10
JODA 2026-K	–10.69	22.71	*Merychippus*	Mascall	12.5
JODA 2026-L	–10.66	23.23	*Merychippus*	Mascall	13.75
JODA 2026-M	–10.68	23.16	*Merychippus*	Mascall	15
JODA 2026-N	–10.16	22.4	*Merychippus*	Mascall	16.25
JODA 2026-O	–10.33	22.49	*Merychippus*	Mascall	17.5
JODA 2026-P	–9.66	22.18	*Merychippus*	Mascall	18.75
JODA 2029-A	–11.19	21.11	*Merychippus*	Mascall	1.25
JODA 2029-B	–10.77	20.93	*Merychippus*	Mascall	2.5
JODA 2029-C	–11.11	21.34	*Merychippus*	Mascall	3.75
JODA 2029-D	–10.99	20.24	*Merychippus*	Mascall	5
JODA 2029-E	–10.95	19.56	*Merychippus*	Mascall	6.25
JODA 2029-F	–11.4	20.14	*Merychippus*	Mascall	7.5
JODA 2029-G	–10.99	21.02	*Merychippus*	Mascall	8.75
JODA 2029-H	–10.93	21.32	*Merychippus*	Mascall	10
JODA 2029-I	–11.47	21.62	*Merychippus*	Mascall	11.25
JODA 2029-J	–11.74	21.71	*Merychippus*	Mascall	12.5
JODA 2029-K	–11.91	21.35	*Merychippus*	Mascall	13.75
JODA-2029-M	–11.76	23.09	*Merychippus*	Mascall	15

Identification number	$\delta^{13}C$ (VPDB)	$\delta^{18}O$ (VSMOW)	Taxon	Location or Formation	Distance from occlusal surface (mm)
JODA-2029-N	–12.31	22.25	*Merychippus*	Mascall	16.25
JODA-2029-P	–12.45	23.31	*Merychippus*	Mascall	17.5
JODA-2029-Q	–11.64	21.09	*Merychippus*	Mascall	18.75
F-23851-C	–9.48	19.76	*Merychippus*	Mascall	3.75
F-23851-D	–9.57	19.16	*Merychippus*	Mascall	5
F-23851-E	–9.6	19.32	*Merychippus*	Mascall	6.25
F-23851-F	–9.7	18.82	*Merychippus*	Mascall	7.5
F-23851-G	–10.2	19.62	*Merychippus*	Mascall	8.75
F-23851-H	–10.03	19.61	*Merychippus*	Mascall	10
F-23851-I	–10.29	18.64	*Merychippus*	Mascall	11.25
F-23851-J	–9.87	18.3	*Merychippus*	Mascall	12.5
F-23851-L	–9.8	18.8	*Merychippus*	Mascall	15
F-23851-M	–10.14	18.68	*Merychippus*	Mascall	16.25
F-30988-B	–12.19	22.84	*Merychippus*	Mascall	2.5
F-30988-D	–11.24	20.32	*Merychippus*	Mascall	5
F-30989-C	–11.5	24.52	*Merychippus*	Mascall	3.75
F-30989-F	–12.05	23.77	*Merychippus*	Mascall	7.5
F-30989-G	–12.52	25.58	*Merychippus*	Mascall	8.75
F-30989-J	–12.46	26.02	*Merychippus*	Mascall	11.25
F-30989-I	–12.89	25.43	*Merychippus*	Mascall	10
F-30989-K	–14.82	25.05	*Merychippus*	Mascall	12.5
F-23852-A+B	–10.75	20.74	*Merychippus*	Mascall	2.5
F-23852-C	–10.1	20.45	*Merychippus*	Mascall	3.75

Identification number	$\delta^{13}C$ (VPDB)	$\delta^{18}O$ (VSMOW)	Taxon	Location or Formation	Distance from occlusal surface (mm)
F-23852-D	–10.94	20.47	*Merychippus*	Mascall	5
F-23852-E	–10.9	20.92	*Merychippus*	Mascall	6.25
F-23852-F	–10.56	19.57	*Merychippus*	Mascall	7.5
F-23852-G	–11.54	20.27	*Merychippus*	Mascall	8.75
F-23852-H	–10.48	18.72	*Merychippus*	Mascall	10
F-23852-I	–10.84	20.31	*Merychippus*	Mascall	11.25
F-23852-J	–10.18	18.94	*Merychippus*	Mascall	12.5
F-23852-K	–10.1	18.99	*Merychippus*	Mascall	13.75
JODA-2000-C	–11.45	20.37	*Merychippus*	Mascall	3.75
JODA-2000-B	–11.29	19.75	*Merychippus*	Mascall	2.5
JODA-2000-E	–11.3	20.42	*Merychippus*	Mascall	6.25
JODA-2000-F	–10.78	20.58	*Merychippus*	Mascall	7.5
JODA-2000-G	–11.66	20.99	*Merychippus*	Mascall	8.75
JODA-2000-I	–11.45	20.99	*Merychippus*	Mascall	11.25
JODA-2000-H	–11.64	21.5	*Merychippus*	Mascall	10
JODA-2000-K	–11.11	21.73	*Merychippus*	Mascall	13.75
JODA-2000-L	–11.49	21.87	*Merychippus*	Mascall	15
JODA-2000-M	–11.5	22.14	*Merychippus*	Mascall	16.25
JODA-2000-N	–11.03	22.12	*Merychippus*	Mascall	17.5
JODA-2018-A	–12.09	21.29	*Merychippus*	Mascall	1.25
JODA-2018-B	–12.32	21.11	*Merychippus*	Mascall	2.5
JODA-2018-C	–12.19	20.85	*Merychippus*	Mascall	3.75
JODA-2018-D	–12.49	20.51	*Merychippus*	Mascall	5

Identification number	$\delta^{13}C$ (VPDB)	$\delta^{18}O$ (VSMOW)	Taxon	Location or Formation	Distance from occlusal surface (mm)
JODA-2018-E	–12.44	20.6	*Merychippus*	Mascall	6.25
JODA-2018-F	–11.24	20.15	*Merychippus*	Mascall	7.5
JODA-2018-G	–11.83	19.45	*Merychippus*	Mascall	10
JODA-2018-H	–11.77	20.32	*Merychippus*	Mascall	11.25
JODA-2018-I	–11.22	20.1	*Merychippus*	Mascall	12.5
JODA-2018-J	–11.67	19.75	*Merychippus*	Mascall	13.75
JODA-2018-K	–12.48	20.25	*Merychippus*	Mascall	15
JODA-2018-M	–11.78	20.23	*Merychippus*	Mascall	16.25
JODA-2018-O	–11.82	20.85	*Merychippus*	Mascall	18.75
JODA-2018-P	–12.16	20.51	*Merychippus*	Mascall	20
JODA 2008-B	–11.39	20.11	*Merychippus*	Mascall	2.5
JODA 2008-C	–11.67	19.39	*Merychippus*	Mascall	3.75
JODA 2008-E	–11.4	19.89	*Merychippus*	Mascall	6.25
JODA 2008-F	–11.32	19.94	*Merychippus*	Mascall	7.5
JODA 2008-G	–11.45	21.93	*Merychippus*	Mascall	8.75
JODA 2008-H	–10.92	21.19	*Merychippus*	Mascall	10
JODA 2008-I	–10.77	19.4	*Merychippus*	Mascall	11.25
JODA 2008-K	–11.01	20.63	*Merychippus*	Mascall	13.75
JODA 2008-L	–11.18	21.17	*Merychippus*	Mascall	15
JODA 2008-M	–11.07	21.27	*Merychippus*	Mascall	16.25
JODA 2008-N	–10.95	20.95	*Merychippus*	Mascall	17.5
JODA 2008-O	–11.11	21.24	*Merychippus*	Mascall	18.75
JODA 2006-A	–8.92	21.9	*Merychippus*	Mascall	1.25

Identification number	$\delta^{13}C$ (VPDB)	$\delta^{18}O$ (VSMOW)	Taxon	Location or Formation	Distance from occlusal surface (mm)
JODA 2006-B	–8.8	21.21	*Merychippus*	Mascall	2.5
JODA 2006-D	–9.17	20.81	*Merychippus*	Mascall	5
JODA 2006-F	–8.9	20.15	*Merychippus*	Mascall	7.5
JODA 2006-I	–8.87	22.95	*Merychippus*	Mascall	11.25
JODA 2006-K	–10.66	21.15	*Merychippus*	Mascall	15
JODA 2006-M	–9.17	22.83	*Merychippus*	Mascall	17.5
JODA 2006-N	–9.84	19.05	*Merychippus*	Mascall	18.75
JODA 2006-P	–9.18	20.1	*Merychippus*	Mascall	21.25
JODA 2006-S	–13.47	18.46	*Merychippus*	Mascall	25
JODA 4269-C	–11.92	20.96	Equidae	Mascall	3.75
JODA 4269-D	–12.03	21.48	Equidae	Mascall	5
JODA 4269-E	–12.14	21.42	Equidae	Mascall	6.25
JODA 4269-F	–11.62	21.46	Equidae	Mascall	7.5
JODA 4269-G	–11.55	22.65	Equidae	Mascall	8.75
JODA 4269-H	–11.66	22.98	Equidae	Mascall	10
JODA 4269-I	–11.7	21.63	Equidae	Mascall	11.25
JODA 4269-J	–12.02	21.78	Equidae	Mascall	12.5
JODA 4269-K	–12.32	22.61	Equidae	Mascall	13.75
JODA 4269-L	–12.21	22.27	Equidae	Mascall	15
JODA 4269-M	–12.65	22.11	Equidae	Mascall	16.25
Sucker Creek (~14.9 Ma)					
Identification number	$\delta^{13}C$ (VPDB)	$\delta^{18}O$ (VSMOW)	Taxon	Location or Formation	Distance from occlusal surface (mm)

Identification number	$\delta^{13}C$ (VPDB)	$\delta^{18}O$ (VSMOW)	Taxon	Location or Formation	Distance from occlusal surface (mm)
JODA 8459 K	–8.99	17.48	*Merychippus*	Sucker Creek	13.75
JODA 8459-A	–9.13	17.69	*Merychippus*	Sucker Creek	1.25
JODA 8459-D	–9.43	17.82	*Merychippus*	Sucker Creek	5
JODA 8459-F	–9.24	17.05	*Merychippus*	Sucker Creek	7.5
JODA 8459-G	–8.94	16.7	*Merychippus*	Sucker Creek	8.75
JODA 8460 B	–9.86	19.93	*Merychippus*	Sucker Creek	2.5
JODA 8460 E	–10.31	20.03	*Merychippus*	Sucker Creek	5
JODA 8460 H	–10.38	20.11	*Merychippus*	Sucker Creek	8.75
JODA 8460 K	–10.5	20.26	*Merychippus*	Sucker Creek	12.5
JODA 8460 N	–10.62	20.23	*Merychippus*	Sucker Creek	16.25
JODA 8451 A	–9.13	16.09	*Merychippus*	Sucker Creek	1.25
JODA 8451 D	–8.99	17.35	*Merychippus*	Sucker Creek	5
JODA 8451 G	–9.32	17.24	*Merychippus*	Sucker Creek	8.75
JODA 8451 J	–8.76	17.88	*Merychippus*	Sucker Creek	12.5
JODA 8451 L	–8.52	17.22	*Merychippus*	Sucker Creek	15
JODA 8464 E	–9.43	18.99	*Merychippus*	Sucker Creek	6.25
JODA 8464 H	–9.54	19.57	*Merychippus*	Sucker Cree	10
JODA 8464 K	–9.24	19.53	*Merychippus*	Sucker Creek	13.75
JODA 8464 N (Root)	–8.53	18.85	*Merychippus*	Sucker Creek	17.5
JODA 8463-E/H	–9.87	20.55	Equid	Sucker Creek	10
JODA 8463-K/N	–9.9	16.05	Equid	Sucker Creek	16.25
JODA 8453-A (TOP)	–9.17	17.59	Equid	Sucker Creek	1.25

Identification number	$\delta^{13}C$ (VPDB)	$\delta^{18}O$ (VSMOW)	Taxon	Location or Formation	Distance from occlusal surface (mm)
JODA 8453-F	–9.06	18.23	Equid	Sucker Creek	7.5
JODA 8453-H	–9.21	18.03	Equid	Sucker Creek	10
JODA 8454-A (TOP)	–11.26	18.39	Equid	Sucker Creek	1.25
JODA 8454-D/F	–10.58	19.09	Equid	Sucker Creek	7.5
JODA 8454-H	–10.14	18.91	Equid	Sucker Creek	10
JODA 8457-C	–10.23	16.28	Equid	Sucker Creek	3.75
JODA 8457-E/G	–10.47	17.08	Equid	Sucker Creek	8.75
JODA 8457-I	–10.26	18.02	Equid	Sucker Creek	11.25
JODA 8458-D	–9.1	18.55	Rhino	Sucker Creek	5
JODA 8458-F	–10.03	17.44	Rhino	Sucker Creek	7.5
JODA 8458-H	–10.28	17.01	Rhino	Sucker Creek	10
JODA 8458-J	–9.99	16.81	Rhino	Sucker Creek	12.5
JODA 8458-L	–10.02	16.78	Rhino	Sucker Creek	15
JODA 8465-A	–8.19	18.05	Artiodactyl	Sucker Creek	1.25
JODA 8465-C/E	–8.59	13.31	Artiodactyl	Sucker Creek	6.25
JODA 8466-C	–9.99	15.02	Artiodactyl	Sucker Creek	1.25
JODA 8466-E	–8.38	15.56	Artiodactyl	Sucker Creek	6.25
Quartz Basin (14.3-14.8 Ma)					
Identification number	$\delta^{13}C$ (VPDB)	$\delta^{18}O$ (VSMOW)	Taxon	Location or Formation	Distance from occlusal surface (mm)
JODA 8468 J	–9.34	20.3	*Merychippus*	Quartz Basin	12.5
JODA 8468 M	–9.39	20.01	*Merychippus*	Quartz Basin	16.25

Identification number	$\delta^{13}C$ (VPDB)	$\delta^{18}O$ (VSMOW)	Taxon	Location or Formation	Distance from occlusal surface (mm)
JODA 8468 P	–9.43	18.93	*Merychippus*	Quartz Basin	20
JODA 8468 S	–9.66	18.94	*Merychippus*	Quartz Basin	23.75
JODA 8468 V	–9.55	18.3	*Merychippus*	Quartz Basin	27.5
JODA 8468 X	–9.93	19.15	*Merychippus*	Quartz Basin	31.25
JODA 8472 E	–9.3	21.05	*Merychippus*	Quartz Basin	6.25
JODA 8472 H	–9.25	20.53	*Merychippus*	Quartz Basin	10
JODA 8472 J	–9.12	20.64	*Merychippus*	Quartz Basin	12.5
JODA 8475-A/D	–9.59	19.6	Equid	Quartz Basin	5
JODA 8475-G/J	–9.18	18.2	Equid	Quartz Basin	12.5
Red Basin (~12.5-14.8 Ma)					
Identification number	$\delta^{13}C$ (VPDB)	$\delta^{18}O$ (VSMOW)	Taxon	Location or Formation	Distance from occlusal surface (mm)
23236-M1-B	–11.27	26.22	*Dromomeryx*	Red Basin	2.5
23236-M1-D	–9.58	28.06	*Dromomeryx*	Red Basin	5
23236-M1-F	–9.45	28.2	*Dromomeryx*	Red Basin	7.5
unlabled-M1-A	–11.37	26.11	*Dromomeryx*	Red Basin	1.25
unlabled-M1-C	–10.09	27.51	*Dromomeryx*	Red Basin	3.75
unlabled-M1-E	–10.12	27.47	*Dromomeryx*	Red Basin	6.25
20740-M2-B	–9.75	27.87	*Dromomeryx*	Red Basin	2.5
20740-M2-D	–9.81	27.81	*Dromomeryx*	Red Basin	5
20740-M2-F	–10.1	27.49	*Dromomeryx*	Red Basin	7.5
20740-M2-H	–10.65	26.89	*Dromomeryx*	Red Basin	10
20740-M2-J	–10.83	26.7	*Dromomeryx*	Red Basin	12.5

Identification number	$\delta^{13}C$ (VPDB)	$\delta^{18}O$ (VSMOW)	Taxon	Location or Formation	Distance from occlusal surface (mm)
unlabled-M2-A	–10.53	27.02	*Dromomeryx*	Red Basin	1.25
unlabled-M2-C	–9.93	27.68	*Dromomeryx*	Red Basin	3.75
unlabled-M2-E	–10.06	27.53	*Dromomeryx*	Red Basin	6.25
23235-M3-B	–9.86	27.75	*Dromomeryx*	Red Basin	2.5
23235-M3-D	–9.92	27.69	*Dromomeryx*	Red Basin	5
23235-M3-F	–10.52	27.03	*Dromomeryx*	Red Basin	7.5
23235-M3-H	–10.96	26.56	*Dromomeryx*	Red Basin	10
21255-M3-B	–10.01	27.59	*Dromomeryx*	Red Basin	2.5
21255-M3-D	–10.84	26.69	*Dromomeryx*	Red Basin	5
21255-M3-F	–10.85	26.67	*Dromomeryx*	Red Basin	7.5
21255-M3-H	–10.78	26.75	*Dromomeryx*	Red Basin	10
22127-P2-B	–9.16	28.52	*Dromomeryx*	Red Basin	2.5
22127-P2-D	–9.76	27.86	*Dromomeryx*	Red Basin	5
22127-P2-F	–10.5	27.06	*Dromomeryx*	Red Basin	7.5
22127-P2-H	–8.97	28.73	*Dromomeryx*	Red Basin	10
unlabled-P2-B	–9.71	27.92	*Dromomeryx*	Red Basin	2.5
unlabled-P2-D	–9.84	27.77	*Dromomeryx*	Red Basin	5
23239-P4-A	–10.37	27.2	*Dromomeryx*	Red Basin	1.25
23239-P4-C	–10.01	27.58	*Dromomeryx*	Red Basin	3.75
23239-P4-D	–10.2	27.38	*Dromomeryx*	Red Basin	5
23239-P4-F	–9.9	27.71	*Dromomeryx*	Red Basin	7.5
23239-P4-H	–10.11	27.48	*Dromomeryx*	Red Basin	10
Drewsey Formation (~9.8 Ma)					

Identification number	$\delta^{13}C$ (VPDB)	$\delta^{18}O$ (VSMOW)	Taxon	Location or Formation	Distance from occlusal surface (mm)
JODA 8479 A	–9.52	18.9	*Hipparion*	Drewsey	1.25
JODA 8479 B	–9.28	20.28	*Hipparion*	Drewsey	2.5
JODA 8479 F	–9.13	19.97	*Hipparion*	Drewsey	7.5
JODA 8479 I	–9.05	20.52	*Hipparion*	Drewsey	11.25
JODA 8479 J	–10.75	19.35	*Hipparion*	Drewsey	12.5
JODA 8479 L	–9.17	20.51	*Hipparion*	Drewsey	15
JODA 8479 M	–9.3	20.55	*Hipparion*	Drewsey	16.25
JODA 8479 P	–9.02	21.16	*Hipparion*	Drewsey	20
JODA 8479 Q	–8.67	20.58	*Hipparion*	Drewsey	21.25
JODA 8479 T	–8.81	20	*Hipparion*	Drewsey	25
JODA 8479 V	–8.81	20.56	*Hipparion*	Drewsey	27.5
JODA 8479 Z	–8.21	20.04	*Hipparion*	Drewsey	32.5
JODA 8479 AA	–8.74	20.31	*Hipparion*	Drewsey	33.75
JODA 8479 DD	–8.44	20.88	*Hipparion*	Drewsey	37.5
JODA 8479 GG	–9.13	20.72	*Hipparion*	Drewsey	35
JODA 8479 HH	–8.75	21.86	*Hipparion*	Drewsey	38.75
JODA 8479 II	–8.6	20.93	*Hipparion*	Drewsey	36.25
JODA 8479 JJ	0.9	20.69	*Hipparion*	Drewsey	37.5
JODA 8485 A	–9.04	19.11	*Pliohippus*	Drewsey	1.25
JODA 8485 D	–9.01	18.47	*Pliohippus*	Drewsey	6.25
JODA 8485 J	–8.58	17.59	*Pliohippus*	Drewsey	13.75
JODA 8485 B	–9.25	19.08	*Pliohippus*	Drewsey	2.5
JODA 8485 E	–8.6	18.69	*Pliohippus*	Drewsey	7.5

Identification number	$\delta^{13}C$ (VPDB)	$\delta^{18}O$ (VSMOW)	Taxon	Location or Formation	Distance from occlusal surface (mm)
JODA 8485 G	–8.52	18.2	*Pliohippus*	Drewsey	10
JODA 8485 H	–8.81	18.15	*Pliohippus*	Drewsey	12.5
JODA 8485 K	–8.51	17.48	*Pliohippus*	Drewsey	15
JODA 8485 N	–8.44	17.22	*Pliohippus*	Drewsey	18.5
JODA 8485 Q	–8.57	17.72	*Pliohippus*	Drewsey	22
JODA 8485 R	–8.94	17.83	*Pliohippus*	Drewsey	23.25
JODA 8491-I/L	–8.76	20.09	*Pliohippus*	Drewsey	15
JODA 8491-O	–9.07	19.83	*Pliohippus*	Drewsey	20
JODA 8491-Q	–8.86	18.9	*Pliohippus*	Drewsey	22.5
JODA 8494 F	–7.54	14.61	*Pliohippus*	Drewsey	7.5
JODA 8494 I	–7.25	13.84	*Pliohippus*	Drewsey	11.25
JODA 8494 L	–7.48	13.38	*Pliohippus*	Drewsey	15
JODA 8494 M	–6.99	13.75	*Pliohippus*	Drewsey	16.25
JODA 8498b A	–10.11	22.86	*Megatylopus*	Drewsey	1.25
JODA 8498b D	–9.74	23.53	*Megatylopus*	Drewsey	5
JODA 8498b G	–10.11	23.1	*Megatylopus*	Drewsey	8.75
JODA 8498b J	–9.94	23.52	*Megatylopus*	Drewsey	12.5
JODA 8498c B	–9.2	23.74	*Megatylopus*	Drewsey	2.5
JODA 8498c H	–9.24	22.54	*Megatylopus*	Drewsey	10
JODA 8498c K	–9.32	20.33	*Megatylopus*	Drewsey	13.75
JODA 8498a A	–11.12	20.97	Gomphothere	Drewsey	1.25
JODA 8498a D	–11.35	20.81	Gomphothere	Drewsey	5
JODA 8490-A	–10.61	18.89	Equid	Drewsey	1.25

Identification number	$\delta^{13}C$ (VPDB)	$\delta^{18}O$ (VSMOW)	Taxon	Location or Formation	Distance from occlusal surface (mm)
JODA 8490-E	–9.27	17.45	Equid	Drewsey	6.25
JODA 8490-B	–9.76	20.41	Equid	Drewsey	2.5
JODA 8490-D	–10.04	19.65	Equid	Drewsey	5
JODA 8490-F	–10.08	19.51	Equid	Drewsey	7.5
JODA 8490-H	–10.08	19	Equid	Drewsey	10
JODA 8490-L	–10.22	19.33	Equid	Drewsey	15
JODA 8490-E	–9.96	18.27	Rhino	Drewsey	6.25
JODA 8490-I	–10.07	18	Rhino	Drewsey	11.25
JODA 8490-K	–9.72	18.46	Rhino	Drewsey	13.75
Rattlesnake Formation (~7.1 Ma)					
Identification number	$\delta^{13}C$ (VPDB)	$\delta^{18}O$ (VSMOW)	Taxon	Location or Formation	Distance from occlusal surface (mm)
JODA 4389c-B	–11.12	23.54	Equid	Rattlesnake	2.5
JODA 4389c-C	–10.70	23.93	Equid	Rattlesnake	3.75
JODA 4389c-D	–9.93	22.32	Equid	Rattlesnake	5
JODA 4389c-E	–8.84	21.85	Equid	Rattlesnake	6.25
JODA 4389c-F	–10.26	23.85	Equid	Rattlesnake	7.5
JODA 4389c-G	–9.79	22.49	Equid	Rattlesnake	8.75
JODA 4389c-H	–10.24	23.69	Equid	Rattlesnake	10
JODA 4389c-I	–11.83	22.81	Equid	Rattlesnake	11.25
JODA 4389c-J	–10.11	22.21	Equid	Rattlesnake	12.5
JODA 4389d-B	–11.34	19.83	Equid	Rattlesnake	2.5
JODA 4389d-F	–11.22	21.57	Equid	Rattlesnake	7.5

Identification number	$\delta^{13}C$ (VPDB)	$\delta^{18}O$ (VSMOW)	Taxon	Location or Formation	Distance from occlusal surface (mm)
JODA 4389d-G	–11.04	19.69	Equid	Rattlesnake	8.75
JODA 2067a-C	–12.04	24.21	Equid	Rattlesnake	3.75
JODA 2067a-D	–11.66	25.97	Equid	Rattlesnake	5
JODA 2067a-H	–11.68	22.48	Equid	Rattlesnake	10
JODA 2067a-J	–11.91	22.7	Equid	Rattlesnake	12.5
JODA 2076b-B	–12.48	23.26	Equid	Rattlesnake	2.5
JODA 2076b-C	–11.38	22.93	Equid	Rattlesnake	3.75
JODA 2076b-D	–12.56	23.94	Equid	Rattlesnake	5
JODA 2076b-O	–12.26	25.5	Equid	Rattlesnake	18.75
Glenns Ferry Formation (Hagerman; ~3.2 Ma)					
Identification number	$\delta^{13}C$ (VPDB)	$\delta^{18}O$ (VSMOW)	Taxon	Location or Formation	Distance from occlusal surface (mm)
HAFO 16491-1	–10.4	19.87	*Camelops*	Glenns Ferry	0
HAFO 16491-2	–10.47	19.36	*Camelops*	Glenns Ferry	1.25
HAFO 16491-3	–10.07	18.81	*Camelops*	Glenns Ferry	2.5
HAFO 16491-4	–10.42	20.7	*Camelops*	Glenns Ferry	3.75
HAFO 16491-5	–10.45	20.71	*Camelops*	Glenns Ferry	5
HAFO 16491-6	–10.58	21.13	*Camelops*	Glenns Ferry	6.25
HAFO 16491-7	–9.63	18.3	*Camelops*	Glenns Ferry	7.5
HAFO 16491-8	–9.47	18.35	*Camelops*	Glenns Ferry	8.75
HAFO 17991-1	–8.02	19.39	*Equus*	Glenns Ferry	0
HAFO 17991-2	–8.18	19.03	*Equus*	Glenns Ferry	1.25
HAFO 17991-3	–8.54	18.9	*Equus*	Glenns Ferry	2.5

Identification number	$\delta^{13}C$ (VPDB)	$\delta^{18}O$ (VSMOW)	Taxon	Location or Formation	Distance from occlusal surface (mm)
HAFO 17991-4	–8.57	19.2	*Equus*	Glenns Ferry	3.75
HAFO 17991-5	–8.98	19.27	*Equus*	Glenns Ferry	5
HAFO 17991-6	–8.89	19.49	*Equus*	Glenns Ferry	6.25
HAFO 17991-7	–10.64	19.54	*Equus*	Glenns Ferry	7.5
HAFO 17991-8	–9.01	19.82	*Equus*	Glenns Ferry	8.75
HAFO 17991-9	–9.06	19.53	*Equus*	Glenns Ferry	10
HAFO 17991-10	–9.05	19.49	*Equus*	Glenns Ferry	11.25
HAFO 17991-11	–9.09	19.34	*Equus*	Glenns Ferry	12.5
HAFO 17991-12	–8.96	19.48	*Equus*	Glenns Ferry	13.75
HAFO 17991-13	–8.95	19.51	*Equus*	Glenns Ferry	15
HAFO 17991-14	–8.9	19.65	*Equus*	Glenns Ferry	16.25
HAFO 17991-15	–8.85	19.55	*Equus*	Glenns Ferry	17.5
HAFO 17991-16	–8.9	19.54	*Equus*	Glenns Ferry	18.75
HAFO 18057-1	–7.6	16.4	*Equus*	Glenns Ferry	0
HAFO 18057-2	–8.1	18	*Equus*	Glenns Ferry	1.3
HAFO 18057-3	–8.4	19	*Equus*	Glenns Ferry	2.5
HAFO 18057-4	–8.9	19.1	*Equus*	Glenns Ferry	3.8
HAFO 18057-5	–9.4	20.1	*Equus*	Glenns Ferry	5
HAFO 18057-6	–9.3	19.6	*Equus*	Glenns Ferry	6.3
HAFO 18057-7	–9.8	20.4	*Equus*	Glenns Ferry	7.5
HAFO 18057-9	–9.9	20.4	*Equus*	Glenns Ferry	10
HAFO 18057-10	–9.8	19.9	*Equus*	Glenns Ferry	11.3
HAFO 18057-11	–9.8	19.6	*Equus*	Glenns Ferry	12.5

Identification number	$\delta^{13}C$ (VPDB)	$\delta^{18}O$ (VSMOW)	Taxon	Location or Formation	Distance from occlusal surface (mm)
HAFO 18057-12	–9.8	20.3	*Equus*	Glenns Ferry	13.8
HAFO 18057-13	–9.7	20	*Equus*	Glenns Ferry	15
HAFO 18057-14	–9.6	20.3	*Equus*	Glenns Ferry	16.3
HAFO 18057-15	–9.8	20.6	*Equus*	Glenns Ferry	17.5
HAFO 18057-16	–9.6	19.9	*Equus*	Glenns Ferry	18.8
HAFO 18057-17	–9.8	20.1	*Equus*	Glenns Ferry	20
HAFO 18057-18	–9.8	19.7	*Equus*	Glenns Ferry	21.3
HAFO 389-1	–9.9	22	*Mammut*	Glenns Ferry	0
HAFO 389-2	–9.9	21.1	*Mammut*	Glenns Ferry	1.3
HAFO 389-3	–9.8	21.5	*Mammut*	Glenns Ferry	2.5
HAFO 389-4	–9.8	21.4	*Mammut*	Glenns Ferry	3.8
HAFO 389-5	–9.8	20.8	*Mammut*	Glenns Ferry	5
HAFO 389-6	–9.9	21.7	*Mammut*	Glenns Ferry	6.3
HAFO 389-7	–9.7	21.8	*Mammut*	Glenns Ferry	7.5
HAFO 389-8	–9.4	20.9	*Mammut*	Glenns Ferry	8.8
HAFO 7997-1	–10.3	19.1	*Mammut*	Glenns Ferry	0
HAFO 7997-2	–10.2	19.1	*Mammut*	Glenns Ferry	1.3
HAFO 7997-3	–10.2	19	*Mammut*	Glenns Ferry	2.5
HAFO 7997-4	–10.3	18.8	*Mammut*	Glenns Ferry	3.8
HAFO 7997-5	–10.1	18.8	*Mammut*	Glenns Ferry	5
HAFO 7997-6	–10.1	19	*Mammut*	Glenns Ferry	6.3
HAFO 7997-7	–9.9	19	*Mammut*	Glenns Ferry	7.5
HAFO 7997-8	–9.9	18.8	*Mammut*	Glenns Ferry	8.8

Identification number	$\delta^{13}C$ (VPDB)	$\delta^{18}O$ (VSMOW)	Taxon	Location or Formation	Distance from occlusal surface (mm)
HAFO 7997-9	–10	18.7	*Mammut*	Glenns Ferry	10
HAFO 7997-10	–9	19.5	*Mammut*	Glenns Ferry	11.3
HAFO 7997-11	–10	18.8	*Mammut*	Glenns Ferry	12.5
HAFO 17581-1	–9.2	17.6	*Castor*	Glenns Ferry	0
HAFO 17581-2	–9	17.2	*Castor*	Glenns Ferry	1.3
HAFO 17581-3	–9	17.6	*Castor*	Glenns Ferry	2.5
HAFO 17581-4	–8.9	17.7	*Castor*	Glenns Ferry	3.8
HAFO 17581-5	–8.9	17.8	*Castor*	Glenns Ferry	5
HAFO 17581-6	–8.7	17.7	*Castor*	Glenns Ferry	6.3
HAFO 17581-7	–8.8	17.9	*Castor*	Glenns Ferry	7.5
HAFO 17581-8	–8.9	18.1	*Castor*	Glenns Ferry	8.8
HAFO 17581-9	–8.6	18.1	*Castor*	Glenns Ferry	10
HAFO 17581-10	–8.5	17.9	*Castor*	Glenns Ferry	11.3
HAFO 17581-11	–8.6	18	*Castor*	Glenns Ferry	12.5
HAFO 17581-12	–9	18.1	*Castor*	Glenns Ferry	13.8
HAFO 17581-13	–9.3	18.3	*Castor*	Glenns Ferry	15
HAFO 17581-14	–9.1	18.2	*Castor*	Glenns Ferry	16.3
HAFO 19145-1	–9.7	20.5	Proboscidea	Glenns Ferry	0
HAFO 19145-2	–9.6	20.6	Proboscidea	Glenns Ferry	1.3
HAFO 19145-3	–9.6	20.5	Proboscidea	Glenns Ferry	2.5
HAFO 19145-4	–9.5	20.6	Proboscidea	Glenns Ferry	3.8
HAFO 19145-5	–9.5	20.4	Proboscidea	Glenns Ferry	5
HAFO 19145-6	–9.6	20	Proboscidea	Glenns Ferry	6.3

Identification number	$\delta^{13}C$ (VPDB)	$\delta^{18}O$ (VSMOW)	Taxon	Location or Formation	Distance from occlusal surface (mm)
HAFO 19145-7	–8.4	17.6	Proboscidea	Glenns Ferry	7.5
HAFO 19145-8	–8.2	17.2	Proboscidea	Glenns Ferry	8.8
HAFO 170581-1	–8.9	17.9	*Castor*	Glenns Ferry	0
HAFO 170581-2	–8.9	17.6	*Castor*	Glenns Ferry	1.3
HAFO 170581-3	–8.8	17.7	*Castor*	Glenns Ferry	2.5
HAFO 170581-4	–8.6	17.7	*Castor*	Glenns Ferry	3.8
HAFO 170581-5	–8.7	18.1	*Castor*	Glenns Ferry	5
HAFO 170581-6	–8.4	17.7	*Castor*	Glenns Ferry	6.3
HAFO 170581-7	–8.6	17.6	*Castor*	Glenns Ferry	7.5
HAFO 170581-8	–8.8	17.9	*Castor*	Glenns Ferry	8.8
HAFO 170581-9	–8.3	16.9	*Castor*	Glenns Ferry	10
HAFO 170581-10	–8.4	17.5	*Castor*	Glenns Ferry	11.3
HAFO 170581-11	–8.4	18.1	*Castor*	Glenns Ferry	12.5
HAFO 170581-12	–8.6	18	*Castor*	Glenns Ferry	13.8
HAFO 170581-13	–9.3	18.2	*Castor*	Glenns Ferry	15
HAFO 170581-14	–8.9	17.8	*Castor*	Glenns Ferry	16.3
HAFO 2191-1	–9.8	19.8	*Equus*	Glenns Ferry	0
HAFO 2191-2	–9.5	18.7	*Equus*	Glenns Ferry	1.3
HAFO 2191-3	–9.3	18.9	*Equus*	Glenns Ferry	2.5
HAFO 2191-4	–9.4	18	*Equus*	Glenns Ferry	3.8
HAFO 2191-5	–9.4	18.4	*Equus*	Glenns Ferry	5
HAFO 2191-6	–9.3	17.4	*Equus*	Glenns Ferry	6.3
HAFO 2191-7	–9.1	18.5	*Equus*	Glenns Ferry	7.5

Identification number	$\delta^{13}C$ (VPDB)	$\delta^{18}O$ (VSMOW)	Taxon	Location or Formation	Distance from occlusal surface (mm)
HAFO 2191-8	–9.1	19.2	*Equus*	Glenns Ferry	8.8
HAFO 2191-9	–9.3	18.9	*Equus*	Glenns Ferry	10
HAFO 2191-10	–9.4	19.2	*Equus*	Glenns Ferry	11.3
HAFO 2191-11	–9.2	18.8	*Equus*	Glenns Ferry	12.5
HAFO 2191-12	–9.4	19.6	*Equus*	Glenns Ferry	13.8
HAFO 2126-1	–9.4	18.3	*Castor*	Glenns Ferry	0
HAFO 2126-2	–10	18.7	*Castor*	Glenns Ferry	1.3
HAFO 2126-3	–9.7	18.3	*Castor*	Glenns Ferry	2.5
HAFO 2126-4	–9.7	18.7	*Castor*	Glenns Ferry	3.8
HAFO 2126-5	–10	18.6	*Castor*	Glenns Ferry	5
HAFO 2126-6	–9.8	18.5	*Castor*	Glenns Ferry	6.3
HAFO 2126-7	–9.6	18.3	*Castor*	Glenns Ferry	7.5
HAFO 2126-8	–9.2	18.4	*Castor*	Glenns Ferry	8.8
HAFO 2126-9	–9.1	17.7	*Castor*	Glenns Ferry	10
HAFO 2126-10	–9	18.4	*Castor*	Glenns Ferry	11.3
HAFO 2126-11	–8.8	17.2	*Castor*	Glenns Ferry	12.5
HAFO 2126-12	–8.7	18.4	*Castor*	Glenns Ferry	13.8
HAFO 2126-13	–8.6	19.4	*Castor*	Glenns Ferry	15
HAFO 2126-14	–8.4	17.9	*Castor*	Glenns Ferry	16.3
HAFO 986-1	–10	19.1	*Mammut*	Glenns Ferry	0
HAFO 986-2	–10.4	18.8	*Mammut*	Glenns Ferry	1.3
HAFO 986-3	–10.2	19.2	*Mammut*	Glenns Ferry	2.5
HAFO 986-4	–10.3	19	*Mammut*	Glenns Ferry	3.8

Identification number	$\delta^{13}C$ (VPDB)	$\delta^{18}O$ (VSMOW)	Taxon	Location or Formation	Distance from occlusal surface (mm)
HAFO 986-5	–10.2	18.7	*Mammut*	Glenns Ferry	5
HAFO 986-6	–10.3	18.6	*Mammut*	Glenns Ferry	6.3
HAFO 986-7	–10.3	18.9	*Mammut*	Glenns Ferry	7.5
HAFO 8870-1	–9.7	18.2	*Mammut*	Glenns Ferry	0
HAFO 8870-2	–9.6	18	*Mammut*	Glenns Ferry	1.3
HAFO 8870-3	–9.6	18.1	*Mammut*	Glenns Ferry	2.5
HAFO 8870-4	–9.8	17.9	*Mammut*	Glenns Ferry	3.8
HAFO 8870-5	–10	17.8	*Mammut*	Glenns Ferry	5
HAFO 8870-6	–9.7	18.1	*Mammut*	Glenns Ferry	6.3
HAFO 8870-7	–10.1	18.1	*Mammut*	Glenns Ferry	7.5
HAFO 8870-8	–9.4	18	*Mammut*	Glenns Ferry	8.8
HAFO 19021-4	–8	17.8	Castoridae	Glenns Ferry	3.8
HAFO 19021-5	–7.7	17.9	Castoridae	Glenns Ferry	5
HAFO 19021-6	–7.7	17.2	Castoridae	Glenns Ferry	6.3
HAFO 19021-7	–7.7	17.4	Castoridae	Glenns Ferry	7.5
HAFO 19021-8	–7.7	18.1	Castoridae	Glenns Ferry	8.8
HAFO 19021-9	–7.8	18.2	Castoridae	Glenns Ferry	10
HAFO 19021-10	–7.8	18.1	Castoridae	Glenns Ferry	11.3
HAFO 18051-1	–8.7	16.4	*Equus*	Glenns Ferry	0
HAFO 18051-2	–9	16.5	*Equus*	Glenns Ferry	1.3
HAFO 18051-3	–8.5	17.3	*Equus*	Glenns Ferry	2.5
HAFO 18051-4	–8.6	17.4	*Equus*	Glenns Ferry	3.8
HAFO 18051-5	–8.5	17.6	*Equus*	Glenns Ferry	5

Identification number	$\delta^{13}C$ (VPDB)	$\delta^{18}O$ (VSMOW)	Taxon	Location or Formation	Distance from occlusal surface (mm)
HAFO 18051-6	–8.4	18.1	*Equus*	Glenns Ferry	6.3
HAFO 18051-7	–8.5	18.6	*Equus*	Glenns Ferry	7.5
HAFO 203-1	–10.3	19.4	Camelidae	Glenns Ferry	0
HAFO 203-2	–10.8	20.5	Camelidae	Glenns Ferry	1.3
HAFO 203-3	–10.7	22.1	Camelidae	Glenns Ferry	2.5
HAFO 203-4	–10.8	22.1	Camelidae	Glenns Ferry	3.8
HAFO 203-5	–10.7	22.8	Camelidae	Glenns Ferry	5
HAFO 203-6	–10.8	22.7	Camelidae	Glenns Ferry	6.3
HAFO 203-7	–10.6	22.8	Camelidae	Glenns Ferry	7.5
HAFO 203-8	–10.6	22.4	Camelidae	Glenns Ferry	8.8
HAFO 203-10	–10.6	22.5	Camelidae	Glenns Ferry	10
HAFO 203-11	–10.5	22.2	Camelidae	Glenns Ferry	11.3
HAFO 203-12	–10.4	21.6	Camelidae	Glenns Ferry	12.5
HAFO 203-13	–10.3	21.4	Camelidae	Glenns Ferry	13.8
HAFO 203-14	–10.2	21.1	Camelidae	Glenns Ferry	15
Birch Creek (~2.4 Ma)					
Identification number	$\delta^{13}C$ (VPDB)	$\delta^{18}O$ (VSMOW)	Taxon	Location or Formation	Distance from occlusal surface (mm)
IMNH 315-C	–9.2	18.51	*Equus*	Birch Creek	3.75
IMNH 315-F	–11.5	17.18	*Equus*	Birch Creek	6.25
IMNH 315-H	–9.2	19.25	*Equus*	Birch Creek	8.75
IMNH 315-Q	–10.7	20.2	*Equus*	Birch Creek	20
IMNH 315-R	–11.0	18.8	*Equus*	Birch Creek	21.25

Identification number	$\delta^{13}C$ (VPDB)	$\delta^{18}O$ (VSMOW)	Taxon	Location or Formation	Distance from occlusal surface (mm)
IMNH 315-X	–10.7	19	*Equus*	Birch Creek	28.75
IMNH 315-Z	–10.0	20.3	*Equus*	Birch Creek	31.25
IMNH 315-AA	–10.3	19.7	*Equus*	Birch Creek	32.5
IMNH 315-CC	–13.4	17.7	*Equus*	Birch Creek	35
IMNH 315-FF	–11.3	18.8	*Equus*	Birch Creek	38.75
IMNH 315-II	–10.1	21.1	*Equus*	Birch Creek	41.25
IMNH 315-JJ	–11.2	19.4	*Equus*	Birch Creek	42.5
IMNH 315-KK	–10.7	19.6	*Equus*	Birch Creek	43.75
IMNH 315-LL	–11.5	22.1	*Equus*	Birch Creek	45
Tyson Ranch (~1.9 Ma)					
Identification number	$\delta^{13}C$ (VPDB)	$\delta^{18}O$ (VSMOW)	Taxon	Location or Formation	Distance from occlusal surface (mm)
IMNH 231-F	–8.1	21.9	*Equus*	Tyson Creek	7.5
IMNH 231-G	–6.9	22.1	*Equus*	Tyson Creek	8.75
IMNH 231-J	–10.1	25.8	*Equus*	Tyson Creek	12.5
IMNH 231-L	–8.1	23.4	*Equus*	Tyson Creek	15
IMNH 231-M	–8.0	22.3	*Equus*	Tyson Creek	16.25
IMNH 231-N	–7.6	22.9	*Equus*	Tyson Creek	17.5
IMNH 231-O	–7.4	20.5	*Equus*	Tyson Creek	18.75
IMNH 231-P	–6.9	20.8	*Equus*	Tyson Creek	20
IMNH 231-Q	–6.9	21.9	*Equus*	Tyson Creek	21.25
IMNH 231-R	–7.2	24.6	*Equus*	Tyson Creek	22.5
IMNH 231-X	–7.3	25.7	*Equus*	Tyson Creek	30

Identification number	$\delta^{13}C$ (VPDB)	$\delta^{18}O$ (VSMOW)	Taxon	Location or Formation	Distance from occlusal surface (mm)
IMNH 231-Y	–8.7	23.6	*Equus*	Tyson Creek	31.25
IMNH 231-Z	–7.3	24.3	*Equus*	Tyson Creek	33.75
IMNH 231-BB	–7.2	23.4	*Equus*	Tyson Creek	35
IMNH 231-CC	–8.8	24.9	*Equus*	Tyson Creek	36.25
IMNH 231-DD	–7.7	24.1	*Equus*	Tyson Creek	37.5
IMNH 231-JJ	–11.0	26	*Equus*	Tyson Creek	45
IMNH 231-MM	–7.2	23.1	*Equus*	Tyson Creek	48.75
IMNH 231-LL	–8.5	24	*Equus*	Tyson Creek	50
IMNH 231-PP	–7.6	20.9	*Equus*	Tyson Creek	53.75
IMNH 231-TT	–8.0	24.6	*Equus*	Tyson Creek	57.75

APPENDIX B

Seasonal Precipitation Patterns in the American Southwest During the Late Pleistocene Inferred from Stable Isotopes in Tooth Enamel and Tufa

X-RAY DIFFRACTION

Mineral contents of tufa were determined by X-ray diffraction (XRD). Powdered tufa was split into 5 - 8 aliquots and transferred onto glass slides for analysis (Moore and Reynolds, 1997). Powder XRD analyses of whole-tufa samples were analyzed on a Rigaku MiniFlex X-ray diffractometer at the Federal Center USGS, Colorado, XRD laboratory. Samples were X-rayed from 20º to 25ºθ at a counting time of 2 s per step.

XRD analyses were completed to verify samples collected in the field, were in fact tufa (calcium carbonate). The highest intensity within the samples was calcite, confirming samples were tufa (Appendix Fig 2). Detrital silicate and carbonate grains were noticed during optical inspection of tufa samples, and detrital material peaks were also noted on XRD plots.

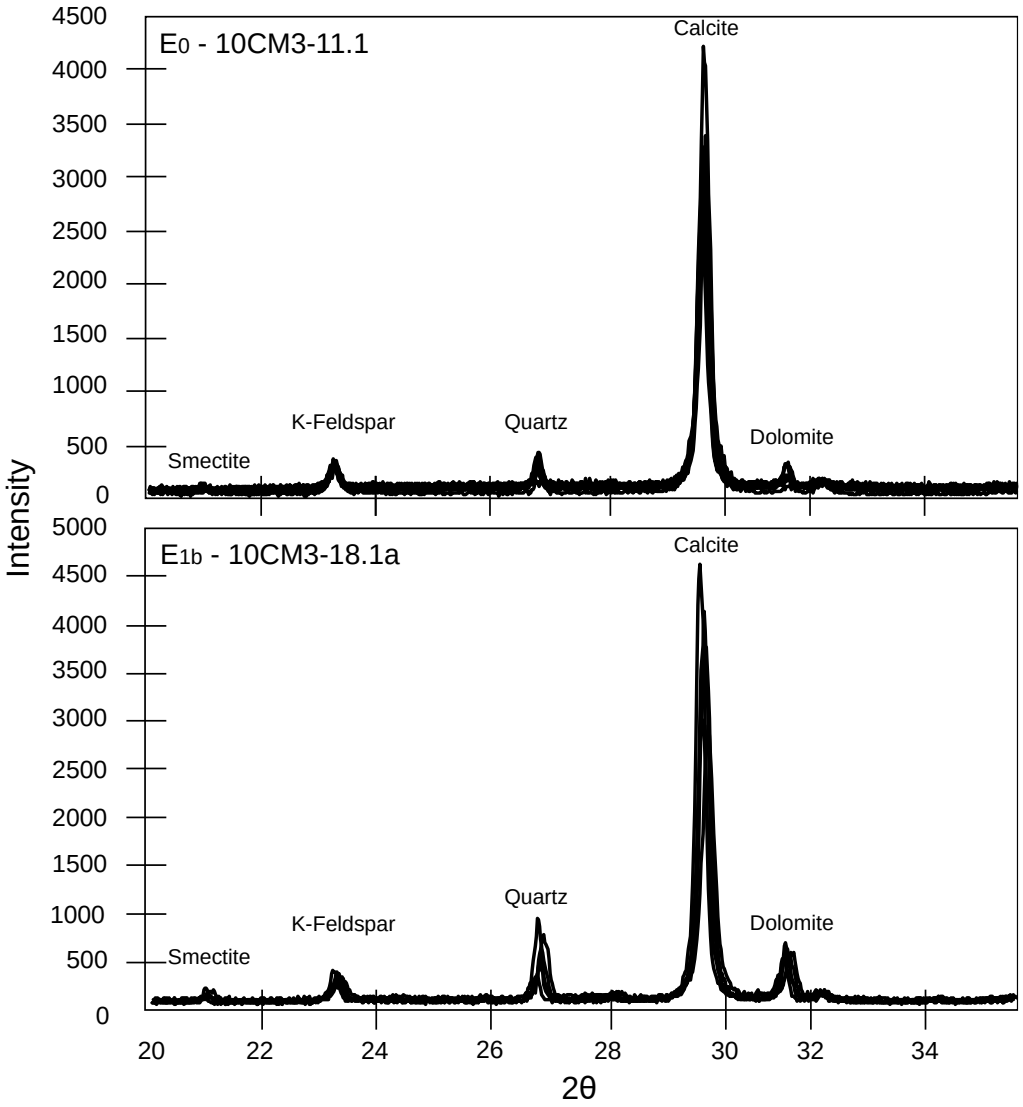

Figure A. 2. Two X-ray diffraction plots of two tufa samples, from units E0 (10CM3-11) and E1b (10CM3-18.1a), showing that tufas primarily consist of calcite, with a small amount of clay, silicates, and dolomite.

Table A. 3. $\delta^{18}O$ and $\delta^{13}C$ values for tooth enamel along with identification number, taxa, distance along each tooth, dating technique, age, and error.

Unit E_{1d}							
Identification number	$\delta^{13}C$ (‰, VPDB)	$\delta^{18}O$ (‰, VSMOW)	Taxa	Distance (mm)	Dating Technique	Age (cal ka BP)	±
03KS9-23.1-1	-8.13	32.14	*Camelops*	1.25	^{14}C	13.69	0.14
03KS9-23.1-3	-8.49	31.59	*Camelops*	2.5	^{14}C	13.69	0.14
03KS9-23.1-5	-8.71	31.70	*Camelops*	3.75	^{14}C	13.69	0.14
03KS9-23.1-7	-8.44	32.30	*Camelops*	5	^{14}C	13.69	0.14
03KS9-23.1-9	-8.35	34.35	*Camelops*	6.25	^{14}C	13.69	0.14
03KS9-23.1-11	-8.58	31.08	*Camelops*	7.5	^{14}C	13.69	0.14
03KS9-23.1-13	-9.42	30.91	*Camelops*	8.75	^{14}C	13.69	0.14
03KS9-23.1-15	-8.64	30.27	*Camelops*	10	^{14}C	13.69	0.14
03KS9-23.1-1b	-7.70	22.31	*Equus*	1.25	^{14}C	13.69	0.14
03KS9-23.1-3b	-7.47	22.86	*Equus*	2.5	^{14}C	13.69	0.14
03KS9-23.1-5b	-7.17	23.18	*Equus*	3.75	^{14}C	13.69	0.14
03KS9-23.1-7b	-7.12	23.23	*Equus*	5	^{14}C	13.69	0.14
03KS9-23.1-9b	-6.97	23.40	*Equus*	6.25	^{14}C	13.69	0.14
03KS9-23.1-11b	-6.87	23.51	*Equus*	7.5	^{14}C	13.69	0.14
03KS9-23.1-13b	-6.63	23.78	*Equus*	8.75	^{14}C	13.69	0.14
03KS9-23.1-15b	-6.68	23.72	*Equus*	10	^{14}C	13.69	0.14
03KS9-23.1-17b	-6.84	23.55	*Equus*	11.25	^{14}C	13.69	0.14
Identification number	$\delta^{13}C$ (‰, VPDB)	$\delta^{18}O$ (‰, VSMOW)	Taxa	Distance (mm)	Dating Technique	Age (cal ka BP)	±
Unit E_{1c}							

Identification number	$\delta^{13}C$ (‰, VPDB)	$\delta^{18}O$ (‰, VSMOW)	Taxa	Distance (mm)	Dating Technique	Age (cal ka BP)	±
03MRR10-1.2-1	-7.21	25.35	*Equus*	1.25	^{14}C	14.12	0.21
03MRR10-1.2-3	-7.37	25.84	*Equus*	2.5	^{14}C	14.12	0.21
03MRR10-1.2-5	-7.15	25.14	*Equus*	3.75	^{14}C	14.12	0.21
03MRR10-1.2-9	-7.18	24.02	*Equus*	6.25	^{14}C	14.12	0.21
03MRR10-1.2-11	-6.93	23.24	*Equus*	7.5	^{14}C	14.12	0.21
03MRR10-1.2-15	-6.52	23.91	*Equus*	10	^{14}C	14.12	0.21
03MRR10-1.2-17	-5.91	24.11	*Equus*	11.25	^{14}C	14.12	0.21
03MRR10-1.2-19	-6.30	24.37	*Equus*	12.5	^{14}C	14.12	0.21
03MRR10-1.2-21	-6.90	24.58	*Equus*	13.75	^{14}C	14.12	0.21
03MRR10-1.2-23	-7.37	24.09	*Equus*	15	^{14}C	14.12	0.21
03MRR10-1.2-25	-6.24	25.15	*Equus*	16.25	^{14}C	14.12	0.21
03MRR10-1.2-27	-7.49	24.92	*Equus*	17.5	^{14}C	14.12	0.21
03MRR10-1.2-29	-8.39	24.26	*Equus*	18.75	^{14}C	14.12	0.21
03MRR10-1.2-31	-5.92	25.58	*Equus*	20	^{14}C	14.12	0.21
03MRR10-1.2-33	-5.86	25.88	*Equus*	21.25	^{14}C	14.12	0.21
03MRR10-1.2-35	-6.48	26.63	*Equus*	22.5	^{14}C	14.12	0.21

Unit E_{1b}							
Identification number	$\delta^{13}C$ (‰, VPDB)	$\delta^{18}O$ (‰, VSMOW)	Taxa	Distance (mm)	Dating Technique	Age (cal ka BP)	±
03CM10-8.2A-1	-15.81	14.16	*Mammuthus*	1.25	^{14}C	14.59	0.50
03CM10-8.2A-3	-11.22	15.74	*Mammuthus*	2.5	^{14}C	14.59	0.50
03CM10-8.2A-5	-12.14	16.35	*Mammuthus*	3.75	^{14}C	14.59	0.50
03CM10-8.2A-7	-11.92	17.01	*Mammuthus*	5	^{14}C	14.59	0.50
03CM10-8.2A-9	-10.15	18.14	*Mammuthus*	6.25	^{14}C	14.59	0.50
03CM10-8.2A-11	-11.05	17.63	*Mammuthus*	7.5	^{14}C	14.59	0.50
03CM10-8.2A-13	-12.27	17.00	*Mammuthus*	8.75	^{14}C	14.59	0.50
03CM10-8.2A-15	-11.69	17.09	*Mammuthus*	10	^{14}C	14.59	0.50
03CM10-8.2A-17	-11.11	17.67	*Mammuthus*	11.25	^{14}C	14.59	0.50
03M10-18.24-19	-12.56	16.30	*Mammuthus*	12.5	^{14}C	14.59	0.50
10CM6-17.2-5	-1.96	22.75	*Camelops*	3.75	^{14}C	14.56	0.38
10CM6-17.2-7	-2.24	22.30	*Camelops*	5	^{14}C	14.56	0.38
10CM6-17.2-9	-2.28	22.21	*Camelops*	6.25	^{14}C	14.56	0.38
10CM6-17.2-11	-0.53	23.47	*Camelops*	7.5	^{14}C	14.56	0.38
10CM6-17.2-13	-1.21	24.24	*Camelops*	8.75	^{14}C	14.56	0.38
10CM6-17.2-15	-0.87	24.57	*Camelops*	10	^{14}C	14.56	0.38
10CM6-17.2-17	-1.15	25.36	*Camelops*	11.25	^{14}C	14.56	0.38
10CM6-17.1-1	-12.36	22.23	*Camelops*	1.25	^{14}C	14.56	0.38
10CM6-17.1-3	-9.10	23.01	*Camelops*	2.5	^{14}C	14.56	0.38
10CM6-17.1-5	-9.19	21.08	*Camelops*	3.75	^{14}C	14.56	0.38

Identification number	$\delta^{13}C$ (‰, VPDB)	$\delta^{18}O$ (‰, VSMOW)	Taxa	Distance (mm)	Dating Technique	Age (cal ka BP)	±
10CM6-17.1-7	-10.08	20.02	*Camelops*	5	^{14}C	14.56	0.38
10CM6-17.1-9	-7.53	23.83	*Camelops*	6.25	^{14}C	14.56	0.38
10CM6-17.1-11	-6.77	19.37	*Camelops*	7.5	^{14}C	14.56	0.38
10CM6-17.1-13	-13.23	21.09	*Camelops*	8.75	^{14}C	14.56	0.38
10CM6-17.1-17	-10.00	26.79	*Camelops*	11.25	^{14}C	14.56	0.38
10CM6-17.1-21	-6.86	29.38	*Camelops*	12.5	^{14}C	14.56	0.38
10CM6-17.1-23	-6.73	27.27	*Camelops*	13.75	^{14}C	14.56	0.38
10CM6-17.1-25	-10.49	21.76	*Camelops*	15	^{14}C	14.56	0.38
10CM6-17.1-27	-11.28	20.06	*Camelops*	16.25	^{14}C	14.56	0.38
03MJS-10-1.2-1	-5.09	24.44	*Camelops*	1.25	^{14}C	14.56	0.38
03MJS-10-1.2-3	-5.13	24.93	*Camelops*	2.5	^{14}C	14.56	0.38
03MJS-10-1.2-5	-5.50	24.86	*Camelops*	3.75	^{14}C	14.56	0.38
03MJS-10-1.2-9	-5.17	24.46	*Camelops*	5	^{14}C	14.56	0.38
03MJS-10-1.2-11	-4.35	24.22	*Camelops*	6.25	^{14}C	14.56	0.38
03MJS-10-1.2-13	-4.57	24.80	*Camelops*	7.5	^{14}C	14.56	0.38
03MJS-10-1.2-15	-9.85	19.26	*Camelops*	8.75	^{14}C	14.56	0.38
03MJS-10-1.2-17	-7.04	21.56	*Camelops*	10	^{14}C	14.56	0.38
03MJS-10-1.2-19	-7.53	21.54	*Camelops*	11.25	^{14}C	14.56	0.38
03MJS-10-1.2-21	-4.39	23.83	*Camelops*	12.5	^{14}C	14.56	0.38
03MJS-10-1.2-25	-7.83	23.10	*Camelops*	15	^{14}C	14.56	0.38
03MJS-10-1.2-27	-10.35	21.31	*Camelops*	16.25	^{14}C	14.56	0.38

Identification number	$\delta^{13}C$ (‰, VPDB)	$\delta^{18}O$ (‰, VSMOW)	Taxa	Distance (mm)	Dating Technique	Age (cal ka BP)	±
03MJS-10-1.2-29	-8.40	22.90	*Camelops*	17.5	^{14}C	14.56	0.38
03MJS-10-1.2-31	-7.98	20.93	*Camelops*	18.75	^{14}C	14.56	0.38
03MJS-10-1.2-33	-6.50	24.61	*Camelops*	20	^{14}C	14.56	0.38
Unit E_{1a}							
Identification number	$\delta^{13}C$ (‰, VPDB)	$\delta^{18}O$ (‰, VSMOW)	Taxa	Distance (mm)	Dating Technique	Age (cal ka BP)	±
03GAM10-15.1.1-3	-7.32	20.32	*Mammoth*	2.5	^{14}C	16.10	0.21
03GAM10-15.1.1-5	-7.37	19.74	*Mammoth*	3.75	^{14}C	16.10	0.21
03GAM10-15.1.1-7	-6.74	19.86	*Mammoth*	5	^{14}C	16.10	0.21
03GAM10-15.1.1-9	-7.41	19.36	*Mammoth*	6.25	^{14}C	16.10	0.21
03GAM10-15.1.1-11	-7.67	19.55	*Mammoth*	7.5	^{14}C	16.10	0.21
03GAM10-15.1.2-1	-7.44	20.13	*Mammoth*	1.25	^{14}C	16.10	0.21
03GAM10-15.1.2-3	-5.91	19.47	*Mammoth*	2.5	^{14}C	16.10	0.21
03GAM10-15.1.2-5	-8.26	19.73	*Mammoth*	3.75	^{14}C	16.10	0.21
03GAM10-15.1.3-1	-7.78	20.37	*Mammoth*	1.25	^{14}C	16.10	0.21
03GAM10-15.1.3-3	-8.37	21.14	*Mammoth*	2.5	^{14}C	16.10	0.21
03GAM10-15.1.3-5	-9.41	19.90	*Mammoth*	3.75	^{14}C	16.10	0.21
03GAM10-15.1.4-3	-7.67	20.14	*Mammoth*	1.25	^{14}C	16.10	0.21
03GAM10-15.1.4-4	-7.36	19.21	*Mammoth*	2.45	^{14}C	16.10	0.21
03GAM10-15.1.4-5	-7.78	20.01	*Mammoth*	3.65	^{14}C	16.10	0.21
03GAM10-15.1.4-6	-7.69	19.54	*Mammoth*	4.85	^{14}C	16.10	0.21
03GAM10-15.1.4-7	-8.26	19.37	*Mammoth*	6.05	^{14}C	16.10	0.21

Unit E_0							
Identification number	$\delta^{13}C$ (‰, VPDB)	$\delta^{18}O$ (‰, VSMOW)	Taxa	Distance (mm)	Dating Technique	Age (cal ka BP)	±
L3160-773.3-9	-8.57	21.62	*Camelops*	6.25	^{14}C	19.80	0.22
L3160-773.3-11	-8.30	21.09	*Camelops*	7.5	^{14}C	19.80	0.22
L3160-773.3-13	-7.68	21.49	*Camelops*	8.75	^{14}C	19.80	0.22
L3160-773.3-15	-10.97	20.40	*Camelops*	10	^{14}C	19.80	0.22
L3160-773.3-17	-7.28	20.45	*Camelops*	11.25	^{14}C	19.80	0.22
L3160-773.3-19	-5.03	21.75	*Camelops*	12.5	^{14}C	19.80	0.22
L3160-773.3-21	-6.34	20.41	*Camelops*	13.75	^{14}C	19.80	0.22
L3160-773.3-23	-8.02	20.37	*Camelops*	15	^{14}C	19.80	0.22
L3160-207.1-1	-5.39	22.92	*Equus*	1.25	^{14}C	19.80	0.22
L3160-207.1-3	-5.00	23.72	*Equus*	2.5	^{14}C	19.80	0.22
L3160-207.1-5	-6.06	23.12	*Equus*	3.75	^{14}C	19.80	0.22
L3160-207.1-7	-5.40	22.47	*Equus*	5	^{14}C	19.80	0.22
L3160-207.2-1	-5.79	22.13	*Equus*	1.25	^{14}C	19.80	0.22
L3160-207.2-5	-6.46	22.88	*Equus*	3.75	^{14}C	19.80	0.22
L3160-207.2-7	-5.20	21.82	*Equus*	5	^{14}C	19.80	0.22
L3160-207.2-9	-5.73	22.70	*Equus*	6.25	^{14}C	19.80	0.22
L3160-207.2-11	-4.81	21.55	*Equus*	7.5	^{14}C	19.80	0.22
L3088-390a-1	-9.72	18.62	*Bison*	1.25	^{14}C	19.80	0.22
L3088-390a-3	-7.75	20.68	*Bison*	2.5	^{14}C	19.80	0.22
L3088-390a-5	-7.93	20.82	*Bison*	3.75	^{14}C	19.80	0.22

Identification number	$\delta^{13}C$ (‰, VPDB)	$\delta^{18}O$ (‰, VSMOW)	Taxa	Distance (mm)	Dating Technique	Age (cal ka BP)	±
L3088-390a-7	-7.27	22.02	*Bison*	5	^{14}C	19.80	0.22
L3088-390a-9	-7.47	21.23	*Bison*	6.25	^{14}C	19.80	0.22
L3088-390a-11	-7.08	20.88	*Bison*	7.5	^{14}C	19.80	0.22
L3088-459-3	-7.18	17.53	*Camelops*	2.5	^{14}C	19.80	0.22
L3088-459-5	-4.89	22.78	*Camelops*	3.75	^{14}C	19.80	0.22
L3088-459-7	-5.75	23.59	*Camelops*	5	^{14}C	19.80	0.22
L3088-459-9	-5.80	23.44	*Camelops*	6.25	^{14}C	19.80	0.22
L3088-459-11	-5.67	23.92	*Camelops*	7.5	^{14}C	19.80	0.22
L3088-459-13	-6.16	22.63	*Camelops*	8.75	^{14}C	19.80	0.22
L3088-459-15	-5.94	23.27	*Camelops*	10	^{14}C	19.80	0.22
L3088-459-17	-6.81	22.47	*Camelops*	11.25	^{14}C	19.80	0.22
L3088-459-19	-6.36	21.21	*Camelops*	12.5	^{14}C	19.80	0.22
L3160-953-3	-8.50	24.66	*Camelops*	2.5	^{14}C	19.80	0.22
L3160-953-5	-9.69	25.39	*Camelops*	3.75	^{14}C	19.80	0.22
L3160-953-7	-10.33	25.45	*Camelops*	5	^{14}C	19.80	0.22
L3160-953-9	-10.87	25.60	*Camelops*	6.25	^{14}C	19.80	0.22
L3160-953-11	-11.33	25.94	*Camelops*	7.5	^{14}C	19.80	0.22
L3160-953-13	-11.20	26.18	*Camelops*	8.75	^{14}C	19.80	0.22
L3160-953-15	-11.00	26.21	*Camelops*	10	^{14}C	19.80	0.22
L3160-953-17	-10.61	25.90	*Camelops*	11.25	^{14}C	19.80	0.22
L3160-953-21	-10.30	25.73	*Camelops*	13.75	^{14}C	19.80	0.22

Identification number	$\delta^{13}C$ (‰, VPDB)	$\delta^{18}O$ (‰, VSMOW)	Taxa	Distance (mm)	Dating Technique	Age (cal ka BP)	±
L3160-953-23	-10.21	25.67	*Camelops*	15	^{14}C	19.80	0.22
L3160-773.1-1	-6.80	24.47	*Camelops*	1.25	^{14}C	19.80	0.22
L3160-773.1-3	-7.30	22.95	*Camelops*	2.5	^{14}C	19.80	0.22
L3160-773.1-5	-6.81	23.07	*Camelops*	3.75	^{14}C	19.80	0.22
L3160-773.1-7	-7.36	22.68	*Camelops*	5	^{14}C	19.80	0.22
L3160-773.1-9	-7.17	22.12	*Camelops*	6.25	^{14}C	19.80	0.22
L3160-773.1-11	-7.13	22.11	*Camelops*	7.5	^{14}C	19.80	0.22
L3160-773.1-13	-7.17	21.60	*Camelops*	8.75	^{14}C	19.80	0.22
L3160-773.1-15	-7.06	21.87	*Camelops*	10	^{14}C	19.80	0.22
L3160-773.1-19	-8.47	22.61	*Camelops*	11.25	^{14}C	19.80	0.22
L3160-773.1-21	-8.48	23.10	*Camelops*	12.5	^{14}C	19.80	0.22
L3160-773.1-23	-8.87	23.54	*Camelops*	13.75	^{14}C	19.80	0.22
L3160-773.1-25	-8.88	22.35	*Camelops*	15	^{14}C	19.80	0.22
L3160-773.2-3+5	-7.23	21.22	*Camelops*	3	^{14}C	19.80	0.22
L3160-773.2-7	-7.17	20.54	*Camelops*	4.25	^{14}C	19.80	0.22
L3088-391-1	-6.03	23.42	*Camelops*	1.25	^{14}C	19.80	0.22
L3088-391-3	-6.31	23.20	*Camelops*	2.5	^{14}C	19.80	0.22
L3088-391-5	-5.77	22.99	*Camelops*	3.75	^{14}C	19.80	0.22
L3088-391-7	-5.99	22.68	*Camelops*	5	^{14}C	19.80	0.22
L3088-391-9	-6.06	22.51	*Camelops*	6.25	^{14}C	19.80	0.22
L3088-391-11	-6.54	22.42	*Camelops*	7.5	^{14}C	19.80	0.22

Identification number	$\delta^{13}C$ (‰, VPDB)	$\delta^{18}O$ (‰, VSMOW)	Taxa	Distance (mm)	Dating Technique	Age (cal ka BP)	±
L3088-391-13	-6.57	22.43	*Camelops*	8.75	^{14}C	19.80	0.22
L3088-391-15	-6.89	22.47	*Camelops*	10	^{14}C	19.80	0.22
L3088-391-17	-7.37	23.07	*Camelops*	11.25	^{14}C	19.80	0.22
L3088-391-19	-7.58	23.23	*Camelops*	12.5	^{14}C	19.80	0.22
L3088-391-21	-7.57	23.64	*Camelops*	13.75	^{14}C	19.80	0.22
L3088-391-23	-7.53	23.75	*Camelops*	15	^{14}C	19.80	0.22
L3088-391-25	-7.66	23.49	*Camelops*	16.25	^{14}C	19.80	0.22
L3088-391-27	-7.55	23.64	*Camelops*	17.5	^{14}C	19.80	0.22
L3088-391-29	-7.19	23.02	*Camelops*	18.75	^{14}C	19.80	0.22
L3088-391-31	-7.11	22.59	*Camelops*	20	^{14}C	19.80	0.22
L3088-391-33	-6.69	22.31	*Camelops*	21.25	^{14}C	19.80	0.22
L3088-391-35	-6.28	24.92	*Camelops*	22.5	^{14}C	19.80	0.22
L3088-391-39	-6.48	22.46	*Camelops*	23.75	^{14}C	19.80	0.22
L3088-391-41	-6.53	22.59	*Camelops*	25	^{14}C	19.80	0.22
L3088-520-5	-5.47	23.96	*Camelops*	7.5	^{14}C	19.80	0.22
L3088-520-7	-4.87	23.45	*Camelops*	8.75	^{14}C	19.80	0.22
L3088-520-9	-4.82	22.92	*Camelops*	10	^{14}C	19.80	0.22
L3088-520-11	-4.71	23.41	*Camelops*	11.25	^{14}C	19.80	0.22
L3088-520-13	-5.47	24.05	*Camelops*	12.5	^{14}C	19.80	0.22
L3088-520-15	-5.65	23.96	*Camelops*	13.75	^{14}C	19.80	0.22
L3088-520-17	-6.11	24.45	*Camelops*	15	^{14}C	19.80	0.22

Identification number	$\delta^{13}C$ (‰, VPDB)	$\delta^{18}O$ (‰, VSMOW)	Taxa	Distance (mm)	Dating Technique	Age (cal ka BP)	±
L3088-520-22	-7.01	25.39	*Camelops*	16.25	^{14}C	19.80	0.22
L3088-520-23	-6.74	25.18	*Camelops*	17.5	^{14}C	19.80	0.22
L3088-520-25	-6.68	25.07	*Camelops*	18.75	^{14}C	19.80	0.22
L3088-520-27	-6.25	24.54	*Camelops*	20	^{14}C	19.80	0.22
L3088-520-29	-6.50	24.28	*Camelops*	21.25	^{14}C	19.80	0.22
L3088-520-31	-6.17	24.40	*Camelops*	22.5	^{14}C	19.80	0.22
L3088-520-33	-6.03	23.49	*Camelops*	23.75	^{14}C	19.80	0.22
L3160-875	-8.00	20.74	*Mammuthus*	BULK	^{14}C	21.04	0.52
Unit D_2							
Identifier	$\delta^{13}C$ (‰, VPDB)	$\delta^{18}O$ (‰, VSMOW)	Taxa	Distance (mm)	Dating Technique	Age (cal ka BP)	±
L3160-39a-3	-3.64	20.70	*Mammuthus*	2.5	^{14}C	29.63	2.05
L3160-39a-5	-3.81	20.70	*Mammuthus*	3.75	^{14}C	29.63	2.05
L3160-39a-7	-3.84	21.05	*Mammuthus*	5	^{14}C	29.63	2.05
L3160-39a-9	-3.91	20.59	*Mammuthus*	6.25	^{14}C	29.63	2.05
L3160-39a-15	-2.29	19.88	*Mammuthus*	10	^{14}C	29.63	2.05
L3160-39a-21	-4.99	20.85	*Mammuthus*	16.25	^{14}C	29.63	2.05
L3160-39a-22	-4.73	20.34	*Mammuthus*	17.1	^{14}C	29.63	2.05
L3160-39a-23	-4.73	20.28	*Mammuthus*	17.95	^{14}C	29.63	2.05
L3160-39a-24	-4.53	20.12	*Mammuthus*	18.8	^{14}C	29.63	2.05
L3160-39a-25	-4.65	20.44	*Mammuthus*	19.65	^{14}C	29.63	2.05
L3160-39a-31	-6.14	20.72	*Mammuthus*	23.4	^{14}C	29.63	2.05

Identification number	$\delta^{13}C$ (‰, VPDB)	$\delta^{18}O$ (‰, VSMOW)	Taxa	Distance (mm)	Dating Technique	Age (cal ka BP)	±
L3160-39a-32	-5.18	20.12	*Mammuthus*	24.65	^{14}C	29.63	2.05
L3160-39a-35	-2.60	19.22	*Mammuthus*	27.15	^{14}C	29.63	2.05
L3160-39a-39	-2.61	19.81	*Mammuthus*	29.4	^{14}C	29.63	2.05
L3160-39a-43	-4.38	19.72	*Mammuthus*	31.9	^{14}C	29.63	2.05
L3160-39a-47	-4.57	19.64	*Mammuthus*	33.15	^{14}C	29.63	2.05
L3160-39a-49	-3.76	19.84	*Mammuthus*	34.4	^{14}C	29.63	2.05
L3160-6-5	-4.64	21.01	*Mammuthus*	6.25	^{14}C	29.63	2.05
L3160-6-7	-4.63	21.20	*Mammuthus*	8.75	^{14}C	29.63	2.05
L3160-6-11	-4.54	21.03	*Mammuthus*	11.25	^{14}C	29.63	2.05
L3160-6-15	-4.51	20.85	*Mammuthus*	13.75	^{14}C	29.63	2.05
L3160-6-17	-4.49	21.51	*Mammuthus*	15	^{14}C	29.63	2.05
L3160-6-19	-4.60	20.60	*Mammuthus*	16.25	^{14}C	29.63	2.05
L3160-6-21	-4.42	20.54	*Mammuthus*	17.5	^{14}C	29.63	2.05
L3160-6-23	-4.02	20.14	*Mammuthus*	18.75	^{14}C	29.63	2.05
L3160-6-25	-3.47	19.84	*Mammuthus*	20	^{14}C	29.63	2.05
L3160-6-27	-3.65	19.86	*Mammuthus*	21.25	^{14}C	29.63	2.05
L3160-6-29	-3.55	20.51	*Mammuthus*	22.5	^{14}C	29.63	2.05
L3160-6-31	-3.68	20.71	*Mammuthus*	23.75	^{14}C	29.63	2.05
L3160-6-33	-3.27	21.04	*Mammuthus*	25	^{14}C	29.63	2.05
L3160-6-35	-3.51	20.77	*Mammuthus*	26.25	^{14}C	29.63	2.05
L3160-6-37	-3.43	21.81	*Mammuthus*	27.5	^{14}C	29.63	2.05

Identification number	$\delta^{13}C$ (‰, VPDB)	$\delta^{18}O$ (‰, VSMOW)	Taxa	Distance (mm)	Dating Technique	Age (cal ka BP)	±
L3160-6-39	-4.07	21.20	*Mammuthus*	28.75	^{14}C	29.63	2.05
L3160-6-41	-4.15	21.11	*Mammuthus*	30	^{14}C	29.63	2.05
L3160-6-43	-4.74	21.41	*Mammuthus*	31.25	^{14}C	29.63	2.05
L3160-6-45	-4.57	20.69	*Mammuthus*	32.5	^{14}C	29.63	2.05
L3160-6-47	-5.13	20.39	*Mammuthus*	33.75	^{14}C	29.63	2.05
L3160-6-51	-4.45	21.85	*Mammuthus*	35	^{14}C	29.63	2.05
L3160-6-53	-4.39	21.26	*Mammuthus*	36.25	^{14}C	29.63	2.05
L3160-6-55	-4.65	21.28	*Mammuthus*	37.5	^{14}C	29.63	2.05
L3160-6-57	-5.18	21.04	*Mammuthus*	38.75	^{14}C	29.63	2.05
L3160-6-59	-4.29	20.68	*Mammuthus*	40	^{14}C	29.63	2.05
L3160-6-61	-4.29	20.77	*Mammuthus*	41.25	^{14}C	29.63	2.05
L3160-6-63	-4.96	21.04	*Mammuthus*	42.5	^{14}C	29.63	2.05
L3160-6-65	-4.60	20.88	*Mammuthus*	43.75	^{14}C	29.63	2.05
L3160-6-67	-4.68	20.69	*Mammuthus*	45	^{14}C	29.63	2.05
L3160-6-69	-4.51	20.23	*Mammuthus*	46.25	^{14}C	29.63	2.05
L3160-6-71	-4.81	20.59	*Mammuthus*	47.5	^{14}C	29.63	2.05
L3160-6-73	-5.04	20.49	*Mammuthus*	48.75	^{14}C	29.63	2.05
Unit D_1							
Identifier	$\delta^{13}C$ (‰, VPDB)	$\delta^{18}O$ (‰, VSMOW)	Taxa	Distance (mm)	Dating Technique	Age (cal ka BP)	±
L3160-654.2-1	-3.05	22.57	*Equus*	1.25	^{14}C	35.04	0.50
L3160-654.2-3	-2.71	22.58	*Equus*	2.5	^{14}C	35.04	0.50

Identification number	$\delta^{13}C$ (‰, VPDB)	$\delta^{18}O$ (‰, VSMOW)	Taxa	Distance (mm)	Dating Technique	Age (cal ka BP)	±
L3160-654.1-3	-8.89	32.12	*Equus*	2.5	^{14}C	35.04	0.50
L3160-654.1-5	-8.90	32.90	*Equus*	3.75	^{14}C	35.04	0.50
L3160-779-1	-5.34	22.28	*Equus*	1.25	^{14}C	35.04	0.50
L3160-779-3	-5.43	22.07	*Equus*	3.75	^{14}C	35.04	0.50
L3160-779-5	-6.46	22.20	*Equus*	6.25	^{14}C	35.04	0.50
L3160-779-7	-6.62	22.92	*Equus*	8.75	^{14}C	35.04	0.50
L3160-779-9	-6.45	22.90	*Equus*	11.25	^{14}C	35.04	0.50
L3160-779-11	-5.86	23.08	*Equus*	13.75	^{14}C	35.04	0.50
L3160-779-13	-5.56	22.70	*Equus*	16.25	^{14}C	35.04	0.50
L3160-917-3	-1.97	21.23	*Bison*	3.75	^{14}C	35.04	0.50
L3160-917-5	-1.42	21.14	*Bison*	6.25	^{14}C	35.04	0.50
L3160-917-9	-1.89	21.32	*Bison*	11.25	^{14}C	35.04	0.50
L3160-917-11	-2.38	21.82	*Bison*	13.75	^{14}C	35.04	0.50
L3160-917-13	-2.84	22.31	*Bison*	16.25	^{14}C	35.04	0.50
L3160-917-15	-3.05	23.53	*Bison*	18.75	^{14}C	35.04	0.50
L3160-917-17	-2.96	23.33	*Bison*	21.25	^{14}C	35.04	0.50
L3160-917-19	-2.49	21.61	*Bison*	23.75	^{14}C	35.04	0.50
L3160-917-23	-2.30	22.24	*Bison*	26.25	^{14}C	35.04	0.50
L3160-917-25	-2.10	21.24	*Bison*	28.75	^{14}C	35.04	0.50
L3160-917-27	-1.97	20.87	*Bison*	31.25	^{14}C	35.04	0.50
L3160-781-1	-1.85	20.73	*Bison*	1.25	^{14}C	35.04	0.50

Identification number	$\delta^{13}C$ (‰, VPDB)	$\delta^{18}O$ (‰, VSMOW)	Taxa	Distance (mm)	Dating Technique	Age (cal ka BP)	±
L3160-781-3	-3.23	20.14	*Bison*	2.5	^{14}C	35.04	0.50
L3160-781-5	-3.49	20.72	*Bison*	3.75	^{14}C	35.04	0.50
L3160-781-7	-2.86	21.37	*Bison*	5	^{14}C	35.04	0.50
L3160-781-11	-2.91	20.47	*Bison*	7.5	^{14}C	35.04	0.50
L3160-781-13	-3.08	21.31	*Bison*	8.75	^{14}C	35.04	0.50
L3160-781-15	-3.08	21.82	*Bison*	10	^{14}C	35.04	0.50
L3160-781-19	-1.66	20.89	*Bison*	12.5	^{14}C	35.04	0.50
L3160-647-1	-8.31	19.51	*Mammuthus columbi*	1.25	^{14}C	35.04	0.50
L3160-647-3	-8.54	19.73	*Mammuthus columbi*	2.5	^{14}C	35.04	0.50
L3160-647-5	-8.38	19.90	*Mammuthus columbi*	3.75	^{14}C	35.04	0.50
L3160-647-7	-8.49	19.65	*Mammuthus columbi*	5	^{14}C	35.04	0.50
L3160-647-9	-8.16	19.80	*Mammuthus columbi*	6.25	^{14}C	35.04	0.50
L3160-647-11	-8.26	19.33	*Mammuthus columbi*	7.5	^{14}C	35.04	0.50
L3160-647-13	-8.05	19.57	*Mammuthus columbi*	8.75	^{14}C	35.04	0.50
L3160-647-15	-7.96	19.46	*Mammuthus columbi*	10	^{14}C	35.04	0.50
L3160-647-17	-7.79	19.25	*Mammuthus columbi*	11.25	^{14}C	35.04	0.50
L3160-647-19	-7.98	19.05	*Mammuthus columbi*	12.5	^{14}C	35.04	0.50

Identification number	$\delta^{13}C$ (‰, VPDB)	$\delta^{18}O$ (‰, VSMOW)	Taxa	Distance (mm)	Dating Technique	Age (cal ka BP)	±
L3160-647-21	-8.18	18.88	*Mammuthus columbi*	13.75	^{14}C	35.04	0.50
L3160-647-23	-7.82	19.15	*Mammuthus columbi*	15	^{14}C	35.04	0.50
Unit B_2							
Identification number	$\delta^{13}C$ (‰, VPDB)	$\delta^{18}O$ (‰, VSMOW)	Taxa	Distance (mm)	Dating Technique	Age (cal ka BP)	±
L3160-748-1	-4.28	16.55	*Equus*	2.5	OSL	50.00	5.0
L3160-748-3	-3.85	18.49	*Equus*	3.75	OSL	50.00	5.0
L3160-748-5	-3.48	19.43	*Equus*	6.25	OSL	50.00	5.0
L3160-748-7	-3.58	19.86	*Equus*	8.75	OSL	50.00	5.0
L3160-748-9	-4.21	20.13	*Equus*	11.25	OSL	50.00	5.0
L3160-748-11	-4.37	20.88	*Equus*	13.75	OSL	50.00	5.0
L3160-748-13	-4.41	21.27	*Equus*	16.25	OSL	50.00	5.0
L3160-748-15	-4.39	21.36	*Equus*	18.75	OSL	50.00	5.0
L3160-751-3	-8.10	22.06	*Bison*	3.75	OSL	50.00	5.0
L3160-751-7	-8.29	25.75	*Bison*	8.75	OSL	50.00	5.0
L3160-751-9	-8.58	24.18	*Bison*	11.25	OSL	50.00	5.0
L3160-751-11	-8.36	23.63	*Bison*	13.75	OSL	50.00	5.0
L3160-751-15	-7.59	27.08	*Bison*	18.75	OSL	50.00	5.0
L3160-751-17	-7.14	25.85	*Bison*	21.25	OSL	50.00	5.0
L3160-751-19	-6.88	23.05	*Bison*	23.75	OSL	50.00	5.0
L3160-751-23	-6.91	18.51	*Bison*	28.75	OSL	50.00	5.0

Identification number	$\delta^{13}C$ (‰, VPDB)	$\delta^{18}O$ (‰, VSMOW)	Taxa	Distance (mm)	Dating Technique	Age (cal ka BP)	±
L3160-946-3	-5.66	20.12	*Bison*	3.75	OSL	50.00	5.0
L3160-946-5	-5.07	19.86	*Bison*	6.25	OSL	50.00	5.0
L3160-946-7	-4.30	20.39	*Bison*	8.75	OSL	50.00	5.0
L3160-946-9	-4.52	19.04	*Bison*	11.25	OSL	50.00	5.0
L3160-230.2-3	-4.95	20.46	*Equus*	2.5	OSL	50.00	5.0
L3160-230.2-5	-4.75	20.80	*Equus*	3.75	OSL	50.00	5.0
L3160-230.2-7	-4.61	20.80	*Equus*	5	OSL	50.00	5.0
L3160-230.2-9	-5.40	20.45	*Equus*	6.25	OSL	50.00	5.0
L3160-230.2-11	-4.71	20.79	*Equus*	7.5	OSL	50.00	5.0
L3160-230.2-13	-4.51	21.13	*Equus*	8.75	OSL	50.00	5.0
L3160-230.2-17	-5.19	20.52	*Equus*	11.25	OSL	50.00	5.0
L3160-230.2-19	-5.97	18.83	*Equus*	12.5	OSL	50.00	5.0
L3160-230.2-25	-4.86	20.75	*Equus*	17.5	OSL	50.00	5.0
L3160-230.2-27	-4.69	21.02	*Equus*	18.75	OSL	50.00	5.0
L3160-230.2-29	-4.98	20.51	*Equus*	20	OSL	50.00	5.0
L3160-230.2-35	-4.41	21.11	*Equus*	23.75	OSL	50.00	5.0
L3160-230.2-37	-5.01	20.90	*Equus*	26.25	OSL	50.00	5.0
L3160-230.2-39	-5.09	20.55	*Equus*	27.5	OSL	50.00	5.0
L3160-230.2-41	-4.91	20.81	*Equus*	28.75	OSL	50.00	5.0
L3160-230.2-43	-4.97	20.71	*Equus*	30	OSL	50.00	5.0
L3160-230.2-47	-4.91	20.41	*Equus*	32.5	OSL	50.00	5.0
L3160-230.2-49	-4.40	21.18	*Equus*	33.75	OSL	50.00	5.0
L3160-230.2-52	-4.02	21.26	*Equus*	35.25	OSL	50.00	5.0
L3160-230.2-53	-4.32	20.63	*Equus*	36	OSL	50.00	5.0

Identification number	$\delta^{13}C$ (‰, VPDB)	$\delta^{18}O$ (‰, VSMOW)	Taxa	Distance (mm)	Dating Technique	Age (cal ka BP)	±
L3160-230.2-55	-4.61	20.58	*Equus*	37.25	OSL	50.00	5.0
L3160-230.2-57	-4.51	20.64	*Equus*	38.5	OSL	50.00	5.0
L3160-230.2-59	-3.95	21.06	*Equus*	39.75	OSL	50.00	5.0
L3160-230.2-61	-4.30	21.23	*Equus*	41	OSL	50.00	5.0
L3160-230.2-63	-4.34	21.01	*Equus*	42.25	OSL	50.00	5.0
L3160-230.4-1	-5.17	22.57	*Bison*	1.25	OSL	50.00	5.0
L3160-230.4-3	-5.01	22.94	*Bison*	2.5	OSL	50.00	5.0
L3160-230.4-5	-4.87	22.77	*Bison*	3.75	OSL	50.00	5.0
L3160-230.4-7	-5.45	23.00	*Bison*	5	OSL	50.00	5.0
L3160-230.4-9	-5.63	23.11	*Bison*	6.25	OSL	50.00	5.0
L3160-230.4-11	-5.28	22.95	*Bison*	7.5	OSL	50.00	5.0
L3160-230.4-13	-5.01	22.85	*Bison*	8.75	OSL	50.00	5.0
L3160-230.4-15	-4.86	22.73	*Bison*	10	OSL	50.00	5.0
L3160-230.4-17	-4.94	22.74	*Bison*	11.25	OSL	50.00	5.0
L3160-230.4-19	-4.74	22.69	*Bison*	12.5	OSL	50.00	5.0
L3160-818.2-2	-3.98	21.15	*Bison*	1.5	OSL	50.00	5.0
L3160-818.2-3	-4.13	21.54	*Bison*	2.25	OSL	50.00	5.0
L3160-818.2-5	-3.82	21.15	*Bison*	3.5	OSL	50.00	5.0
L3160-818.2-7	-3.34	21.34	*Bison*	4.75	OSL	50.00	5.0
Unit B_1							
Identification number	$\delta^{13}C$ (‰, VPDB)	$\delta^{18}O$ (‰, VSMOW)	Taxa	Distance (mm)	Dating Technique	Age (cal ka BP)	±
04MRR1-28.1-3	-2.46	23.18	*Bison*	2.5	OSL	77.5	22.5
04MRR1-28.1-5	-2.52	23.62	*Bison*	3.75	OSL	77.5	22.5

Identification number	$\delta^{13}C$ (‰, VPDB)	$\delta^{18}O$ (‰, VSMOW)	Taxa	Distance (mm)	Dating Technique	Age (cal ka BP)	±
04MRR1-28.1-7	-2.67	24.48	*Bison*	5	OSL	77.5	22.5
04MRR1-28.1-9	-2.83	25.00	*Bison*	6.25	OSL	77.5	22.5
04MRR1-28.1-13	-2.12	22.48	*Bison*	8.75	OSL	77.5	22.5

APPENDIX C

The Interpretability of Stable Hydrogen Isotopes in Modern Herbivore Tooth Enamel

INTRODUCTION

In herbivores, $\delta^{13}C$ values in enamel carbonate reflect an animal's diet and ultimately local plant compositions (Koch, 1998; Cerling and Harris, 1999; Passey et al., 2005). Herbivores tend to consume either C_3 or C_4 vegetation, which differ in photosynthetic pathways, and these difference result in isotopically distinct ranges. C_4 grasses tend to outcompete C_3 grasses when pCO_2 is low, but C_3 grasses outcompete C_4 grasses in climates with intensified winter moisture (Kohn and Cerling, 2002). Climate studies have not utilized tooth enamel δD values for climate or environmental reconstructions, therefore it is unclear whether stable hydrogen isotopes correlate with vegetation signals.

In herbivores, omnivores, and carnivores, collagen $\delta^{13}C$ and δD values exhibit the trophic level effect, with herbivores displaying lower $\delta^{13}C$ and δD values when compared to carnivores (Reynard and Hedges, 2008; Birchnall et al., 2005). Other organic substrates, such has hair (keratin), alternatively display a decoupling between $\delta^{13}C$ and δD values in human specimens (Bowen et al., 2005b). Here we analyzed herbivore tooth enamel and measured $\delta^{13}C$ and δD values to evaluate whether these two isotopes correlate.

METHODS

Stable carbon isotopic compositions were measured by dissolving 1.5 to 2.0 mg of powdered enamel with supersaturated H_3PO_4. The subsequent CO_2 was measured using a ThermoFisher GasBench II, in-line with a Thermo Delta V Plus Mass Spectrometer, housed in the Stable Isotope Laboratory at Boise State University. Five to six NIST-120c ($\delta^{13}C = -6.55‰$, VPDB; Kohn et al., 2015) aliquots were prepared using the same cleaning and pretreatment methods and analyzed with each sample set. Each sample set was standardized to VPDB using eight to nine aliquots of the NBS-18 ($\delta^{13}C = -5.014‰$) and NBS-19 ($\delta^{13}C = +1.95‰$) calcite standards. Analytical reproducibility for carbon isotopes, reproducibility was: NIST-120c = ±4.03‰ (2σ); NBS-18 = ±0.40‰, and NBS-19 = ±0.40‰. All further $\delta^{13}C$ values are reported in VPDB.

STABLE CARON ISOTOPE RESULTS

Mean tooth enamel $\delta^{13}C$ values ranged from −18.08±0.35‰ (2 s.e.; specimen BTM) to +0.00±0.13‰ (O2120; Appendix Fig 3). The equation for the hydrogen and carbon (Appendix Fig 3; Appendix Table 3) regression is:

δD_{enamel} vs. $\delta^{13}C_{enamel}$: $\delta D = 0.75 \pm 0.70(\delta^{13}C) - 137 \pm 9‰$ ($R^2 = 0.10$) (Eq. A1)

STABLE HYDROGEN AND CARBON ISOTOPES IN TOOTH ENAMEL

A low R^2 value (0.10) for the stable hydrogen-carbon isotope regression, suggests no significant correlation between mean tooth δD and $\delta^{13}C$ values (Appendix Fig 3; Appendix Table 3). Decoupling between stable hydrogen and carbon isotopes is also

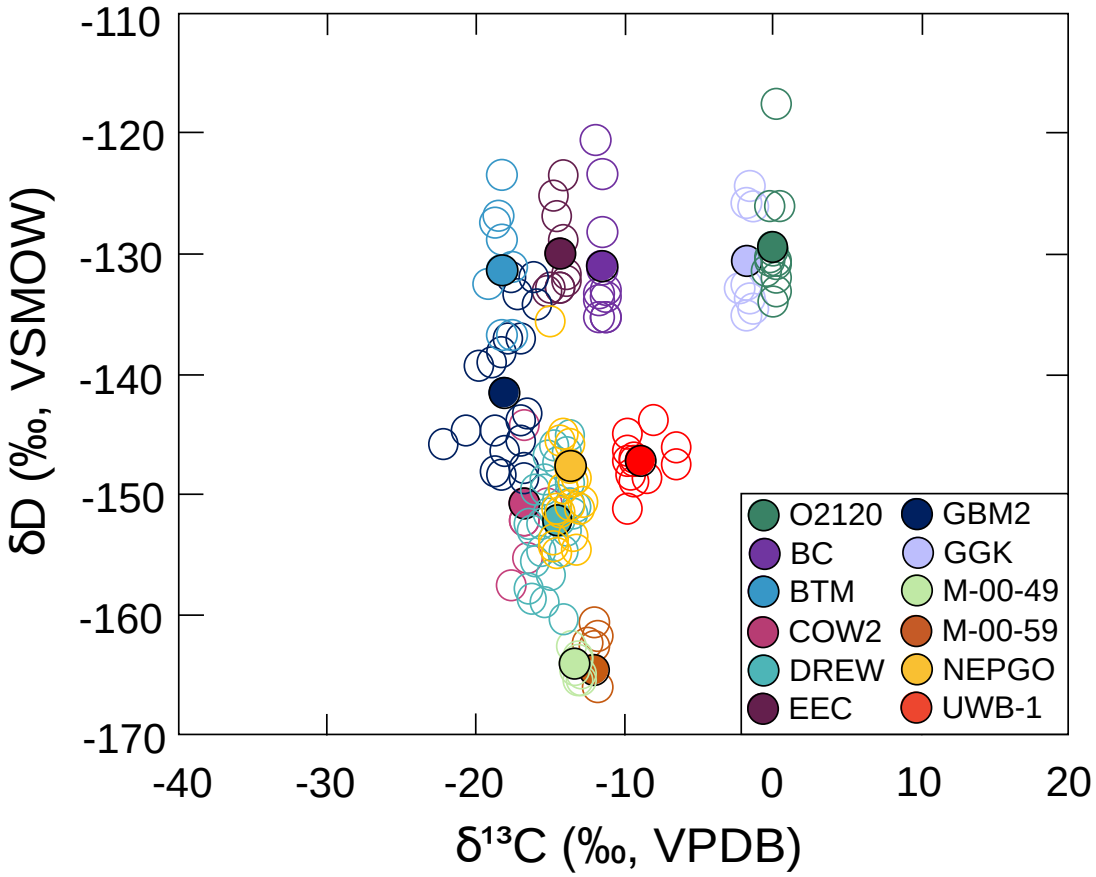

Figure A. 3. $\delta^{13}C$ vs. δD values. A weak correlation (R2 = 0.10), suggests stable carbon and hydrogen isotopes in tooth enamel do not correlate.

Table A. 4. Intra-tooth sample identification numbers, δD, $\delta^{18}O$, and $\delta^{13}C$ values, hydrogen peak area, sample weight (mg), and distance (mm) along each tooth

Castor - Canyon County, CO						
Identification number	δD (‰, VSMOW)	Hydrogen peak area	sample weight (mg)	$\delta^{18}O$ (‰, VSMOW)	$\delta^{13}C$ (‰, VPDB)	Distance (mm)
BTM a	−139.20	18.89	1.19	20.10		2.30
BTM c	−136.86	48.54	1.01	19.86	−17.39	3.53
BTM d	−129.12	33.68	0.77	19.64	−18.15	4.76
BTM e	−131.22	36.63	1.17	17.46	−17.49	5.99
BTM f	−123.64	25.50	1.86	18.99	−17.98	7.22
BTM g	−127.64	88.07	1.17	20.46	−18.39	8.45
BTM h	−136.92	60.77	1.17	18.05	−18.02	9.68
BTM i	−127.07	43.30	1.15	18.45	−18.32	10.91
BTM j	−132.80	46.43	1.10	19.79	−18.91	12.14
Bos tarus - Uni. of Wisconsin, WI						
Identification number	δD (‰, VSMOW)	Hydrogen peak area	sample weight (mg)	$\delta^{18}O$ (‰, VSMOW)	$\delta^{13}C$ (‰, VPDB)	Distance (mm)
UWB-1 1	−147.86	46.84	1.23	23.34	−6.59	2.84
UWB-1 2	−146.45	22.37	2.81	23.23	−6.41	4.38
UWB-1 3	−148.24	49.20	2.01			5.80
UWB-1 4	−148.97	35.67	1.41	22.56	−8.40	7.33
UWB-1 5	−149.23	24.59	2.54	21.80	−9.23	9.02
UWB-1 6	−151.38	46.25	1.49	20.82	−9.65	10.84

Identification number	δD (‰, VSMOW)	Hydrogen peak area	sample weight (mg)	$\delta^{18}O$ (‰, VSMOW)	$\delta^{13}C$ (‰, VPDB)	Distance (mm)
UWB-1 7	−147.33	31.69	1.82	21.27	−9.31	13.07
UWB-1 8	−146.77	18.52	1.98	19.37	−9.76	15.75
UWB-1 9	−147.55	36.82	2.10	18.42	−9.72	17.67
UWB-1 10	−148.55	40.45	1.35	18.32	−9.41	19.08
UWB-1 11	−144.21	32.66	1.96	15.81	−8.05	21.63
UWB-1 12	−147.65	38.13	1.72	17.74	−9.36	22.89
UWB-1 13	−145.21	35.21	2.83		−9.72	25.12
Bison - Catalina, CA						
Identification number	δD (‰, VSMOW)	Hydrogen peak area	sample weight (mg)	$\delta^{18}O$ (‰, VSMOW)	$\delta^{13}C$ (‰, VPDB)	Distance (mm)
BC 1	−120.72	50.48	2.30	28.44	−11.78	1.60
BC 2	−123.59	61.68	2.94	27.06	−11.52	3.62
BC 3	−131.57	34.64	1.94	28.69	−11.42	5.51
BC 4	−128.47	52.55	2.21	29.06	−11.44	7.02
BC 5	−135.66	36.94	2.41	29.11	−11.29	8.79
BC 6	−133.22	38.84	2.15	29.40	−11.20	10.28
BC 7	−135.47	45.09	2.77	28.53	−11.27	12.11
BC 8	−133.74	43.29	2.37	28.29	−11.29	13.78
BC 9	−134.02	38.19	2.43	26.94	−11.73	15.23
BC 10	−135.68	32.63	2.00	27.04	−11.64	16.93
BC 11	−133.53	44.58	2.52	27.56	−11.69	18.24
Bos tarus - Juntura, OR						

Identification number	δD (‰, VSMOW)	Hydrogen peak area	sample weight (mg)	$\delta^{18}O$ (‰, VSMOW)	$\delta^{13}C$ (‰, VPDB)	Distance (mm)
COW2 M2 1	−144.25	42.42	1.89	21.82	−16.55	1.25
COW2 M2 2	−144.33	7.28	0.45	24.53		3.00
COW2 M2 3	−147.75	9.39	0.58			4.74
COW2 M2 4	−152.38	25.81	1.47	20.36	−16.60	6.49
COW2 M2 5	−155.44	27.23	1.58	20.46	−16.36	8.23
COW2 M2 6	−157.90	31.45	1.95	19.11	−17.50	9.98
COW2 M2 7	−150.98	24.28	1.40	22.63	−15.15	11.72
COW2 M2 8	−152.23	18.04	1.09	19.75	−16.58	13.47
COW2 M2 9	−147.84	13.11	0.72			15.21
COW2 M2 10	−149.11	34.69	1.67			16.96
COW2 M2 11	−149.62	47.69	2.51			18.70
Equus - el Criado, Argentina						
Identification number	δD (‰, VSMOW)	Hydrogen peak area	sample weight (mg)	$\delta^{18}O$ (‰, VSMOW)	$\delta^{13}C$ (‰, VPDB)	Distance (mm)
EEC M2 1	−132.91	42.08	1.36	25.52	−14.82	1.40
EEC M2 2	−127.03	44.67	1.71	26.39	−14.50	2.72
EEC M2 3	−129.09	20.03	0.83	24.17	−13.93	4.03
EEC M2 4	−133.2359	51.46	2.11	24.45	−15.07	5.35
EEC M2 5	−132.37	35.31	1.58	23.58	−13.77	6.66
EEC M2 6	−133.24	45.98	2.21			7.98
EEC M2 7	−131.99	57.19	2.53	23.45	−13.78	9.29
EEC M2 8	−133.02	37.99	1.71	23.58	−14.24	10.61
EEC M2 9	−132.97	43.30	2.07	28.84	−14.30	11.92

Identification number	δD (‰, VSMOW)	Hydrogen peak area	sample weight (mg)	$\delta^{18}O$ (‰, VSMOW)	$\delta^{13}C$ (‰, VPDB)	Distance (mm)
EEC M2 10	−123.62	54.84	2.04	23.45	−14.82	13.24
EEC M2 11	−130.30	7.62	0.38		−14.07	14.55
EEC M2 12	−125.21	56.72	2.47	24.48	−14.56	15.87
Nanger granti - Sibiloi National Park, Kenya						
Identification number	δD (‰, VSMOW)	Hydrogen peak area	sample weight (mg)	$\delta^{18}O$ (‰, VSMOW)	$\delta^{13}C$ (‰, VPDB)	Distance (mm)
GGK 1	−125.80	40.87	2.01	31.37	−1.65	1.98
GGK 2	−133.10	43.12	2.11	32.41	−1.98	2.72
GGK 3	−135.15	37.31	1.93	33.00	−1.52	4.50
GGK 4	−133.94	38.51	2.19	33.77	−1.32	5.59
GGK 5	−132.64	45.73	2.47	33.72	−1.48	6.75
GGK 6	−124.58	58.54	3.00	33.62	−1.40	8.71
GGK 7	−126.07	42.40	2.15	32.88	−1.11	10.43
GGK 8	−134.60	33.28	1.92	32.86	−1.21	12.53
Oryx - Sibiloi National Park, Kenya						
Identification number	δD (‰, VSMOW)	Hydrogen peak area	sample weight (mg)	$\delta^{18}O$ (‰, VSMOW)	$\delta^{13}C$ (‰, VPDB)	Distance (mm)
O2120-1	-126.08	41.79	0.65		0.41	
O2120-2	-132.23	42.99	0.99		0.08	
O2120-3	-133.17	13.12	1.76	35.75	0.16	3.42
O2120-4	-131.11	20.49	0.91		0.19	
O2120-5	-117.54	52.17	1.49	36.07	0.10	6.02

Identification number	δD (‰, VSMOW)	Hydrogen peak area	sample weight (mg)	$\delta^{18}O$ (‰, VSMOW)	$\delta^{13}C$ (‰, VPDB)	Distance (mm)
O2120-6	-126.25	28.94	1.72	36.34	-0.31	7.30
O2120-7	-130.59	50.92	1.40	35.99	0.12	9.14
O2120-8	-133.99	19.36	1.12		0.05	
O2120-9	-130.42	38.86	1.24	35.94	-0.16	12.38
O2120-10	-129.84	33.06	2.18	35.38	-0.14	14.59
O2120-11	-131.65	28.96	1.30	34.76	-0.38	14.90
O2120-12	-130.83	34.01	1.80	34.64	-0.17	15.84
Equus - Gran Barranca, Argentina						
Identification number	δD (‰, VSMOW)	Hydrogen peak area	sample weight (mg)	$\delta^{18}O$ (‰, VSMOW)	$\delta^{13}C$ (‰, VPDB)	Distance (mm)
GBM2-1	−134.47	15.06	1.91	27.45	−15.88	1.30
GBM2-2	−132.24	6.20	2.32	30.54	−17.73	2.57
GBM2-3	−139.59	28.38	1.50	22.10	−19.67	3.84
GBM2-4	−148.05	28.16	2.94	25.79	−16.68	5.11
GBM2-5	−137.12	15.70	0.86	25.44	−16.95	6.38
GBM2-6	−143.59	43.30	1.24	25.56	−16.55	7.65
GBM2-7	−137.25	19.32	2.18	25.00	−17.90	8.92
GBM2-8	−145.04	23.93	0.90	24.10	−18.74	10.19
GBM2-9	−133.66	22.55	1.13	26.36	−17.18	11.46
GBM2-10	−145.80	70.99	2.30		−17.03	
GBM2-11	−148.36	27.45	0.78	26.04	−18.78	12.73
GBM2-12	−139.38	14.93	0.87	23.74	−18.88	14.00
GBM2-13	−138.40	11.31	1.73	24.50	−18.23	15.27

Identification number	δD (‰, VSMOW)	Hydrogen peak area	sample weight (mg)	$\delta^{18}O$ (‰, VSMOW)	$\delta^{13}C$ (‰, VPDB)	Distance (mm)
GBM2-14	−132.10	23.27	0.92	25.05	−16.13	16.54
GBM2-15	−144.13	39.04	2.37	26.98	−17.03	17.81
GBM2-16	−148.57	11.74	0.91	26.57	−18.18	19.08
GBM2-17	−148.85	8.69	0.55	25.05	−16.81	20.35
GBM2-18	−146.81	19.46	1.15	26.30	−18.10	21.62
GBM2-19	−144.94	4.16	0.48	24.23	−20.54	22.89
GBM2-20	−145.96	28.24	1.45	21.38	−22.204	24.16
GBM2-21	−146.75	29.96	1.32	19.19		25.43
Equus - Drewsey, OR						
Identification number	δD (‰, VSMOW)	Hydrogen peak area	sample weight (mg)	$\delta^{18}O$ (‰, VSMOW)	$\delta^{13}C$ (‰, VPDB)	Distance (mm)
DREW-c				24.37	−8.38	1.25
DREW-e	−150.67	53.69	2.31	24.71	−14.38	2.48
DREW-f	−153.31	50.61	2.12	22.84	−16.04	3.71
DREW-g	−152.79	20.03	0.82	23.89	−15.39	4.94
DREW-h	−149.71	65.23	2.43	23.18	−15.25	6.17
DREW-i	−149.00	30.43	0.98	22.58	−15.19	7.40
DREW-j	−146.82	27.57	0.90	22.06	−15.09	8.63
DREW-k	−146.08	20.21	0.69	22.09	−14.72	9.86
DREW-l	−147.58	21.05	0.74	21.96	−14.4	11.09
DREW-m	−151.05	36.38	1.11	21.9	−13.64	12.32
DREW-n	−145.38	33.77	1.05	21.51	−13.49	13.55

Identification number	δD (‰, VSMOW)	Hydrogen peak area	sample weight (mg)	$\delta^{18}O$ (‰, VSMOW)	$\delta^{13}C$ (‰, VPDB)	Distance (mm)
DREW-o	−151.69	44.42	1.54	20.95	−13.27	14.78
DREW-p	−151.33	50.48	1.75	21.00	−13.03	16.01
DREW-q	−149.71	34.83	1.18	19.62	−16.00	17.24
DREW-r	−152.66	34.62	1.23	18.85	−16.26	18.47
DREW-s	−154.86	65.32	2.54	18.64	−15.55	19.70
DREW-t	−155.76	68.17	2.46	18.07	−15.93	20.93
DREW-u	−153.34	26.37	0.96	18.9	−13.68	22.16
DREW-w	−152.39	17.58	0.64	18.4	−14.14	23.39
DREW-x	−155.01	25.51	0.94	17.81	−13.91	24.62
DREW-y	−146.68	31.46	0.97	18.16	−13.83	25.85
DREW-z	−151.86	25.63	0.86	17.44	−15.09	27.08
DREW-ab	−158.80	44.12	1.70	17.26	−16.16	28.31
DREW-ac	−160.54	39.97	1.52	18.29	−14.08	29.54
DREW-ad	−156.99	22.42	0.86	18.23	−14.85	30.77
DREW-af	−157.99	19.43	0.75	16.89	−16.33	32.00
DREW-ag	−159.34	36.48	1.35	17.97	−15.22	33.23
DREW-ah				17.53	−12.56	34.46
DREW-ai				19.4	−14.15	35.69
DREW-aj	−149.21	53.31	1.76	19.79	−13.47	36.80
Capra hircus -Nepal						
Identification number	δD (‰, VSMOW)	Hydrogen peak area	sample weight (mg)	$\delta^{18}O$ (‰, VSMOW)	$\delta^{13}C$ (‰, VPDB)	Distance (mm)
NEPGO-A	−135.77	122.38	3.99	20.61	−14.77	1.23

Identification number	δD (‰, VSMOW)	Hydrogen peak area	sample weight (mg)	$\delta^{18}O$ (‰, VSMOW)	$\delta^{13}C$ (‰, VPDB)	Distance (mm)
NEPGO-B	−154.62	51.26	2.66	20.82	−14.53	2.46
NEPGO-C	−154.14	51.92	2.33	20.72	−14.62	3.69
NEPGO-D	−155.34	66.85	3.05	21.06	−14.43	4.92
NEPGO-E	−151.49	46.87	2.13	21.44	−14.31	6.15
NEPGO-F	−151.86	58.29	2.63	21.93	−14.20	7.38
NEPGO-G	−149.67	41.84	2.22	22.28	−14.01	8.61
NEPGO-H	−145.90	55.48	2.31	22.29	−14.2	9.84
NEPGO-I	−145.38	41.22	1.70	22.76	−13.92	11.07
NEPGO-J	−149.90	42.64	1.90	22.59	−13.99	12.30
NEPGO-K	−151.22	49.64	2.31	23.21	−13.53	13.53
NEPGO-L	−147.79	38.56	1.66	23.07	−13.57	14.76
NEPGO-M	−148.13	38.92	1.67	22.98	−13.51	15.99
NEPGO-N	−146.12	47.95	1.93	22.71	−13.62	17.22
NEPGO-O	−149.21	53.81	2.21	21.86	−13.38	18.45
NEPGO-P	−148.97	53.75	1.50	21.39	−13.11	19.68
NEPGO-Q	−154.95	42.20	1.88	20.66	−13.18	20.91
NEPGO-R	−153.65	46.60	2.07	19.99	−13.35	22.14
NEPGO-S	−150.95	43.49	1.87	20.66	−12.74	23.37
NEPGO-T	−151.41	46.76	1.95	19.60	−12.82	24.60
Cervus - Yellowstone, WY						
Identification number	δD (‰, VSMOW)	Hydrogen peak area	sample weight (mg)	$\delta^{18}O$ (‰, VSMOW)	$\delta^{13}C$ (‰, VPDB)	Distance (mm)
M-00-49-A	−162.16	20.50	0.80	16.35	−11.89	1.24

Identification number	δD (‰, VSMOW)	Hydrogen peak area	sample weight (mg)	$\delta^{18}O$ (‰, VSMOW)	$\delta^{13}C$ (‰, VPDB)	Distance (mm)
M-00-49-B	−160.95	23.08	0.83	14.94	−12.00	2.48
M-00-49-C	−166.37	23.74	0.92	14.48	−11.92	3.72
M-00-49-D	−173.90	75.93	2.85		−12.32	4.96
M-00-49-E	−162.83	61.18	1.97	13.47	−12.19	6.20
M-00-49-F	−162.60	53.70	1.70	13.76	−12.50	7.44
M-00-49-G	−161.53	48.94	1.58	13.86		8.68
M-00-49-H	−159.42	86.17	2.26	14.67		9.92
Cervus - Yellowstone, WY						
Identification number	δD (‰, VSMOW)	Hydrogen peak area	sample weight (mg)	$\delta^{18}O$ (‰, VSMOW)	$\delta^{13}C$ (‰, VPDB)	Distance (mm)
M-00-59-A	−165.85	50.04	1.20	16.78	−13.21	1.25
M-00-59-B	−164.0	58.22	1.73	15.55	−13.13	2.49
M-00-59-C	−165.08	85.93	2.31	15.18	−12.98	3.73
M-00-59-D	−165.70	95.20	2.89	14.10	−12.92	4.97
M-00-59-E	−163.80	78.40	2.27	14.96	−13.21	6.21
M-00-59-F	−162.84	89.76	1.93	14.85	−13.58	7.45
M-00-59-G	−165.00	62.67	1.28	15.18	−13.24	8.69

noted in other biological tissues, such as hair (Bowen et al., 2008). However, collagen δD and $\delta^{13}C$ values within animals appear to exhibit a trophic level effect, with lower δD and $\delta^{13}C$ values associated with herbivores when compared to carnivores (Reynard and Hedges, 2008; Birchnall et al., 2005). Because we solely analyzed herbivores, we were unable to determine whether tooth enamel δD and $\delta^{13}C$ values similarly illustrate a trophic level effect.